GDL-GMF-02-04

FLOW/SOOT-FORMATION INTERACTIONS IN NONBUOYANT LAMINAR DIFFUSION FLAMES

by

Z. Dai, K.-C. Lin, P.B. Sunderland, F. Xu and G.M. Faeth

College of Engineering
Department of Aerospace Engineering
The University of Michigan
Ann Arbor, Michigan 48109-2140

GDL-GMF-02-04

FLOW/SOOT-FORMATION INTERACTIONS IN NONBUOYANT LAMINAR DIFFUSION FLAMES

by

Z. Dai,[a] K.-C. Lin,[b] P.B. Sunderland,[c] F. Xu[d] and G.M. Faeth
Department of Aerospace Engineering
The University of Michigan
Ann Arbor, Michigan 48109-2140

Final Report

1 October 1998-30 September 2002

15 December 2002

NASA Grant No. NAG3-661
Office of Biological and Physical Research
National Aeronautics and Space Administration
Washington, DC 20546-0001
D.L. Urban and Z.-G. Yuan, NASA Glenn Research Center, Project Scientists

---

[a]Now at G.E. Aircraft Engines, Cincinnati, Ohio.

[b]Now at Taitech, Inc., Wright-Patterson Air Force Base, Ohio.

[c]Now at the National Center for Microgravity Research, Cleveland, Ohio.

[d]Now at the University of Central Florida, Orlando, Florida.

FLOW/SOOT-FORMATION INTERACTIONS IN NONBUOYANT LAMINAR DIFFUSION FLAMES

Abstract

This is the final report of a research program considering interactions between flow and soot properties within laminar diffusion flames. Laminar diffusion flames were considered because they provide model flame systems that are far more tractable for theoretical and experimental studies than more practical turbulent diffusion flames. In particular, understanding the transport and chemical reaction processes of laminar flames is a necessary precursor to understanding these processes in practical turbulent flames and many aspects of laminar diffusion flames have direct relevance to turbulent diffusion flames through application of the widely recognized laminar flamelet concept of turbulent diffusion flames. The investigation was divided into three phases, considering the shapes of nonbuoyant round laminar jet diffusion flames in still air, the shapes of nonbuoyant round laminar jet diffusion flames in coflowing air, and the hydrodynamic suppression of soot formation in laminar diffusion flames.

The shapes (the luminous flame boundaries) of nonbuoyant round soot-containing hydrocarbon/air laminar jet diffusion flames where observed at microgravity from color video images obtained on orbit in the Space Shuttle Columbia. These test conditions provided truly steady and nonbuoyant flames that were close to the laminar smoke point. These flames had larger luminous flame lengths than earlier ground-based observations at similar flame conditions: 40% larger than the luminous flame lengths of soot-containing low gravity flames observed using an aircraft (KC-135) facility due to reduced effects of accelerative disturbances and unsteadiness; roughly twice as large as the luminous flame lengths of soot-containing flames at normal gravity due to the absence of effects of buoyant mixing and roughly twice as large as luminous flame lengths of soot-free low gravity flames using drop tower facilities due to the presence of soot luminosity and possible effects of reduced unsteadiness. Simplified expressions to estimate the luminous flame boundaries of round nonbuoyant laminar jet diffusion flames were obtained using the classical analysis of Spalding (1979); this approach provided successful correlations of flame shapes for both soot-free and soot-containing flames, except when the soot-containing flames were in the opened-tip configuration that is reached at fuel flow rates that are either near or exceed the laminar smoke-point fuel flow rate.

The shapes (luminous flame boundaries) of steady nonbuoyant round luminous laminar jet diffusion flames burning in coflowing air were studied both theoretically and experimentally. Flame shapes were measured from photographs of flames burning at low pressures in order to

minimize the effects of buoyancy, considering flames close to the laminar smoke point but not soot emitting. Simple expressions to estimate flame shapes were found by extending an earlier analysis of Mahalingam et al. (1990). These formulas provided a good correlation of the present measurements except near the burner exit where the self-similar approximations used in the simplified analysis are no longer appropriate.

Finally, effects of flow (hydrodynamic) properties on limiting conditions needed to obtain soot-free laminar nonpremixed hydrocarbon/air flames (laminar soot-point conditions) were studied emphasizing non-buoyant laminar coflowing jet diffusion flames. The experiments were carried out at reduced pressures to minimize effects of flow acceleration due to the intrusion of buoyancy. The measurements show that laminar soot-point fuel flow rates and flame lengths can be increased, broadening the range of fuel flow rates where the flames remain soot free, by increasing air coflow velocities compared to fuel flow velocities (or the air/fuel velocity ratio) at the burner exit. Flame shape analysis shows that the mechanism of this effect involves the magnitude and direction of flow velocities relative to the flame sheet where increased air/fuel velocity ratios cause a progressive reduction of flame residence times in the fuel-rich soot-formation region. The range of soot-free conditions was limited by both liftoff (at low pressures) and the intrusion of effects of buoyancy (at high pressures). Effective correlations of laminar soot- and smoke-point flame lengths were also found in terms of a corrected fuel flow rate parameter, based on simplified analysis of laminar coflowing jet diffusion flame structure. These results show that laminar smoke-point flame lengths in coflowing air are roughly twice as long as soot-free (blue) flames at comparable conditions due to the presence of luminous soot particles at fuel-lean conditions as smoke-point conditions are approached. This is very similar to findings concerning differences between laminar smoke- and soot-point flame lengths of nonbuoyant flames in still environments. These results also provide an explanation of effects of air atomization that act to reduce soot formation in practical turbulent flames.

Acknowledgments

The authors wish to acknowledge the contributions of the staff of the Gas Dynamics Laboratories of the Department of Aerospace Engineering at the University of Michigan, as follows: C.J. Chartier, M.J. Etzel, T.L. Griffin, T.M. Larrow and D.J. McLean for help with apparatus development and experiments; and S.C. Bauerle and S.B.G. Smith for help with communications, financial management and publications. Finally, the support of the research by the Office of Biological and Physical Research of NASA, with D.L. Urban and Z.G. Yuan of the NASA Glenn Research Center serving as project scientists, is also gratefully acknowledged.

Table of Contents

Table of Contents (continued)

List of Tables

List of Figures

List of Figures (continued)

Nomenclature

Symbol		Description
C_f	=	empirical soot factor
C_n	=	empirical coflow factor
D	=	mass diffusivity
d	=	jet exit diameter
Fr_a,Fr_f	=	air and fuel stream Froude numbers, $u_{a,o}^2/(2gL_f)$ and $u_{f,o}^2/(2gL_f)$
f	=	mixture fraction
g	=	acceleration of gravity
g_e	=	equivalent acceleration of gravity
L_f	=	distance from jet exit to luminous flame tip
L_o	=	distance from jet exit to virtual origin
$\dot{m}$	=	burner mass flow rate
p	=	pressure
Re	=	jet Reynolds number, $4\dot{m}/(\pi d\mu)$
r	=	radial distance
Sc	=	Schmidt number, ν/D
u	=	streamwise velocity
u_d	=	streamwise velocity defect
w	=	luminous flame diameter
$w_{1/2}$	=	luminous flame diameter at $\zeta = 1/2$
x	=	streamwise distance
Y_{FUEL}	=	mass fraction of fuel
Y_{OXYGEN}	=	mass fraction of oxygen

Z_{st}	=	stoichiometric mixture fraction
z	=	streamwise distance
ζ	=	normalized streamwise distance, Eqs. (3) and (7)
μ	=	dynamic viscosity
ν	=	kinematic viscosity
ρ	=	density
σ	=	standard deviation of parameter i
τ_r	=	characteristic flame residence time, Eq. (9)

Subscripts

a	=	airstream property
f	=	fuelstream property
MAX	=	maximum value
o	=	burner exit plane or virtual origin condition

1. Introduction

An investigation of soot formation in laminar diffusion flames is described emphasizing flow/soot-formation interactions that can be used to reduce the formation of soot in practical nonpremixed (diffusion) flames. The findings of the research are relevant to several problems of society, as follows: the particulate soot emissions from flames, the radiant heat loads caused by combustion processes, the hazards of terrestrial and spacecraft fires, and the development of practical and reliable methods of computational combustion. The research was carried out in three phases, as follows: (1) the study of the shapes of nonbuoyant round laminar jet diffusion flames in still air, (2) the study of the shapes of nonbuoyant round laminar jet diffusion flames in coflowing air, and (3) the study of the hydrodynamic suppression of soot formation in laminar diffusion flames. An evident limitation of the study, however, is that both theoretical and experimental considerations were limited to laminar diffusion flames. This was done because soot formation in flames largely occurs when the flames are diffusion flames. In addition, laminar flames were considered because they provide model flame systems that are far more tractable for both theoretical and experimental studies than more practical turbulent diffusion flames. This is not a significant limitation, however, because understanding the transport and chemical reaction processes of laminar flames is a necessary precursor to understanding these processes in practical turbulent flames, and because many aspects of laminar diffusion flames have direct relevance to turbulent diffusion flames through the application of the widely-recognized laminar flamelet concept of turbulent diffusion flames, see Bilger [1], Gore and Faeth [2], and references cited therein.

Motivated by technological and public health problems, several methods have been developed to control the soot content and emissions of hydrocarbon-fueled flames. Among these, soot control methods based on fast mixing for diffusion flames are of interest because they avoid the operational problems of additives and premixed combustion [3-5]. The objective of fast mixing is to minimize residence times of fuel and fuel-decomposition products at fuel-rich conditions so that few soot particles develop, and those that do develop do not reach large sizes and are readily consumed in the soot-oxidation region of the flame. The present investigation seeks improved understanding of fast mixing concepts based on experimental observations of laminar coflowing jet diffusion flames that were studied because they provide relatively tractable models of mixing and reaction within more practical but relatively intractable turbulent diffusion flames, as discussed earlier. Another advantage of the laminar coflowing jet diffusion flame configuration is that it has been widely used to study the soot-formation within diffusion flames, see Schalla and McDonald [6], Schug et al. [7], Flower and Bowman [8], Sunderland et al. [9] and Urban et al. [10].

Although fast mixing reduces soot-formation within diffusion flames, past studies of both laminar opposed and coflowing jet diffusion flames show that the way that mixing is carried out is important as well [11-18]. In fact, existing evidence from both laminar and turbulent diffusion flames, and from empirical industrial practice, suggests that soot reduction can be achieved most effectively by assuring that the component of velocity normal to the flame sheet is directed from the fuel-rich toward the fuel-lean side. This configuration, called the "soot-formation-oxidation flame condition" by Kang et al. [14], tends to reduce the residence times of soot precursors and soot at fuel-rich soot-formation conditions by drawing these materials directly through the flame sheet toward fuel-lean oxidation conditions. In contrast, when the component of velocity normal to the flame sheet is directed from the fuel-lean toward the fuel-rich side, called the "soot formation flame condition" by Kang et al. [14], residence times of soot precursors and soot at fuel-rich soot-formation conditions are enhanced, making oxidation of these materials more problematical when oxidation conditions are finally reached.

Studies of effects of components of velocity normal to the flame sheet have been carried out in laminar opposed and coflowing jet diffusion flames [11-18]. During most of these studies [11-16], velocities normal to the flame sheet were varied by varying the compositions of the oxidant- and fuel-carrying streams. For example, diluting the fuel stream with an inert gas (e.g., nitrogen) while enriching the oxidant stream by removing existing diluent (e.g., removing nitrogen from air) promotes increased velocities normal to the flame sheet directed from the fuel-rich side of the flame sheet toward the fuel-lean side and results in reduced soot concentrations in the flames [10-15]. As pointed out by Sunderland et al. [19], however, the composition changes alone are sufficient to retard soot formation and enhance soot oxidation, which tends to reduce soot concentrations and obscures the effect of hydrodynamics on soot control. In addition, the practical utility of varying reactant-stream compositions to control soot formation in diffusion flames is somewhat questionable.

The present investigation sought a direct evaluation of the effect of velocities normal to the flame sheet on soot formation in diffusion flames by considering pure air and pure fuel reactant streams for laminar coflowing jet diffusion flames. In this configuration, enhanced (retarded) air stream velocities provide entrainment velocities normal to the flame sheet directed from the fuel-rich (fuel-lean) side of the flame toward the fuel-lean (fuel-rich) side of the flame, which should reduce (enhance) the formation of soot within the flame, and correspondingly tend to reduce (increase) the degree of soot emission from the flame.

In order to gain insight concerning the way that retarded (enhanced) fuel stream velocities affect soot formation in laminar coflowing jet diffusion flames, the study proceeded in three phases as noted earlier. In the first two phases, theoretical and experimental studies of

flame shape were undertaken, to help define the way that retarded fuel-stream velocities reduce soot concentrations, and thus soot emissions, from diffusion flames. Given this background, observations of the soot properties within coflowing jet diffusion flames were undertaken in order to directly indicate the effect of retarded fuel stream velocities on the soot properties of flames.

The present description of the research is relatively brief. Additional details can be found in the archival publications, the papers, the conference proceedings, and the reports resulting from the investigation that are summarized in Table 1. This table also provides a summary of invited and contributed oral presentations of the research results, honors and awards obtained during the grant period, and the individuals who participated in the investigation. Finally, for convenience, several articles resulting from the research are reproduced in the appendices, as follows: Lin and Faeth [20] in Appendix A, Lin et al. [21] in Appendix B, Dai and Faeth [22] in Appendix C, Urban et al. [23] in Appendix D, and Xu et al. [24] in Appendix E.

Table 1. Summary of Investigation*

Archival Publications (articles and book chapters):

Z. Dai and G.M. Faeth (2000) Hydrodynamic suppression of soot formation in laminar coflowing jet diffusion flames. *Proc. Combust. Inst.* 28, 2085-2092.

G.M. Faeth (2001) Gaseous laminar and turbulent diffusion flames. *Microgravity Combustion Science* (H.D. Ross, ed.), Academic Press, New York, Chapt. 3, pp. 83-182.

G.M. Faeth, G. Roth, and M. Gunderson (1998) Pollutant emissions from combustion processes of mobile power and propulsion systems. *Modern Developments in Propulsion and Combustion* (G.D. Roy, ed.), Taylor & Francis, Washington, D.C., pp. 359-406.

K.-C. Lin and G.M. Faeth (1996) Hydrodynamic suppression of soot emissions in laminar diffusion flames. *J. Prop. Power* 12, 10-17.

K.-C. Lin and G.M. Faeth (1996) Effects of hydrodynamics on soot formation in laminar opposed-jet diffusion flames. *J. Prop. Power* 12, 691-698.

K.-C. Lin and G.M. Faeth (1998) Structure of laminar permanently-blue opposed-jet ethylene-fueled diffusion flames. *Combust. Flame* 115, 468-480.

K.-C. Lin and G.M. Faeth (1999) Shapes of nonbuoyant round luminous laminar jet diffusion flames in coflowing air. *AIAA J.* 37, 759-765.

K.-C. Lin and G.M. Faeth (2000) State relationships of laminar permanently-blue opposed-jet hydrocarbon-fueled diffusion flames. *Int. J. Environ. Combust. Tech.* 1, 53-79.

K.-C. Lin, G.M. Faeth, P.B. Sunderland, D.L. Urban and Z.-G. Yuan (1999) Shapes of nonbuoyant round luminous hydrocarbon/air laminar jet diffusion flames. *Combust. Flame* 116, 415-431.

D.L. Urban, Z.-G. Yuan, P.B. Sunderland, G.T. Linteris, J.E. Voss, K.-C. Lin, Z. Dai, K. Sun and G.M. Faeth (1998) Structure and soot properties of nonbuoyant ethylene/air laminar jet diffusion flames. *AIAA J.* 36, 1346-1360.

D.L. Urban, Z.-G. Yuan, P.B. Sunderland, K.-C. Lin, Z. Dai and G.M. Faeth (2000) Smoke-point properties of nonbuoyant round laminar jet diffusion flames. *Proc. Combust. Inst.* 28, 1965-1972.

F. Xu, Z. Dai and G.M. Faeth (2002) Flame shapes of nonbuoyant laminar jet diffusion flames. *AIAA J.* 40, 2439-2446.

Papers and Conference Proceedings:

Z. Dai and G.M. Faeth (2000) Soot and smoke-point properties of laminar coflowing jet diffusion flames. *Proceedings of the Spring Technical Meeting*, Central States Section, The Combustion Institute, Pittsburgh, PA, pp. 39-44.

Z. Dai and G.M. Faeth (2000) Shapes of nonbuoyant laminar jet diffusion flames at soot- and smoke-point conditions. *Proceedings of Spring Technical Meeting 2000*, Canadian Section of the Combustion Institute, Ottawa, pp. 22-1 to 22-6.

Z. Dai, F. Xu and G.M. Faeth (2001) Shapes of soot-free hydrocarbon/air laminar coflowing jet diffusion flames. 39th Aerospace Sciences Meeting, Reno, NV, AIAA Paper No. 2001-0322.

G.M. Faeth (1999) The structure, optical and radiative properties of soot in flame environments: a review. *Proceedings of the 5th ASME/JSME Joint Thermal Engineering Conference*, San Diego, CA, Paper No. AJTE99-6530.

G.M. Faeth (1999) Flame-flow interactions during combustion of gases. 52nd Annual Meeting, American Physical Society, Division of Fluid Dynamics, New Orleans, LA, *Bulletin of the American Physical Society*, Vol. 44, No. 8, p. 129.

G.M. Faeth and Z. Dai (1999) Flow/soot-formation interactions in nonbuoyant laminar diffusion flames. *Fifth International Microgravity Combustion Workshop*, NASA/CP-1999-208917, pp. 483-486.

K.-C. Lin and G.M. Faeth (1994) Effect of reactant stream velocities on soot formation within laminar coflowing jet diffusion flames. *Proceedings of the Spring Technical Meeting*, Central States Section, The Combustion Institute, Pittsburgh, PA, pp. 281-286.

K.-C. Lin and G.M. Faeth, Effects of coflow on soot formation in laminar jet diffusion flames. *Twenty-Fifth Symposium (International) on Combustion*, Book of Poster Abstracts, The Combustion Institute, Pittsburgh, PA.

K.-C. Lin and G.M. Faeth (1995) Hydrodynamic suppression of soot emissions in laminar diffusion flames. 33rd AIAA Aerospace Sciences Meeting, Reno, NV, AIAA Paper No. 95-0375.

K.-C. Lin and G.M. Faeth (1995) Effects of hydrodynamics on soot formation in hydrocarbon-fueled laminar opposed jet diffusion flames. *Proceedings of the Fall Technical Meeting*, Eastern Section of the Combustion Institute, Pittsburgh, PA, pp. 423-426.

K.-C. Lin and G.M. Faeth (1996) Structure of laminar permanently-blue opposed-jet hydrocarbon-fueled diffusion flames. *Proceedings of the Spring Technical Meeting*, Central States Section, The Combustion Institute, Pittsburgh, PA, pp. 110-115.

K.-C. Lin and G.M. Faeth (1996) Structure and state relationships for laminar soot-free hydrocarbon-fueled diffusion flames *Proceedings of Fall Technical Meeting*, Eastern Section of the Combustion Institute, Pittsburgh, PA, pp. 429-432.

K.-C. Lin and G.M. Faeth (1997) Generalized state relationships of laminar permanently-blue opposed-jet hydrocarbon-fueled diffusion flames. *Proceedings of Fall Technical Meeting*, Eastern Section of the Combustion Institute, Pittsburgh, PA, pp. 187-190.

K.-C. Lin and G.M. Faeth (1999) Flame shapes of laminar nonbuoyant coflowing jet diffusion flames. *Proceedings of the Joint Meeting of the United States Sections*, The Combustion Institute, Pittsburgh, PA, pp. 336-339.

K.-C. Lin, G.M. Faeth, P.B. Sunderland, D.L. Urban and Z.-G. Yuan (1998) Shapes of nonbuoyant luminous hydrocarbon/air laminar jet diffusion flames. *Proceedings of the Spring Technical Meeting*, Central States Section of the Combustion Institute, Pittsburgh, PA, pp. 357-362.

K.-C. Lin, G.M. Faeth, P.B. Sunderland, D.L. Urban and Z.-G. Yuan (1998) Shapes of nonbuoyant round luminous hydrocarbon/air laminar jet diffusion flames. *Twenty-Seventh Symposium (International) on Combustion*, Book of Poster Abstracts, The Combustion Institute, Pittsburgh, PA.

D.L. Urban, Z.-G. Yuan, P.B. Sunderland, G.T. Linteris, J.E. Voss, K.-C. Lin, Z. Dai, K. Sun and G.M. Faeth (1998) Structure and soot properties of nonbuoyant ethylene/air laminar jet diffusion flames. 36th Aerospace Sciences Meeting, Reno, NV, AIAA Paper No. 98-0568.

D.L. Urban and G.M. Faeth (2001) Soot research in combustion science: introduction and review of current work. 39th Aerospace Sciences Meeting, Reno, NV, AIAA Paper No. 2001-0322.

Z. Dai and G.M. Faeth (2000) Soot and smoke-point properties of plane laminar jet diffusion flames. *Proceedings of the Spring Technical Meeting*, The Canadian Section, The Combustion Institute, Ottawa, pp. 39-44.

F. Xu, Z. Dai and G.M. Faeth (2001) Suppression of soot formation and shapes of laminar jet diffusion flames. *Proceedings of the Sixth International Microgravity Combustion Workshop*, NASA/CP-2001-210826, pp. 169-172.

Reports:

K.T. Aung, M.I. Hassan, S.S. Krishnan, K.-C. Lin, F. Xu and G.M. Faeth (2001) Soot formation in freely-propagating laminar premixed flames. Report No. GDL/GMF-01-01, Department of Aerospace Engineering, The University of Michigan, Ann Arbor, MI.

Z. Dai, K.-C. Lin, P.B. Sunderland, F. Xu and G.M. Faeth (1997) Laminar soot processes (LSP). Report No. GDL/GMF 97-01, Department of Aerospace Engineering, The University of Michigan, Ann Arbor, MI.

Z. Dai, A.M. El-Leathy, K.-C. Lin, P.B. Sunderland, F. Xu and G.M.. Faeth (2000) Laminar soot processes (LSP). Report No. GDL/GMF-00-03, Department of Aerospace Engineering, The University of Michigan, Ann Arbor, MI.

Z. Dai, A.M. El-Leathy, C.H. Kim, S.S. Krishnan, K.-C. Lin, F. Xu and G.M. Faeth (2002) Laminar soot Processes. Report No. GDL/GMF-02-03, Department of Aerospace Engineering, The University of Michigan, Ann Arbor, MI.

Oral Presentations (Invited):

G.M. Faeth (1997) Soot growth in laminar premixed and diffusion flames. UIC Spring Seminar Series, University of Illinois-Chicago, Chicago, IL.

G.M. Faeth (1997) Laminar soot processes. 4th International Microgravity Combustion Workshop, NASA Glenn Research Center, Cleveland, OH,

G.M. Faeth (1997) LSP science results. CM-1 Awards Ceremony, NASA Glenn Research Center, Cleveland, OH,

G.M. Faeth (1997) Structure and soot formation processes of premixed flames. Graduate Research Seminar, School of Mechanical Engineering, Purdue University, West Lafayette, IN.

G.M. Faeth (1997) Academic perspectives on combustion research in the 21st century. ASME, Winter Annual Meeting, Houston, TX.

G.M. Faeth (1998) Space shuttle observations of soot-containing round laminar jet diffusion flames. Mechanical Engineering Seminar, University of Connecticut, Storrs, CT.

G.M. Faeth (1998) Soot formation in laminar premixed flames. Mechanical Engineering Seminar, The Pennsylvania State University, University Park, PA.

G.M. Faeth (1999) Structure, optical and radiative properties of soot in flame environments: a review. 5th ASME/JSME Joint Thermal Engineering Conference, San Diego, CA.

G.M. Faeth (1999) Soot formation in laminar premixed flames. 5th International Microgravity Combustion Workshop, NASA Glenn Research Center, Cleveland, OH.

G.M. Faeth (1999) Laminar soot processes. 5th International Microgravity Combustion Workshop, NASA Glenn Research Center, Cleveland, OH

G.M. Faeth (1999) Flow/soot-formation interactions in nonbuoyant laminar diffusion flames. 5th International Microgravity Combustion Workshop, NASA Glenn Research Center, Cleveland, OH.

G.M. Faeth (1999) Structure and soot properties of laminar jet diffusion flames. Gordon Conference on Gravitational Phenomena in Physico-Chemical Systems. New England College, Henniker, NH.

G.M. Faeth (1999) Flame/flow interactions during the combustion of gases. 52nd Annual Meeting of Division of Fluid Dynamics, American Physical Society, New Orleans, LA.

G.M. Faeth (1999) Observations of nonbuoyant laminar diffusion flames using space shuttle facilities. Department of Mechanical Engineering, University of California-Berkeley, Berkeley, CA.

G.M. Faeth (2000) Laminar soot processes (LSP) science overview. NASA Glenn Research Center, Cleveland, OH.

G.M. Faeth (2000) Combustion module-2: laminar soot processes. NASA Kennedy Space Center, Cape Canaveral, FL.

G.M. Faeth (2000) Laminar soot processes (LSP) overview. Spacehab Corp., Cape Canaveral, FL.

G.M. Faeth (2001) Overview of NASA research in combustion science. Space Studies Board, National Research Council, Washington, DC.

G.M. Faeth (2001) Micro-G and you: space research and benefits on earth in physical sciences/combustion. PanPacific Conference on Micro-G, Los Angeles, CA.

G.M. Faeth (2001) Soot formation and oxidation in flames. LCSR Seminar, University of Orleans, Orleans, LA.

G.M. Faeth (2001) Structure and early soot formation properties of laminar flames. 6th International Microgravity Combustion Workshop, NASA Glenn Research Center, Cleveland, OH.

G.M. Faeth (2001) Structure and soot formation properties of laminar flames. 6th International Microgravity Combustion Workshop, NASA Glenn Research Center, Cleveland, OH.

G.M. Faeth (2001) Suppression of soot formation and shapes of laminar jet diffusion flames. 6th International Microgravity Combustion Workshop, NASA Glenn Research Center, Cleveland, OH.

G.M. Faeth (2001) Soot formation and oxidation in laminar premixed and nonpremixed flames. XXIV Event of the Italian Section of the Combustion Institute, S. Margherita Ligure, Italy.

G.M. Faeth (2001) Current and future challenges in combustion: basic aspects. NSF Workshop on New Combustion Models with Practical Fuels, S. Margherita Ligure, Italy.

G.M. Faeth (2001) Opportunities and challenges of combustion science at microgravity. NASA Headquarters, Washington, DC.

G.M. Faeth (2002) Soot surface growth and oxidation properties of premixed and nonpremixed flames. Distinguished Lecturer Series, Department of Chemical and Fuels Engineering, University of Utah, Salt Lake City, UT.

G.M. Faeth (2003) Laminar soot processes (LSP) overview: science results overview. Combustion Module 2 Awards Ceremony, NASA Glenn Research Center, Cleveland, OH.

G.M. Faeth (2003) Laminar soot processes (LSP) experiment: findings from ground-based measurements. 7th International Workshop on Microgravity Combustion and Chemically Reacting Systems, Cleveland, OH.

G.M. Faeth (2003) Laminar soot processes (LSP) experiment: findings from flight measurements. 7th International Workshop on Microgravity Combustion and Chemically Reacting Systems, Cleveland, OH.

G.M. Faeth (2003) Soot processes in nonbuoyant laminar jet diffusion flames: a paradigm for soot processes in practical nonpremixed flames. Gordon Conference on Gravitational Phenomena in Physico-Chemical Systems, Connecticut College, New London, CT.

Honors/Awards:

G.M. Faeth, NASA Public Service Medal, 1999.

G.M. Faeth, Highly-Cited Researcher Certificate (as one of the 99 most frequently cited engineers in the world), Institute for Scientific Information, Philadelphia, PA, 2000.

G.M. Faeth, Medal of Appreciation, Helwan University, El-Matteria, Cairo, Egypt, 2002.

G.M. Faeth et al., Best Propellants and Combustion Paper, presented at the AIAA 37th Aerospace Sciences Meeting, Reno, NV, 1999.

G.M. Faeth et al., Best Propellants and Combustion Paper, presented at the AIAA 40th Aerospace Sciences Meeting, Reno, NV 1999.

G.M. Faeth, Horace H. Rackham Distinguished Dissertation Award, The University of Michigan, Ann Arbor, MI, 1999.

G.M. Faeth, Invited Plenary Lecture, 6th International Conference on Technologies and Combustion for a Clean Environment, Porto, Portugal, 2001.

G.M. Faeth, Invited James E. Peters Plenary Lecture, Spring Technical Meeting, Central States Section, The Combustion Institute, Pittsburgh, PA, 2002.

G.M. Faeth, Invited Plenary Lecture, The Combustion Institute, Pittsburgh, PA, 2002.

G.M. Faeth, Invited Plenary Lecture, 8th AIAA/ASME Joint Thermophusics and Heat Transfer Conference, St. Louis, MO.

G.M. Faeth, Invited Plenary Lecture, ILASS-Europe, Zaragoza, Spain, 2002.

Participants:

K.T. Aung, Graduate Student Research Assistant, The University of Michigan, Ann Arbor, MI.

Z. Dai, Postdoctoral Research Fellow, The University of Michigan, Ann Arbor, MI.

A.M. El-Leathy, Postdoctoral Research Fellow, The University of Michigan, Ann Arbor, MI.

G.M. Faeth, A.B. Modine Professor, The University of Michigan, Ann Arbor, MI.

C.H. Kim, Graduate Student Research Assistant, The University of Michigan, Ann Arbor, MI.

S.S. Krishnan, Graduate Student Research Assistant, The University of Michigan, Ann Arbor, MI.

F. Xu, Postdoctoral Research Fellow, The University of Michigan, Ann Arbor, MI.

---

*For the period 1 October 1998-31 July 2003.

2. Shapes of Round Laminar Jet Diffusion Flames in Still Air

2.1 Introduction

In order to understand flow/soot-formation interactions it is necessary to understand the flame structure. Work toward this objective was begun with the simplest flow condition; namely, nonbuoyant round laminar jet diffusion flames with combustion of the fuel in still air. As noted earlier, diffusion flames are of interest because soot formation in practical flames is generally observed in nonpremixed (diffusion) flames. Laminar diffusion flames also merit study because understanding laminar flames is a necessary precursor to understanding turbulent and many aspect of laminar diffusion flames have direct relevance to turbulent diffusion flames through application of the laminar flamelet concept of turbulent diffusion flames [1,2].

Observation of nonbuoyant round laminar jet diffusion flames involving combustion of a fuel jet in still air were obtained at microgravity on board the orbiting Space Shuttle Columbia. The present study specifically considered the shapes (the luminous flame boundaries) of laminar diffusion flames, which is a flame property that has attracted numerous investigations since the classical study of Burke and Schumann [25]. A concern about observations of laminar diffusion flames at normal gravity, however, involves the intrusion of disturbances due to buoyancy because they are not relevant to practical diffusion flames, which generally are not significantly buoyant due to their large velocities. Thus, the present study exploited the long-term microgravity environment of an orbiting space shuttle. The present objectives were to document these observations and to employ simplified analysis of nonbuoyant laminar jet diffusion flames in order to help interpret and correlate the measurements.

Past measurements of the shapes of nonbuoyant laminar jet diffusion flames in still air have used either drop tower [26-35] or aircraft [36] facilities to provide low gravity environments. The earliest work along these lines was a series of studies of hydrocarbon fueled laminar jet diffusion flames using a 2.2s free-fall (drop tower) due to Cochran and coworkers [26-28]. Observations of transient development of flame length and questions about the relationships between the boundaries of soot luminosity and the flame sheet (where the local mixture fraction is stoichiometric), however, raised concerns about these results.

Subsequent studies due to Bahadori and coworkers [29-34] sought to resolve potential effects of transient flame development and soot luminosity on measurements of the shape of nonbuoyant round laminar jet diffusion flames using both 2.2 and 5.2s drop towers. Unfortunately, the temperature fields and the radiation emission properties of their flames were

still changing at the end of 5.2s free-fall periods for the conditions they considered, implying that transient effects had still not fully relaxed during the available microgravity test time.

Sunderland et al. [35] considered the luminous flame lengths of nonbuoyant soot-containing round laminar jet diffusion flames as part of a study of the laminar smoke point properties of nonbuoyant laminar diffusion flames using a KC-135 aircraft facility that provided roughly 20s at low gravity conditions. Unfortunately, the facility provided a disturbed low-gravity environment (with significant g-jitter) with the accompanying unsteady effects influencing both flame shapes and laminar smoke point properties [35].

More recently, Sunderland et al. [36] sought to avoid problems of both unsteadiness and soot luminosity by measuring the shapes of soot-free round laminar jet diffusion flames using the 2.2s drop-tower facility. Ambient pressures, jet exit diameters and fuel flow rates were controlled to provide soot-free (blue) flames having small characteristic flame residence times so that unsteady effects were potentially minimized. These tests for soot-free flames yielded shorter flame lengths than corresponding soot-containing flames but limited flame development times at microgravity conditions still introduced uncertainties about potential effects of transient flame development.

Several models of nonbuoyant round laminar jet diffusion flames in still environments, of varying complexity, have appeared in the literature [37-43]. Among these, the analysis of Spalding [39], (which is described in some detail by Kuo [40]) offers a potentially simple and robust method of estimating the shapes of steady nonbuoyant round laminar jet diffusion flames. Nevertheless, modifications of this approach to deal with soot-containing flames (as opposed to soot-free flames), the capabilities of this approach to treat all flame shape properties (as opposed to simply luminous flame lengths), and the performance of this approach for truly steady and nonbuoyant round laminar jet diffusion flames, are all issues that need to be addressed.

In view of these observations, the objectives of this phase of the investigation were to consider nonbuoyant round laminar jet diffusion flames in still air, as follows:

1. Measure the luminous flame boundaries for various fuel types, jet exit diameters, jet exit flow rates (Reynolds numbers) and ambient pressures.

2. Compare present measurements with earlier ground-based observations at similar burner conditions in order to quantify effects of transient flame development, flow disturbances (g-jitter), soot luminosity, and buoyancy on flame shape properties.

3. Exploit the measurements in order to evaluate the simple flame shape analysis of Spalding [39] and develop this approach to provide convenient correlations of flame shape measurements for use by others.

The present observations were limited to soot-containing ethylene- and propane-fueled flames burning in still dry air, at conditions near the laminar smoke point, with the test apparatus at microgravity conditions on board the orbiting Space Shuttle Columbia in order to provide truly steady and nonbuoyant flame conditions.

2.2 Experimental Methods

Experimental methods will only be briefly described, see Urban et al. [10] for more details. A sketch of the test apparatus appears in Fig. 1. The laminar jet diffusion flames were stabilized at the exit of round fuel nozzles injecting along the axis of a windowed test chamber (400 mm diameter and 700 mm length), denoted the Combustion Model (CM-1) test facility on board Space Shuttle Columbia during Space Shuttle flights STS-83 and 94. The chamber was filled with O2/N2 mixtures to provide the nominal composition of dry air (21 ± 1% O2 by volume) at pressures of 35-130 kPa. The properties of the air surrounding the flame changed only moderately as combustion proceeded (O2 consumption never exceeded 2% by volume). Fuel nozzles having exit diameters of 1.6 and 2.7 mm were considered, with the flames ignited by a retractable hot wire ignitor.

Several measurements were made to monitor flame operation: fuel flow rate, fuel temperature, chamber pressure, and chamber temperature. Flame shapes were obtained from a standard color CCD video camera operating at a rate of 30 images per second. Test conditions involved dry air, ambient temperatures and pressures of 300 K and 35-130 kPa, jet exit diameters of 1.6 and 2.7 mm, jet exit velocities of 170-1630 mm/s, jet exit Reynolds numbers of 46-172, and luminous flame lengths of 15-63 mm. See Table 2 for a summary of test conditions.

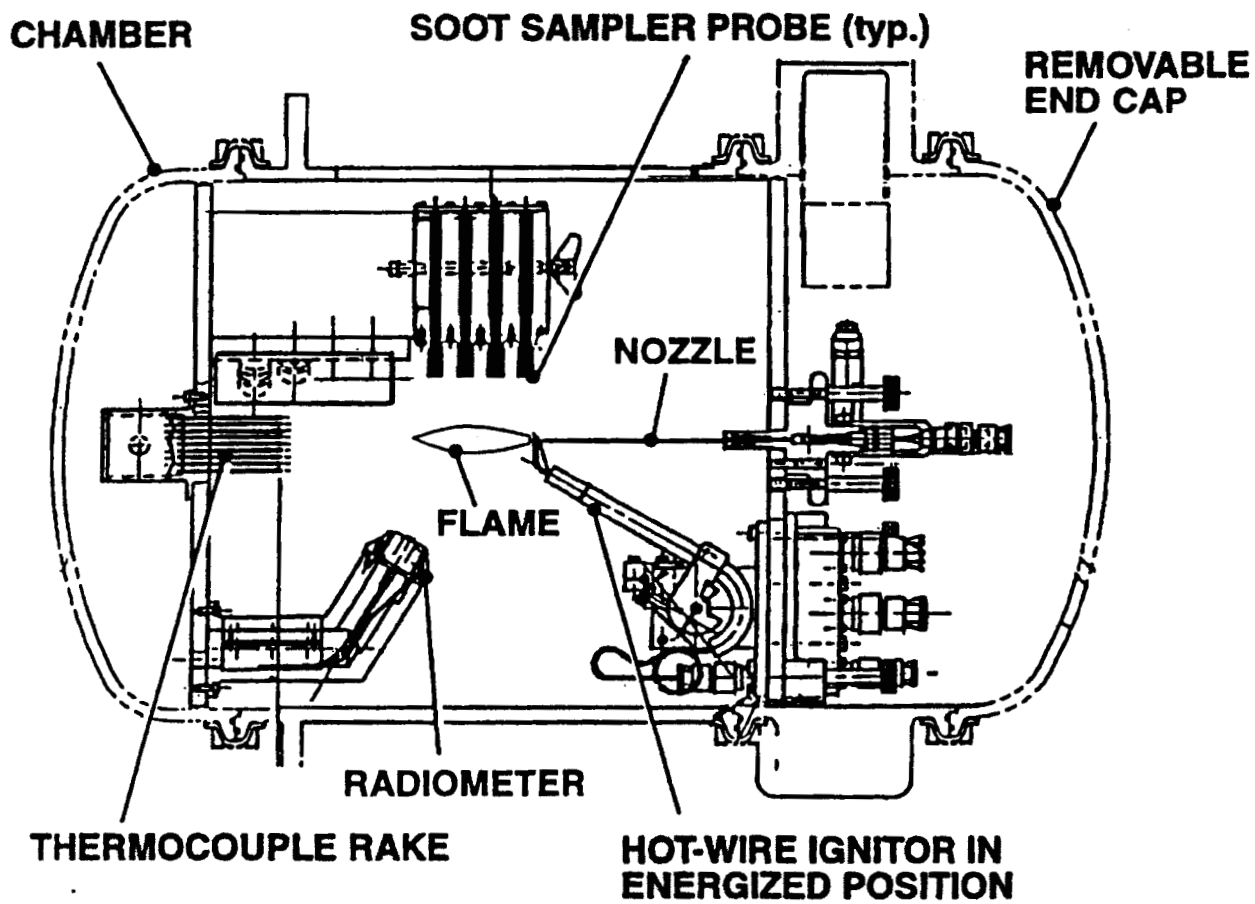

Figure 1. LSP test apparatus for observations of round laminar jet diffusion flames in still air. From Urban et al. (1998).

Table 2. Summary of space shuttle test conditions (STS-83 and 94)[a]

Test	p (kPa)	$\dot{m}$ (mg/s)	u_o (mm/s)	Test	p (kPa)	$\dot{m}$ mg/s)	u_o (mm/s)
C_2H_4 flames, d=66 mm:				C_2H_4 flames, d=2.7 mm:			
O1E*	100	1.84	820	O5E	65	1.14	270
O3E*	50	1.84	1630	O6E	80	1.16	230
O1E	100	0.71	320	O7E	100	1.08	170
O2E	50	0.76	670	O8E	50	1.38	430
O3E	50	1.29	1140	C_3H_8 flames, d=1.6 mm:			
O4E	65	0.91	620	O9P	130	0.78	170
14E	80	0.67	370	10P	50	1.82	1020
15E	100	0.61	270	11P	65	1.22	530
16E	65	0.74	510	12P	100	0.88	250
17E	35	1.34	1690	13P	80	1.04	370
				18P	80	0.82	290
				19P	100	0.71	200

[a]O1E* and O2E* were carried out on STS-83; all other tests were carried out on STS-94. All tests involved combustion in still air at 300 K. Z_{st} = 0.0636 and 0.0602 for ethylene and propane diffusion flames burning in air.

2.3 Theoretical Methods

The goal of the analysis was to find a set of easily used equations, along with recommendations for selecting physical properties appearing in the equations, to help interpret and correlate flame shape measurements. The basis of this approach was the simplified analysis of round nonbuoyant laminar jet diffusion flames in still environments due to Spalding [39]. The major assumptions of this analysis are as follows: (1) steady, axisymmetric laminar jet diffusion flames, (2) effects of buoyancy are negligible, (3) small Mach numbers, (4) large flame aspect ratio so that streamwise molecular transport is negligible, (5) solution of governing equations approximated by far field condition with effects of source disturbances small, (6) thin flame sheet, (7) equal diffusivities of all species, (8) all physical properties constant, and (9) effects of flame radiation are small. See Lin et al. [21] for justification of these assumptions.

Solution of the governing equations yields the following equations after introducing a virtual origin at a distance of L_o from the jet exit and an empirical coefficient, C_f, to treat effects of soot luminosity:

$$(L_f-L_o)/d = C_fC_nReSc/Z_{st} \tag{1}$$

where $C_n = 3/32$ for round laminar jet diffusion flames in a still environment. The corresponding expression for the luminous flame diameter becomes:

$$wZ_{st}/d = 3^{1/2}\zeta(\zeta^{-1/2} - 1)^{1/2} \tag{2}$$

where

$$\zeta = (z-L_o)/(L_f-L_o) \tag{3}$$

Transport properties affect Eqs. (1)-(3) through the Schmidt number and the viscosity used to compute the Reynolds number. It was found that a reasonable correlation of luminous flame lengths could be obtained by approximating these properties by the properties of air at the average of the adiabatic flame temperature and the ambient temperature. This approach seems reasonable because air-like gases dominate the composition of the present flames. The properties needed to find Sc and the mean air viscosity were taken from Braun et al. [44], however, $Sc \approx 0.76$ for present conditions which will be used in the following predictions.

2.4 Results and Discussion

Flame Appearance. Ignition conditions were established during ground-based tests at microgravity and involved fuel flow rates greater than values used during the flame tests. Thus, after ignition, fuel flow rates were reduced to conditions near but generally smaller than the laminar smoke fuel flow rates. Exceptions to this practice were tests 01E*, 03E* and 01E that were soot emitting. After the fuel flow rate was set, an additional 5-10s was required for disturbances to decay away. The flames were then observed during an 80-180s quasi-steady burning period where flame shapes and colors changed slowly due to modest variations of properties within the test chamber, see Urban et al. [10], for typical records of chamber gas properties as a function of time. Flame shape video records were obtained near the start of the quasi-steady burning period; therefore, the test conditions correspond to the nominal conditions summarized in Table 1. Typical flame images can be found in Urban et al. [10,23] and Lin et al. [21].

Typical of many past observations of soot-containing nonbuoyant laminar jet diffusion flames [30-36], present flame shapes could be grouped into closed-tip and open-tip configurations, with open tip configurations associated with near laminar smoke point conditions at large characteristic flame residence times. Such conditions cause radiative quenching at the flame tip which results in tip opening. Remarkably, however, tip opening did not have a major effect on flame shapes except very near the flame tip.

Flame Lengths. Measured and predicted luminous flame lengths of the present round nonbuoyant laminar jet diffusion flames are illustrated in Fig. 2. These results are plotted as suggested by Eq. (1). Results are shown for all the test conditions summarized in Table 2, with non-soot-emitting (non-sooting) and soot-emitting (sooting) flames denoted by closed and open symbols, respectively. Finally, plots of Eq. (1) for $L_o/d = -3.2$ and $C_f = 1.00$ (denoted theory) and the best-fit correlation of the present data at laminar smoke point conditions, $C_f = 1.13$ (denoted correlation) are also shown on Fig. 2 for comparison with the measurements. The comparison between measurements and predictions is remarkably good in view of the approximate nature of the theory. Finally, the predictions confirm a measured linear relationship between the fuel flow rate and flame length, for given burner conditions, and negligible effects of pressure on flame lengths. A surprising feature of these results, however, is that emission of soot, with corresponding tip opening, does not have a large effect on flame length compared to nonsooting laminar smoke point conditions.

Several additional experimental determinations of flame lengths are plotted along with the present measurements in Fig. 3. All these results involve laminar jet diffusion flames in still

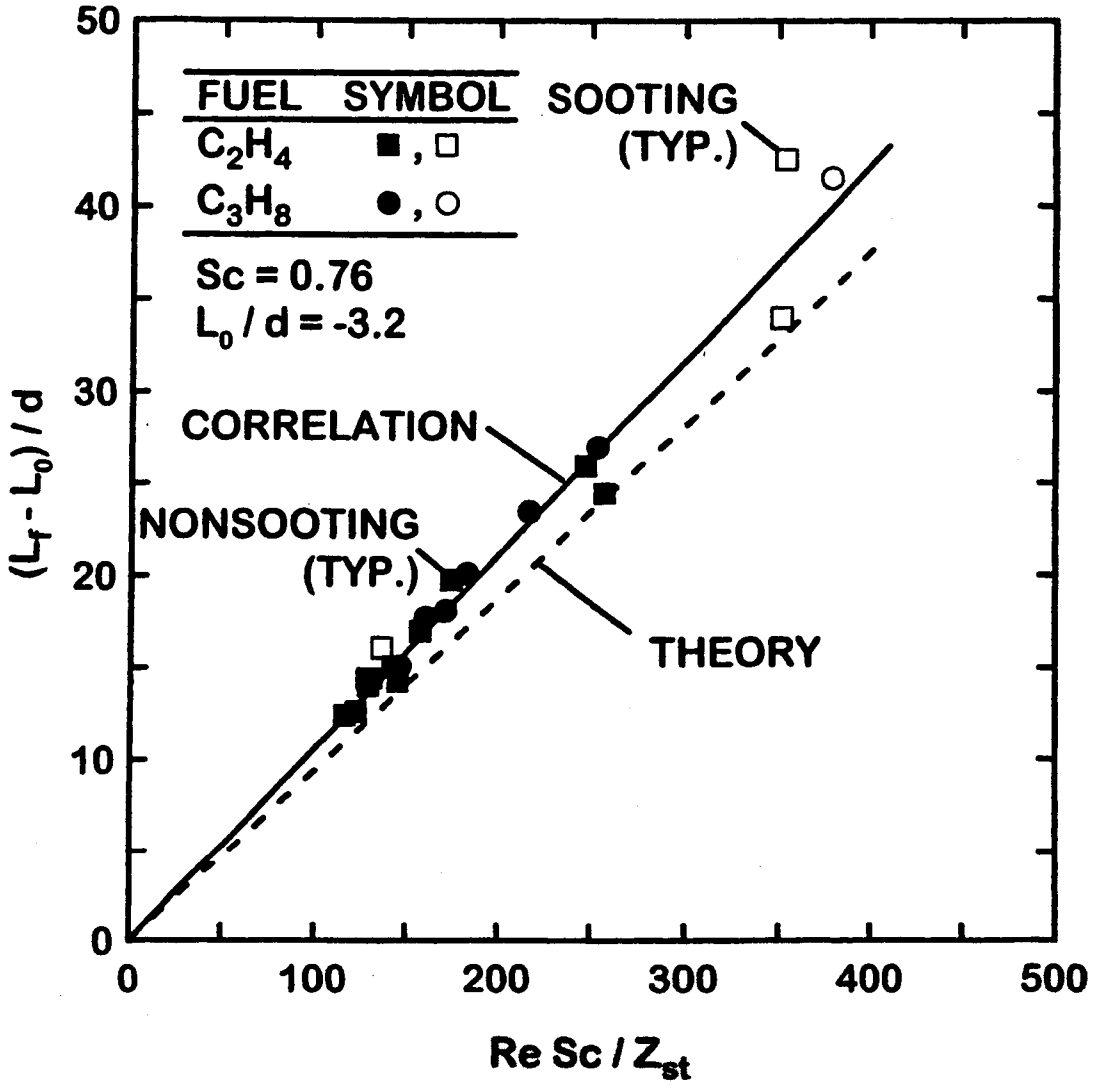

Figure 2. Measured and predicted luminous flame lengths of nonbuoyant hydrocarbon/air laminar jet diffusion flames in still air as a function of $ReSc/Z_{st}$. From Lin et al. (1999).

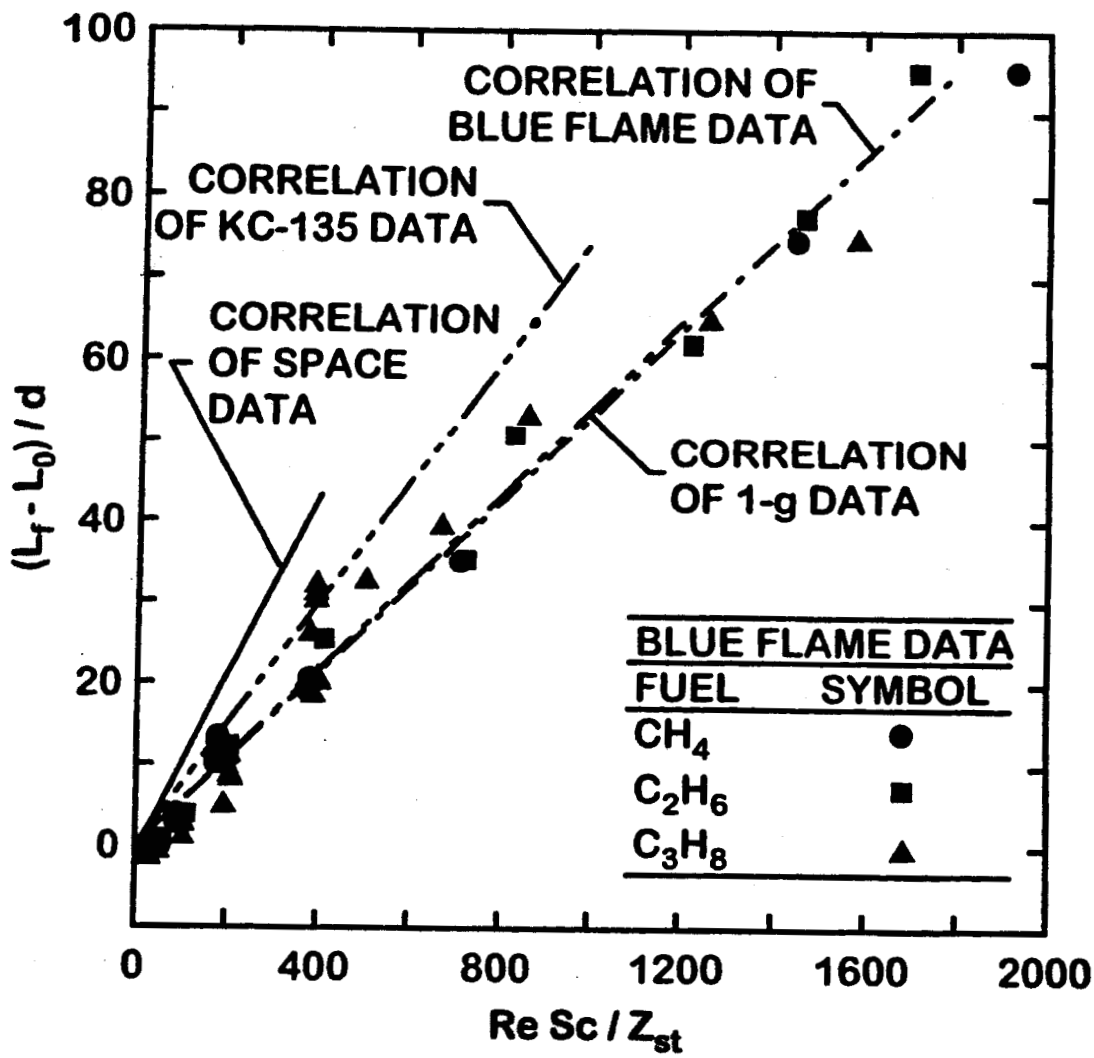

Figure 3. Measured and predicted luminous flame lengths of laminar jet diffusion flames in still air as a function of $ReSc/Z_{st}$: correlation of measurements of soot-free (blue) flames from Sunderland et al. (1998), correlation of measurements of KC-135 flames obtained from Sunderland et al. (1994), measurements (symbols) and correlation of normal gravity flames from Urban et al. (1998) and correlation of LSP flames. From Lin et al. (1999).

air. The results show that g-jitter for the KC-135 tests, lack of soot luminosity for the weakly buoyant (blue)flame data, and effects of buoyancy for soot-containing flames at normal gravity, appreciably shorten flame lengths for given values of $ReSc/Z_{st}$.

Comparisons of predicted and measured flame diameters appear in Lin et al. [21] and will not be reconsidered here. In general, measured and predicted maximum flame diameters were in reasonably good agreement. These results show that flame diameters are proportional to the jet exit diameter but independent of the burner flow rate, whereas, flame lengths are proportional to the burner flow rate but independent of the burner diameter; therefore, rather unusual long narrow laminar jet diffusion flames can be created using large fuel flow rates with small burner diameters.

Predicted and measured flame shapes were compared as a final step in the evaluation of the simplified Spalding [39] analysis of Eqs. (1)-(3). This comparison is shown in Fig. 4 for some typical closed-tip flames, with the radial position of the luminous flame boundary plotted directly as a function of streamwise distance. The agreement between measurements and predictions is seen to be excellent for Tests 03E and 16E. The comparison between measurements and predictions is not quite as good for Test 18P near the flame tip, however, because this flame tends toward open tip behavior. Similar problems are encountered for other open tip flames, see Lin et al. [21].

2.5 Conclusions

The major conclusions of the present study are as follows:

1. The present soot-containing luminous flames had larger luminous flame lengths than earlier ground-based observations: 40% larger than the luminous flame lengths of soot-containing nonbuoyant flames observed using an aircraft (KC-135) facility due to reduced effects of gravitational disturbances (g-jitter), roughly twice as large as the luminous flame lengths of soot-containing buoyant flames at normal gravity due to the absence of effects of buoyant mixing, and roughly twice as large as the luminous flame lengths of soot-free nonbuoyant flames observed by Sunderland et al. [35] using drop tower facilities due to the presence of soot luminosity and possible reduced effects of unsteadiness.

2. Similar to earlier observations of soot-containing nonbuoyant laminar jet diffusion flames [28-34], present luminous flame shapes could be grouped into closed-tip and opened-top configurations, which were observed for fuel flow rates smaller and larger than the laminar

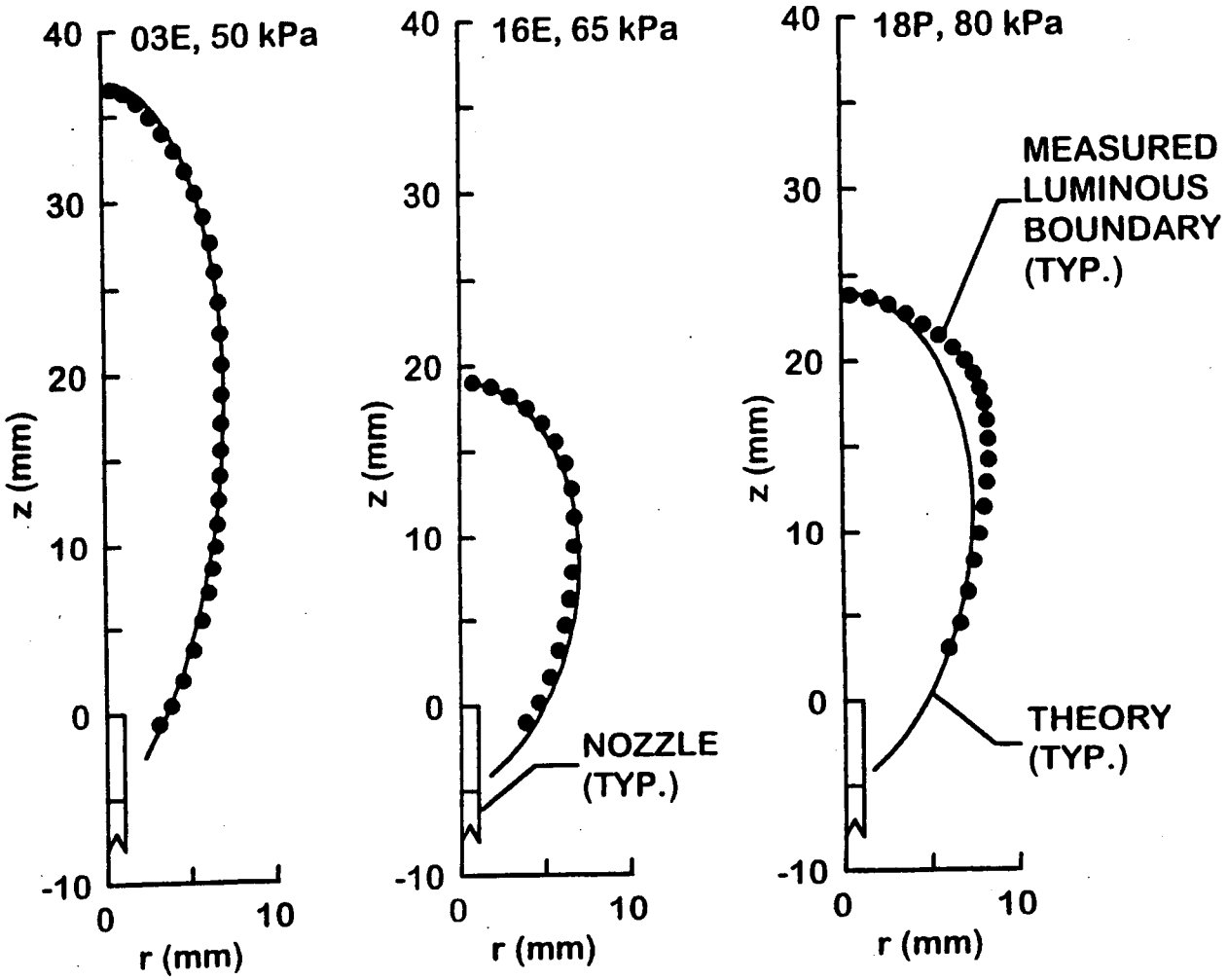

Figure 4. Measured and predicted luminous flame shapes for typical closed-tip nonbuoyant laminar jet diffusion flames in still air (Tests 03E, 16E and 18P). From Lin et al. (1999).

smoke point fuel flow rate, respectively. Blunt-tipped flames were also observed as fuel flow rates approached the tip-opening condition.

3. The simplified theoretical analysis of nonbuoyant laminar jet diffusion flames due to Spalding [39] yielded excellent correlations of the luminous flame shapes of closed-tip soot-containing and soot-free flames upon adjusting an empirical flame length parameter to account for the fact that flame luminosity ends at the location of soot consumption and at the location of the stoichiometric flame sheet along the axis of soot-containing and soot-free flames, respectively. Nevertheless, the slopes of the flame length correlations in Fig. 3 differed by roughly a factor of 2 for nonbuoyant soot-free (blue) and soot-containing (near the laminar smoke point limit) flames. This difference is consistent, however, with the ratios between luminous flame lengths and stoichiometric lengths for soot-containing flames reported previously [36].

4. Remarkably, the simplified theoretical analysis of nonbuoyant laminar jet diffusion flames due to Spalding [39] fortuitously still yields reasonably good predictions of luminous flame shapes for soot-containing nonbuoyant opened-tip flames as well as for conventional buoyant flames, after appropriate selections of empirical flame length parameters. Thus, taken together, the simple formulation of Eqs. (1)-(3) exhibits encouraging potential to correlate the luminous flame boundaries of laminar jet diffusion flames that should be useful for designing imaging systems for nonintrusive measurements of flame properties.

5. Based on the present correlations of luminous flame boundaries for nonbuoyant laminar jet diffusion flames, luminous flame lengths increase linearly with fuel flow rate but are relatively independent of jet exit diameter and pressure, whereas maximum luminous flame diameters increase linearly with jet exit diameter but are relatively independent of fuel flow rate and pressure. Both dimensions, however, are proportional to the stoichiometric mixture fraction, although this parameter was not varied sufficiently during the present experiments to test predictions of this trend.

3. Shapes of Round Laminar Jet Diffusion Flames in Coflowing Air

3.1 Introduction

The objective of this phase of the investigation was to extend the results just discussed in Section 2 to consider nonbuoyant round laminar jet diffusion flames in coflowing air. This work was prompted by the widespread use of this configuration to study the structure and soot formation processes of laminar diffusion flames, see Refs. 6-9 and references cited therein. Similar to the approach used in Section 2 for flames in still air, a way to correlate flame shape was sought, convenient for use by others, based on simplified analysis of nonbuoyant round laminar coflowing jet diffusion flames.

Even though the classical study of Burke and Schumann [28] addressed the shapes of laminar coflowing jet diffusion flames (for the limiting conditions where initial fuel and oxidant velocities were the same and the flow was in a bounded duct) there has been relatively little subsequent consideration of this problem. Exceptions include the theoretical studies of Williams [45] and Mahalingam et al. [46], which extended the Burke and Schumann [28] analysis to treat flames where the outer coflowing stream was unbounded. During this phase of the present investigation, the simple self-similar analysis of Mahalingam et al. [46] was further developed to provide a theoretical basis for correlating the shapes of nonbuoyant round laminar jet diffusion flames in coflowing air, analogous to the use of the simplified analysis of Spalding [29] to provide a theoretical basis for correlating the shape of nonbuoyant round laminar jet diffusion flames in still air by Lin et al. [21].

Based on the previous observations, the objectives of this portion of the investigation were to consider the shape properties of nonbuoyant round laminar jet diffusion flames in coflowing air, as follows:

1. Measure the lengths, diameters and shapes of the flames for various fuel types, coflow velocities, jet exit flow rates and ambient pressures.

2. Compare present measurements with earlier findings for similar flames in still air, e.g., the flames observed by Lin et al. [21], to help quantify effects of coflow on flame-shape properties.

3. Exploit the new measurements to develop a correlation for the shapes of laminar jet diffusion flames in coflowing air, convenient for use by others, analogous to the approach of Lin et al. [21] for laminar jet diffusion flames in still air.

The present observations were limited to weakly-buoyant soot-containing acetylene-, propylene- and 1,3 butadient-fueled laminar jet diffusion flames in coflowing air. Similar to Lin et al. [21], present measurements were limited to conditions near the laminar smoke point except for some preliminary observations to study the effect of the approach to the laminar smoke point on flame shapes.

3.2 Experimental Methods

Experimental methods will only be briefly described, see Lin and Faeth [20] for more details. Effects of buoyancy were controlled based on the observation that the governing equations for laminar coflowing jet diffusion flames scale with pressure to yield an effective gravitational acceleration, $g_e = p^2 g$, with p in atm [47]. Thus, flames at pressures on the order of 0.1 atm have effective gravitational accelerations on the order of 0.01 g, and exhibit relatively weak effects of buoyancy for typical burner exit and coflow velocities.

A sketch of the test apparatus appears in Fig. 5. The burner was a coaxial tube arrangement with fuel flowing from an inner port (6 mm in diameter) and air flowing from an outer port (60 mm in diameter). The burner operated at low pressures within a windowed chamber. Fuel and air were supplied from metered sources whereas combustion products were removed using the laboratory vacuum system. The flames were ignited by a hot wire that could be manually moved out of the flow field once the flames were stabilized. The air coflow velocity remained constant at jet exit conditions for the region where flames were present, providing a constant velocity ambient air flow.

Several measurements were made to monitor flame operation: fuel flow rate, air coflow rate, chamber pressure and fuel and air supply temperatures. Dark field photographs of the flames were obtained using a 35 mm reflex camera. The problem of acetone contaminating acetylene in cylinders, noted by Hamins et al. [48], was small compared to experimental uncertainties of flame shapes. Test conditions varied for the three fuels that were considered and are summarized in Table 3.

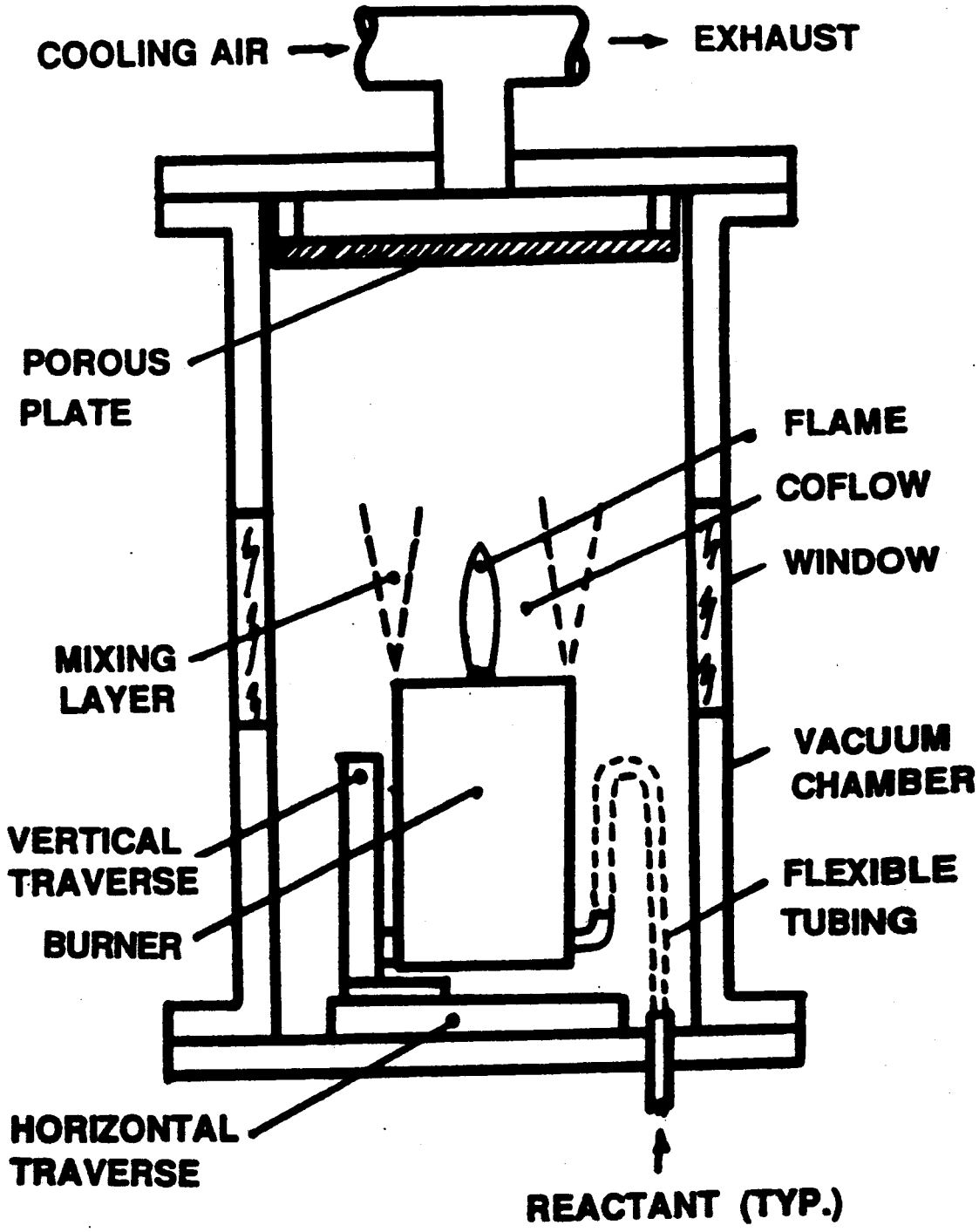

Figure 5. Test apparatus of observations of laminar jet diffusion flames in coflowing air. From Lin and Faeth (1996).

Table 3. Summary of coflowing jet diffusion flame tests[a]

Parameter	Acetylene	Propylene	1,3 Butadiene
Fuel flow rate, mg/s	0.94-5.90	1.53-4.08	0.74-2.71
Re (-)[b]	19-121	38-101	18-66
$u_{a,o}/u_{,f,o}$ (-)	0.22-12.03	0.29-6.99	0.77-32.45
Z_{st} (-)	0.0704	0.0636	0.0667

[a]Reactant temperatures of roughly 300 K with ambient pressures of 19-50 kPa.
[b]Based on jet exit properties, see Lin and Faeth [20] for properties used.

3.3 Theoretical Methods

The assumptions for analysis of nonbuoyant round laminar jet diffusion flames in coflow were the same as those used by Lin et al. [21] for flames in still air, except for the obvious change of coflow velocity. In addition, the streamwise velocity defect

$$u_d = u_{a,o} - u \tag{4}$$

was assumed to be small, similar to the approximate analysis of wakes due to Schlichting [49]. See Lin et al. [20] for justification of all the assumptions and the details of the analysis.

Solution of the governing equations yields the following equations after introducing a virtual origin, etc., similar to the analysis of flames in still air. The luminous flame length becomes

$$(L_f - L_o)/d = C_f C_n ReSc/Z_{st} \tag{5}$$

where $C_n = 1/16$ for round laminar jet diffusion flames in a coflowing environment. The corresponding expression for the luminous flame diameter becomes:

$$w/d = (-\zeta(u_{f,o}/u_{a,o})\ln[\zeta]/Z_{st})^{1/2} \quad (6)$$

where

$$\zeta = (x-L_o)/(L_f-L_o) \quad (7)$$

Transport properties in these equations were found in the same manner as results given by Eqs. (1)-(3) for flames in a still environment. Remarkably, flame length is independent of coflow velocity and is 2/3 as long as flames in still environments at the same fuel port exit condition. For flames in coflow, however, flame diameter decreases as $u_{f,o}/u_{a,o}$ decreases. The present analysis also agrees with Mahalingam et al. [46] at the limiting condition where $u_{f,o} = u_{a,o}$.

Finally, a convenient measure of the flame diameter is its value at $x/L_f = 1/2$, as follows:

$$w_{1/2}/d = [(u_{f,o}/u_{a,o})\ln[2]/(2Z_{st})]^{1/2} \quad (8)$$

3.4 Results and Discussion

Flame Appearance. The present flames were operated steadily so that transient effects were not an issue. Test chamber pressures were kept small enough so that effects of buoyancy were negligible as well. Finally, present results were limited to conditions at the laminar smoke point, similar to conditions considered in Section 2 for flames in still air. In the present case, however, no open tip flames were observed because the large coflow velocities insured relatively small characteristic residence times and thus correspondingly small radiative heat losses and tendencies for quenching at the flame tip.

Flame Lengths. Measured and predicted lengths of flames in coflowing and still air are plotted in Fig. 6. Present measurements have been divided into two groups, as follows: (1) $u_{f,o}/u_{a,o} < 0.5$, which roughly approximates nonbuoyant flames in still air; and (2) $u_{a,o}/u_{f,o} > 1$ for $Fr_a > 0.1$, which roughly approximates nonbuoyant flames in coflowing air. All of the measurements are plotted as suggested by Eqs. (1) and (5). The correlation of flame lengths in still gases according to the Spalding [39] analysis has already been discussed in Section 2. The results illustrated in Fig. 6 for flames in still gases at near laminar smoke point conditions yield an excellent correlation with $C_f = 1.13$, as before. As noted earlier, these luminous flame lengths for near laminar smoke point conditions are roughly twice as long as the measurements of Sunderland et al. [35] for soot-free (blue) flames which correlate with $C_f = 0.56$. Present results for coflow with $u_{a,o}/u_{f,o} > 1$ also yield a good correlation according to the simplified theory of Eq.

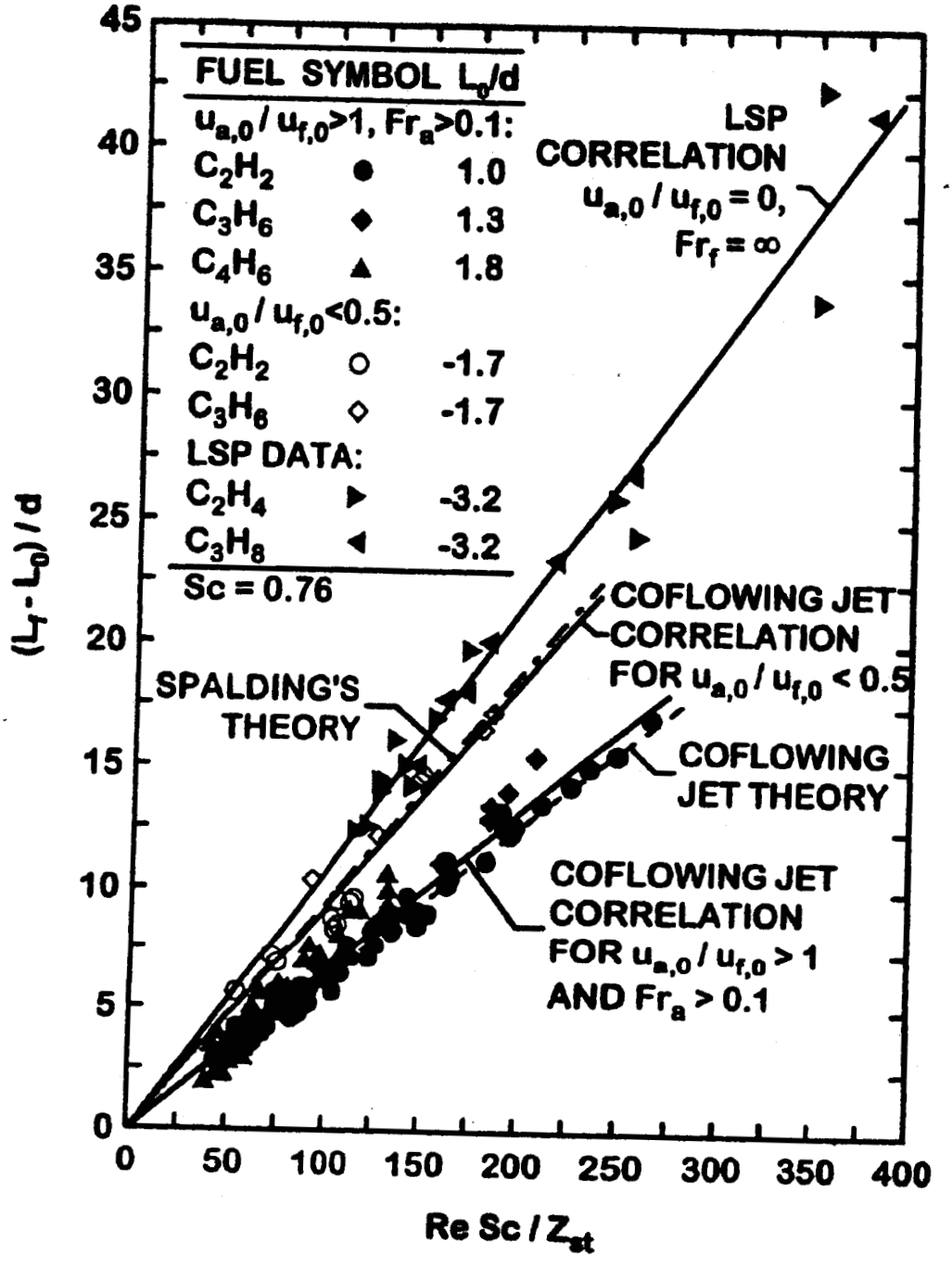

Figure 6. Luminous flame lengths of hydrocarbon-fueled laminar jet diffusion flames burning in coflowing air: correlation of measurements of Lin et al. (1999) for $u_{a,o}/u_{f,o}=0$, predictions of Spalding's (1979) theory for $u_{a,o}/u_{f,o}=0$, correlation and measurements of Lin and Faeth (1999) for $0.22 \leq u_{a,o}/u_{f,o}=0.5$, and correlation and measurementsof Lin and Faeth (1999) for $u_{a,o}/u_{f,o} \geq 1$ and $Fr_a > 0.1$. From Lin and Faeth (1999).

(5) with $C_f = 1.05$, roughly equal to the value of C_f for flames at the laminar smoke point in still air.

Flame Diameters. Flame diameters halfway along the flame length are plotted according to Eq. (8) in Fig. 7. The scatter about the prediction progressively decreases as the normalized flame length increases; therefore, small flame aspect ratios appear to be mainly responsible for the scatter seen in Fig. 7. The agreement between measurements and predictions at large aspect ratios, however, is reasonably good.

Flame Shapes. The comparison between measured and predicted flame shapes was carried out for flames having relatively large aspect ratios to reduce problems of flame diameter predictions at small aspect ratios seen in Fig. 7. Typical results for acetylene- , propylene- and 1,3 butadiene-fueled flames at similar Reynolds numbers (Re of 62-66) and air/fuel velocity ratios ($u_{a,o}/u_{f,o}$ of 3.3-4.2) are illustrated in Fig. 8. The predictions are quite good in the far field but they break down near the jet exit where the far-field approximation is not very satisfactory.

Effects of air/fuel velocity ratios and Reynolds numbers on predictions of flame shape in coflow are illustrated in Fig. 9. The approximate analysis is seen to provide good predictions of trends with respect to air/fuel velocity ratios and Reynolds numbers in the far field. Predictions near the source, however, are not very satisfactory due to failure of the far-field approximations.

Finally, Xu et al. [24] undertook measurements of the luminous flame boundaries of steady, weakly-buoyant round hydrocarbon-fueled laminar jet diffusion flames in still and coflowing air, using optical filters to find the flame sheet in soot-containing flames. These results indicated good predictions of flame sheet shapes, and thus the boundaries of soot-free (blue) flames. Finally, luminous flame lengths at laminar smoke-point conditions were roughly twice as long as at the flame sheet, yielding $C_f \approx 1.$ and 0.5 at laminar smoke-point and soot-free (blue or flame sheet) flame conditions, in both still and coflowing environments.

3.5 Conclusions

The major conclusions of this phase of the present study are as follows:

1. The present extension of the simplified analysis of nonbuoyant round laminar jet diffusion flames in coflow due to Mahalingam et al. [46] provided reasonably good predictions of the luminous shapes of the present flames in the far field for $u_{a,o}/u_{f,o} > 1$ and $Fr_a > 0.1$ after appropriate selections of empirical flame-length parameters, e.g., L_o/d and C_f. The

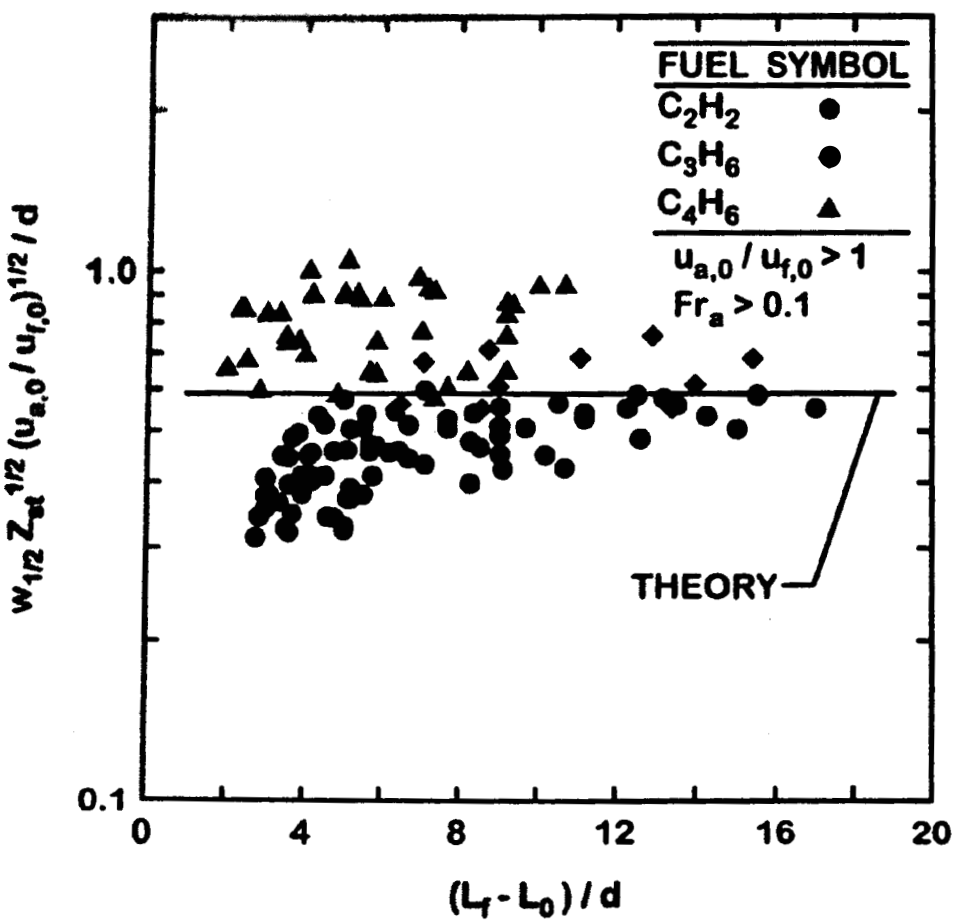

Figure 7. Measured and predicted luminous flame diameters of hydrocarbon-fueled laminar jet diffusion flames burning in coflowing air at various velocity ratios for $u_{a,o}/u_{f,o} > 1$ and $Fr_a > 0.1$. From Lin and Faeth (1999).

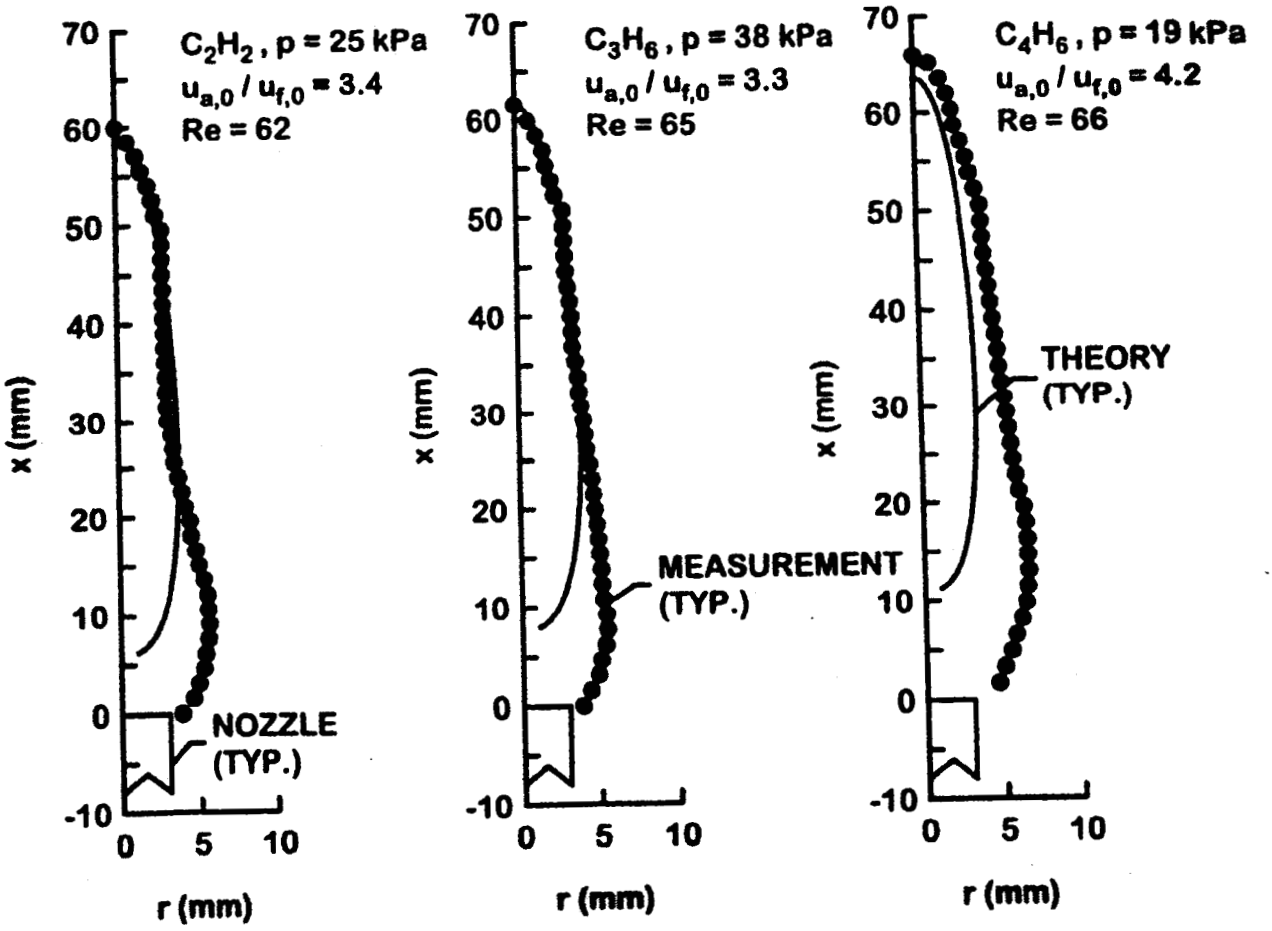

Figure 8. Measured and predicted luminous flame shapes for acetylene-, propylene- and 1,3 butadiene-fueled laminar jet diffusion flames burning in coflowing air. From Lin and Faeth (1999).

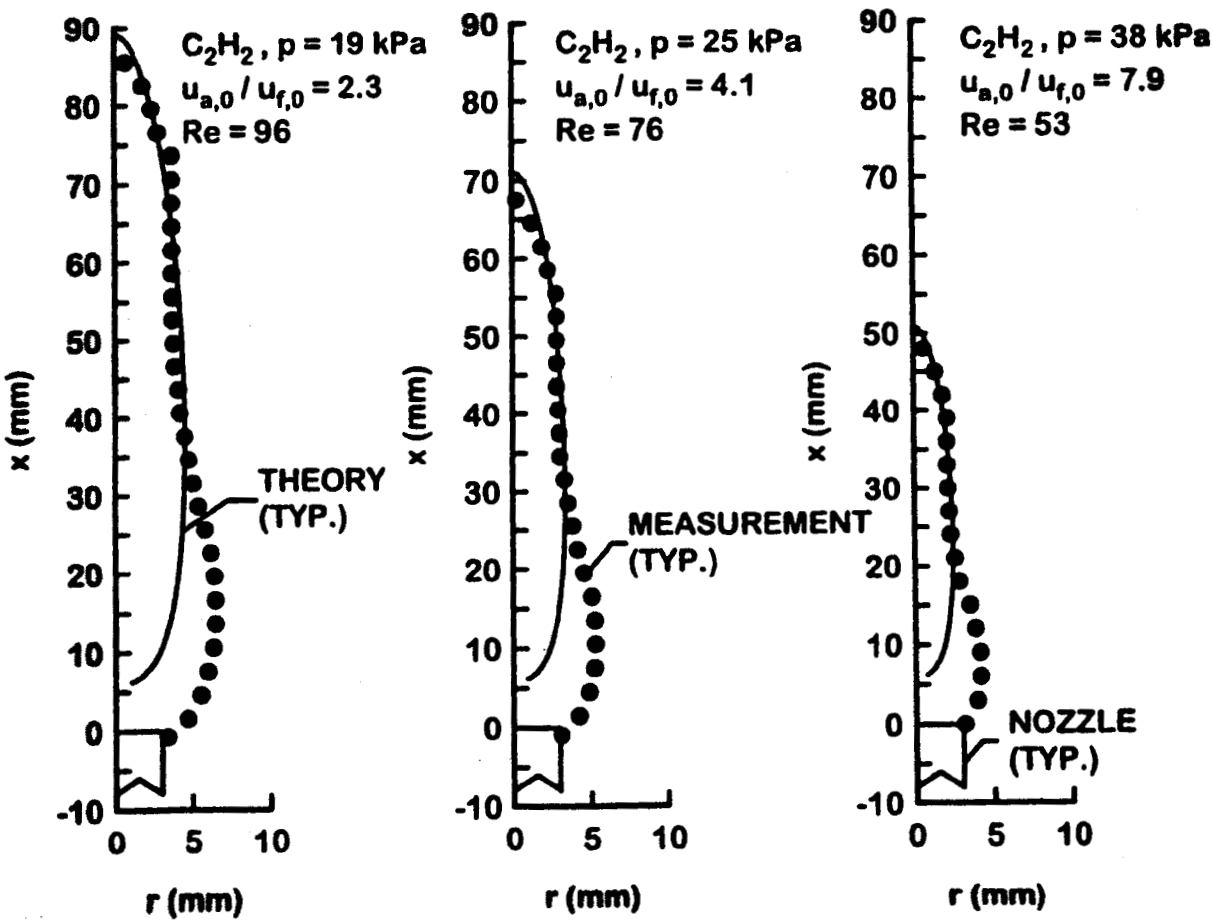

Figure 9. Measured and predicted luminous flame shapes for acetylene-fueled laminar jet diffusion flames burning in coflowing air at various fuel jet and coflow conditions. From Lin and Faeth (1999).

predictions were most satisfactory for large aspect ratio flames and tended to fail near the source where the far-field approximations used in the analysis were no longer valid.

2. The simplified analysis of nonbuoyant laminar jet diffusion flames in still air due to Spalding [39] developed by Lin et al. [21] provided reasonably good predictions of the luminous shapes of the present flames in slow-moving coflow for $0.22 \leq u_{a,o}/u_{f,o} < 0.5$ after appropriate selections of empirical flame-length parameters, e.g., L_o/d and C_f. Present values of the flame lengths (or C_f) for slow coflow ($u_{a,o}/u_{f,o} < 0.5$) were 15% smaller than the earlier results of Lin et al. [21] with no coflow because of enhanced mixing rates caused by coflow.

3. Based on present correlations of the luminous flame boundaries of nonbuoyant laminar jet diffusion flames in still and coflowing air, luminous flame lengths increase linearly with fuel flow rates but are relatively independent of jet-exit diameter, pressure, and air/fuel velocity ratio (for flames in coflow). Nevertheless, flames in still air are roughly 50% longer than flames in significant coflow ($u_{a,o}/u_{f,o} > 1$) at comparable conditions, with this difference being relatively independent of air/fuel velocity ratio and jet-exit Reynolds number.

4. Based on present correlations of the luminous flame boundaries of nonbuoyant laminar jet diffusion flames in still and coflowing air, characteristic luminous flame diameters vary linearly with jet exit diameter and are relatively independent of flow physical properties and jet exit Reynolds numbers. For flames having significant levels of coflow ($u_{a,o}/u_{f,o} > 1$), however, characteristic luminous flame diameters are also inversely proportional to the square root of $u_{a,o}/u_{f,o}$. Thus, large aspect ratio flames can best be achieved using small injector diameters, large injector Reynolds numbers, and large air/fuel velocity ratios, subject to laminar smoke-point limitations if nonsooting flames are desired.

5. Progressive increases of luminous flame lengths at comparable conditions were observed in the laminar smoke point was approached for nonbuoyant laminar jet diffusion flames in coflowing air. This behavior was similar to the observations of Lin et al. [21] that the luminous lengths of nonbuoyant laminar jet diffusion flames in still air were roughly twice as long at near laminar smoke-point conditions as in soot-free (blue) flames at comparable conditions.

4. Hydrodynamic Suppression of Soot Formation in Laminar Diffusion Flames

4.1 Introduction

Given background concerning the structure of laminar diffusion flames, the objective of this third phase of the research was to investigate flow/soot-formation interactions in nonbuoyant laminar diffusion flames. As noted earlier, this involved a direct evaluation of effects of velocities normal to the flame sheet on soot formation in diffusion flames by considering pure air and fuel reactant streams for nonbuoyant laminar coflowing jet diffusion flames. In this configuration, enhanced (retarded) airstream velocities provide entrainment velocities normal to the flame sheet directed from the fuel-rich (fuel-lean) to the fuel-lean (fuel-rich) sides of the flame sheet, which should reduce (increase) both soot concentrations within the flame and the tendency to emit soot from the flame. This behavior has been observed by Lin and Faeth [15] where retarded fuel-stream velocities compared to air-stream velocities caused increased laminar smoke point flame lengths and fuel flow rates for weakly-buoyant laminar coflowing jet diffusion flames at low pressures. This effect became difficult to observe as the pressure was increased toward atmospheric pressure, which caused the effective gravitational acceleration, $g_e = p^2 g$, to increase so that the intrusion of buoyancy reduced the effect of initially retarded fuel-stream velocities. This is probably the main reason why the importance of retarded fuel stream velocities for reducing soot formation in flames has not been recognized earlier.

Based on the results concerning the structure of nonbuoyant buoyant laminar coflowing jet diffusion flames discussed in Section 3 of this report, another rather transparent explanation of the effect of retarded fuel stream velocities can be obtained for this particular flame configuration. In particular, the simplified analysis leading to Eq. (5) for the flame length indicates that flame length is independent of the coflow velocity since this expression is very similar to Eq. (1) for the flame length in a still environment (except for the fact that flame lengths in coflow are only 2/3 as long as in still environments for given fuel-jet exit conditions). On the other hand, the characteristic residence time within the flame, for conditions where the flame aspect ratio is large and u_d is small for most of the flame length, is given by:

$$\tau_r = (L_f - L_o)/u_{a,o} = C_f C_n \mathrm{ReScd}/(Z_{st} u_{a,o}) \qquad (9)$$

Based on Eq. (9), for given values of C_f, C_n, Re_e, Sc, d and Z_{st}, it is evident that τ_r decreases inversely proportional to $u_{a,o}$. Put another way, the residence time for soot formation progressively decreases as $u_{a,o}$ increases (or as the fuel stream velocity becomes increasingly retarded), decreasing the extent of soot formation before soot oxidation conditions are reached, and thus the potential for soot emissions.

Prompted by these observations the present phase of the investigation considered effects of enhanced airstream velocities on laminar soot-point properties — that is on the condition where soot is first observed in laminar diffusion flames. Associated properties, such as luminous flame length and flame liftoff conditions were also observed. Experimental methods were similar to the weakly-buoyant laminar coflowing jet diffusion flames discussed in Section 3, where observations of flames at low pressures were used to minimize the intrusion of effects of buoyancy on initial air-stream/fuel-stream velocity ratios. The present discussion is brief, see Lin and Faeth [15] and Dai and Faeth [22] for more details.

4.2 Experimental Methods

As noted earlier, measurements were carried out at subatmospheric pressures to control effects of buoyancy as discussed by Law and Faeth [47]. The arrangement of the burner was similar to that discussed in Section 3 and illustrated in Fig. 5. The test burner was a vertical coaxial arrangement with fuel flowing from an inner port having inside diameters of 1.7, 3.2 and 6.4 mm and air flowing from an outer port having an inside diameter of 60 mm. The burner was operated within a windowed chamber at reduced pressures with flame ignition and monitoring instrumentation the same as discussed in Section 3.

Acetylene-, ethylene-, propane- and methane-fueled laminar jet diffusion flames in coflowing air were considered. Test conditions included reactant temperatures of roughly 300 K, ambient pressures of 3.7-40.8 kPa, fuel jet exit Reynolds number of 18-121, air coflow velocities of 0-6 m/s, and air/fuel-stream velocity ratios of 0.003-70. Transition to turbulent flames was never observed during the present experiments, whereas characteristic flame residence times were small so that effects of radiative heat losses from the flames were negligible.

4.3 Results and Discussion

Flame Appearance. Color photographs of the flames revealed the presence of soot by the appearance of yellow soot luminosity. As conditions for reduced formation of soot were approached, by increasing air coflow velocities or decreasing the pressure, the yellow soot-containing region became smaller and more confined near the flame tip. The laminar soot-point of the flame, defined as the condition where soot particles first appear in the flame, was then identified as the condition where yellow soot luminosity first appears near the tip of the flame.

Flame Lengths. Similar to the observations of luminous flame lengths at laminar smoke points by Schug et al. [7] and Lin and Faeth [15], the present luminous flame lengths at laminar

smoke points were closely associated with the fuel flow rate. Measurements establishing this behavior and a brief discussion of the simplified theory that helps explain the experimental findings are considered in the following.

Laminar soot- and smoke-point luminous flame lengths are plotted in Fig. 10 as a function of a corrected fuel flow rate suggested by simplified theories of flame shapes for nonbuoyant and laminar jet diffusion flames in still and coflowing gases [22,23] developed in Sections 2 and 3 of this report. The measured laminar smoke point correlations are from Lin and Faeth [15] for acetylene-, propylene- and 1,3 butadiene-fueled flames burning in air at pressures of 19-51 kPa, a burner diameter of 6 mm, and air/fuel-stream velocity ratios of 0.4-6.7. Two sets of correlations (each) are illustrated for the laminar soot- and smoke-point luminous flame lengths in Fig. 10, one for small u_a/u_f (for the following discussion let $u_a/u_f = u_{a,o}/u_{f,o}$)based on analysis of laminar jet diffusion flames in still air, and one for large u_a/u_f based on analysis of laminar jet diffusion flames in coflowing air. There are good correlations between measured luminous flame lengths and the corrected fuel flow rates for both laminar soot- and smoke-point conditions (see Ref. [21] for the latter). As a result, laminar soot-point properties are represented by the laminar soot-point fuel flow rate in the following, similar to past work [15]. It is also evident that the correlation for laminar smoke-point flame lengths is roughly twice as long as that for laminar soot-point flame lengths at both large and small u_a/u_f limits.

An explanation of the flame length behavior observed in Fig. 10 can be obtained from the flame shape correlations of Eqs. (1) and (5). Simple correlations of these expressions were fitted to the measurements illustrated in Fig. 10, taking $C_n = 3/32$ and 1/16 for nonbuoyant flames in still and coflowing gases, and $C_f \approx 1.0$ and 0.5 for flames at laminar soot- and smoke-point conditions, with the latter expression being suitable for soot-free blue flames at fuel flow rates smaller than the soot-point (unless the flame aspect ratio becomes small).

Laminar Soot-Point Properties. Both laminar soot-point and liftoff properties were measured during the present experiments. The tests were conducted by varying the pressure range for each fuel based on its propensity to soot, so that effects of reasonable variations of air/fuel-stream velocity ratios could be measured for flames fueled with each fuel in spite of limitations due to effects of liftoff and the intrusion of buoyancy.

In the following, effects of air coflow on laminar soot-point and liftoff properties are presented as plots of laminar soot-point fuel flow rates as a function of air coflow velocities because this approach provides a compact presentation of the measurements. Effects of air coflow velocities on laminar soot-point fuel flow rates were qualitatively similar for the four fuels that were considered. This can be seen from the plots of fuel mass flow rate at soot-point

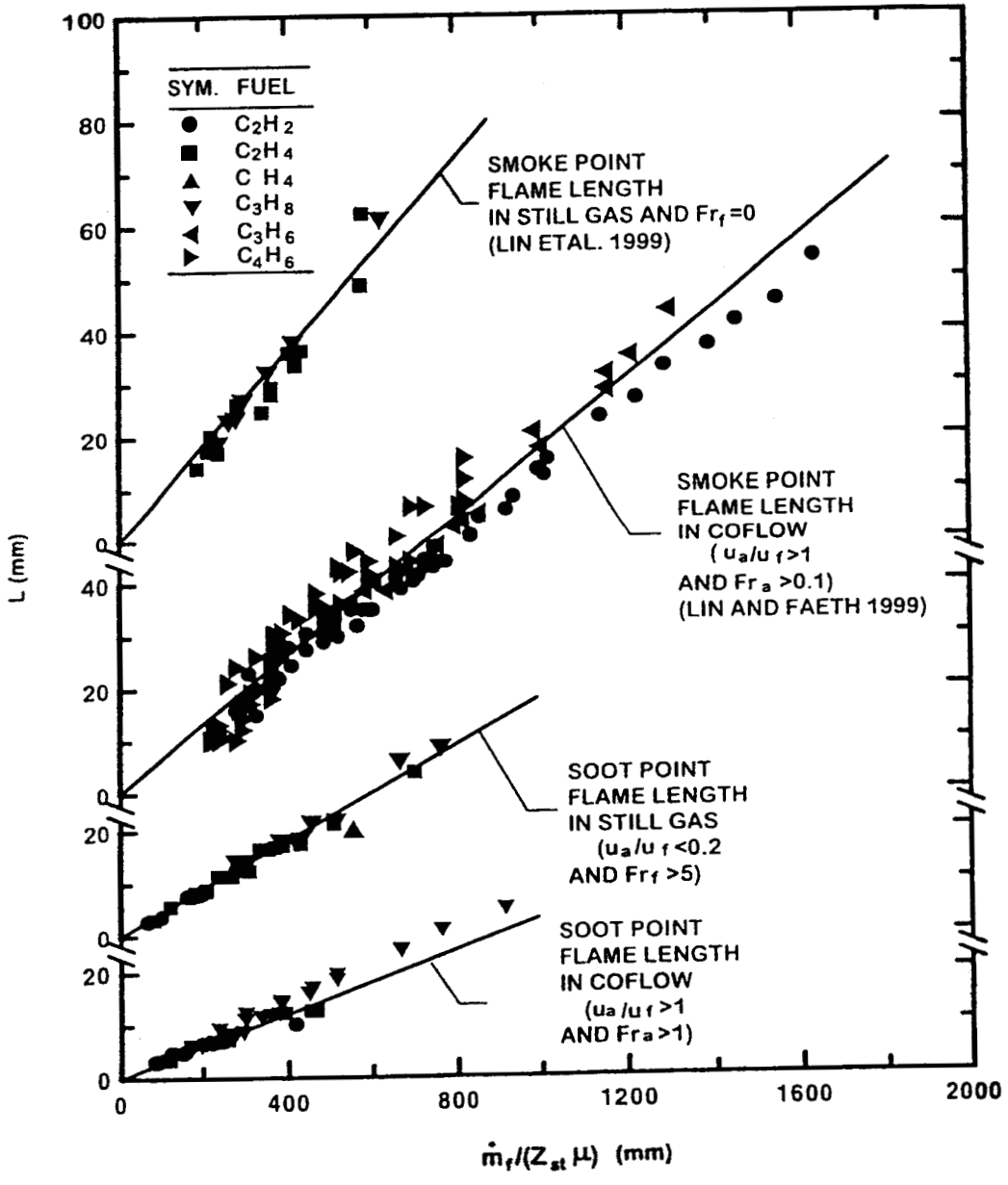

Figure 10. Correlations between laminar soot- and smoke-point flame lengths and corrected fuel flow rates for laminar coflowing jet diffusion flames fueled with acetylene, ethylene, methane, propane, propylene and 1,3 butadiene, burning in air based on the simplified flame shape analyses of Lin et al. [21] and Lin and Faeth [20]. Laminar smoke-point flame length correlations are also from these references. From Dai and Faeth (2000).

conditions as a function of air coflow velocities for the various pressures and fuel port diameters that are illustrated in Figs. 11 and 12 for acetylene/air and propane/air flames, as examples. To indicate the transition between soot formation and soot-formation/oxidation configurations at the base of the test flames, the conditions of $u_a/u_f = 1$ is denoted by reverse-shaded symbols on the plots. Liftoff conditions are denoted by the symbol at the highest air flow rate for each pressure and fuel port diameter, with the extreme liftoff limit denoted by a dashed line.

The measurements illustrated in Figs. 11 and 12 show that increased air coflow velocities increase laminar soot point fuel rates. Notably, this behavior is observed for air/fuel-stream velocity ratios both smaller and larger than unity. Increasing pressures generally reduce allowable fuel mass flow rates and flame lengths for soot free flames due to increased soot formation rates and flame residence times for a given flame length. The relative enhancement of laminar soot point fuel flow rates between small and maximum allowable values of air coflow velocities before liftoff, however, tends to be relatively independent of the pressure for a particular fuel. This behavior comes about because generally more intense reaction rates at elevated pressures accommodate large air coflow velocities before liftoff, which tends to compensate for faster soot reaction rates at elevated pressures. Taken together, it is clear that sufficiently large air coflow velocities are capable of completely suppressing the formation of particulate soot for these conditions, supporting the soot suppression argument discussed in the introduction. The resulting soot free flames also provide potentially useful conditions for evaluating detailed models of diffusion flame chemistry and transport at the computationally tractable limit of soot-free laminar diffusion flames for light hydrocarbons.

Finally, note that the effect of u_a on increasing the allowable fuel flow rate (or flame length) at the laminar soot point progressively decreases as the pressure of the flame increases. This is a direct effect of the intrusion of buoyancy masking the ability of air coflows to reduce soot formation in flames and no doubt explains why this behavior was not recognized earlier because most prior experiments were carried out at atmospheric pressure — far higher than the pressure conditions where effects of the intrusion of buoyancy are first seen in the results of Figs. 11 and 12.

4.4 Conclusions

The present experimental investigation considered the effect of air/fuel-stream velocity ratios on soot processes within laminar coflowing jet diffusion flames for the experimental conditions summarized earlier. Major conclusions of the study are as follows:

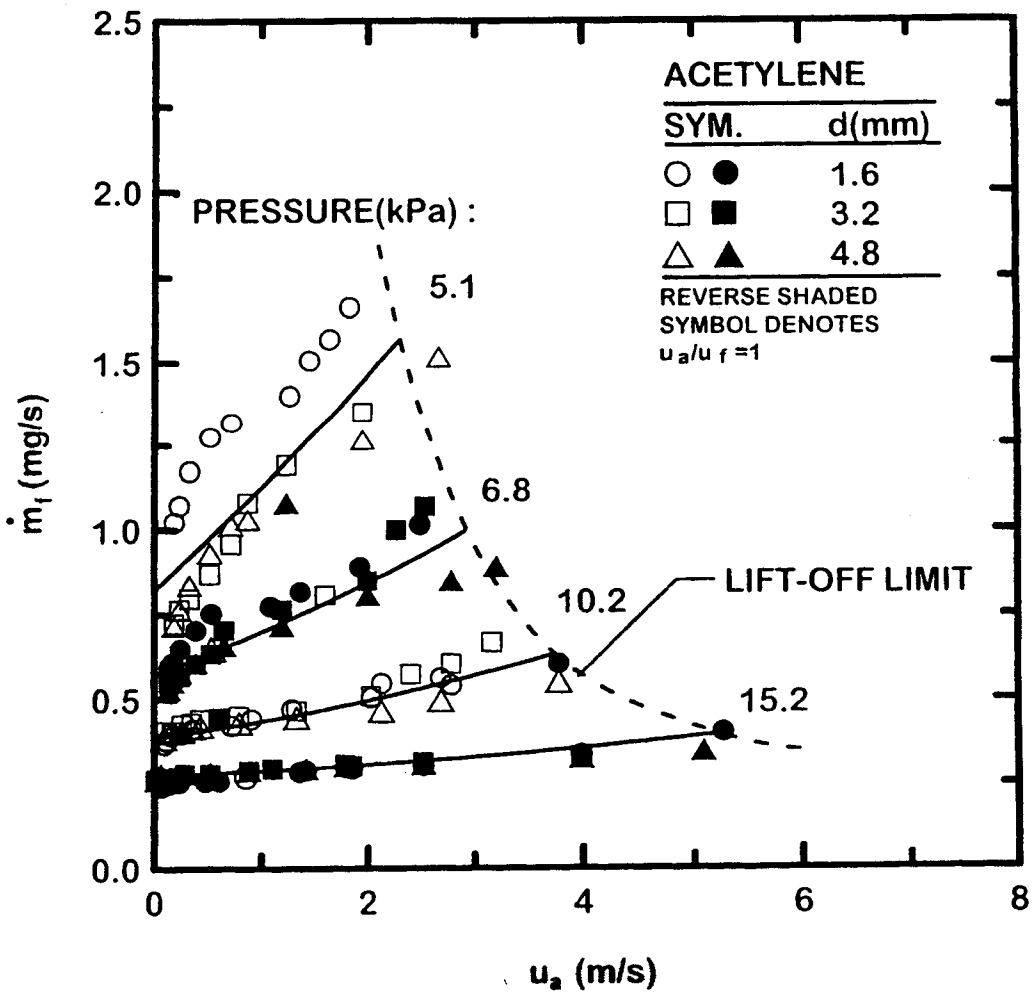

Figure 11. Fuel flow rates at laminar soot-point and liftoff conditions as a function of air coflow velocities, fuel port diameter and pressure for acetylene/air flames. From Dai and Faeth (2000).

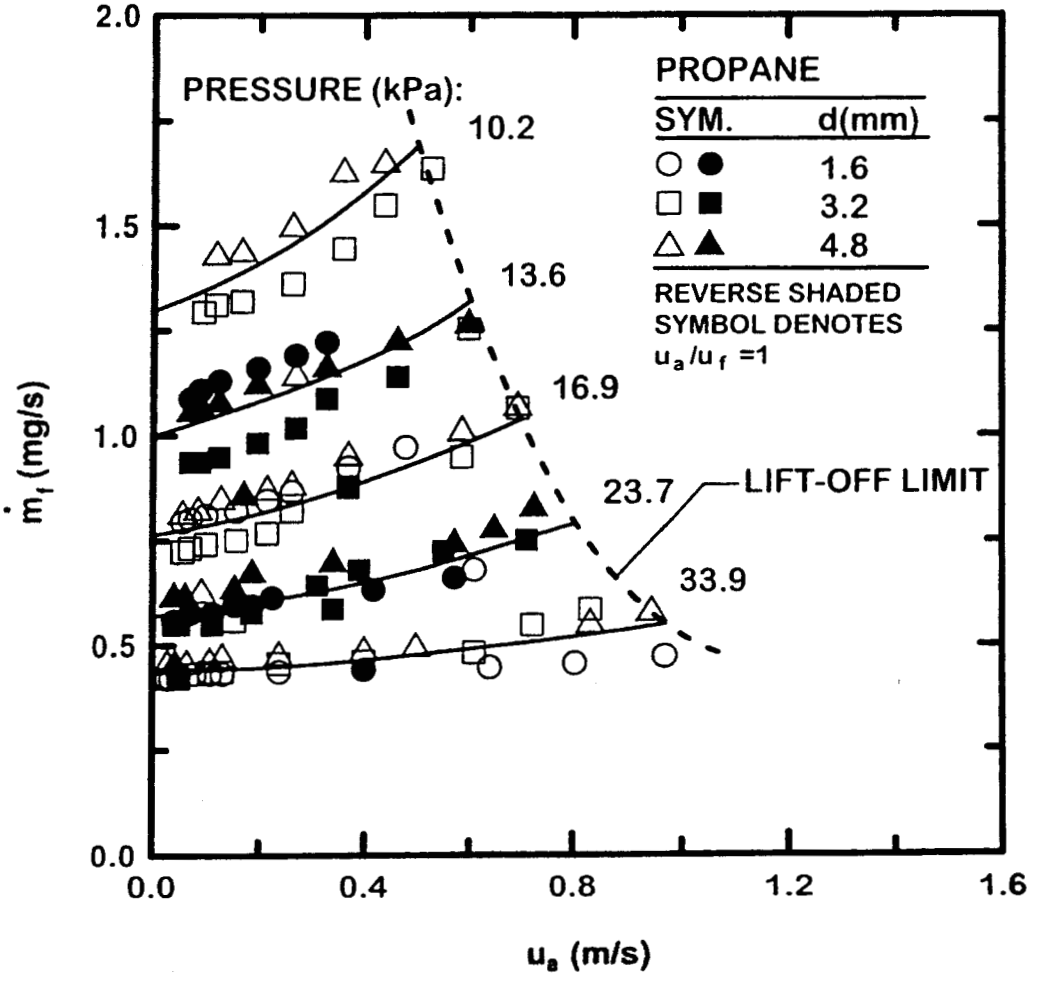

Figure 12. Fuel flow rates at laminar soot-point and liftoff conditions as a function of air coflow velocities, fuel port diameter and pressure for propane/air flames. From Dai and Faeth (2000).

1. Laminar soot point flame lengths and fuel flow rates were increased with increasing air/fuel-stream velocity ratios; these effects were most pronounced at low pressures, where effects of buoyancy were minimized, and initial air/fuel-stream velocity ratios are reasonably representative of the entire visible portion of the flame for the present test conditions. These results are qualitatively similar to earlier measurements of laminar smoke point properties, as well as recent predictions of soot concentration properties [18], for similar flame conditions.

2. Laminar soot point flame lengths were conveniently correlated in terms of a corrected fuel flow rate parameter based on an earlier simplified analysis of the structure of nonbuoyant laminar coflowing jet diffusion flames discussed in Section 3. It is found that laminar smoke point flame lengths in both coflowing and still air environments are roughly twice as long as soot-free (blue) flames at comparable conditions due to the presence of luminous soot particles at fuel-lean conditions as laminar smoke point conditions are approached.

3. The mechanisms of increased resistance to soot formation with increasing air/fuel-stream velocity ratios at low pressures (where buoyancy does not significantly affect flame velocities) involves progressive reduction of flame residence times for soot production, eventually reaching the soot-free (blue) flame limit. Given a critical residence time for the appearance of soot for a particular fuel and pressure, this behavior is consistent with present measurements and the simplified analysis of the shape of nonbuoyant laminar jet diffusion flames in coflowing air. Notably, the shape (length) of these flames is largely controlled by the fuel flow rate, whereas the characteristic residence time is proportional to the flame length divided by the air coflow velocity. Then, laminar soot-point fuel flow rates should increase with increasing air coflow velocities for a given fuel and pressure, relatively independent of fuel-port diameter, as observed at low pressures and large air coflow velocities in Figs. 11 and 12.

References

1. R.W. Bilger, *Prog. Energy Combust. Sci.* 1, 87 (1976).

2. J.P. Gore and G.M. Faeth, *J. Heat Trans.* 110, 173 (1988).

3. D.W. Bahr, *Gas Turbine Combustor Design Problems* (A. H. Lefebvre, ed.), Hemisphere Washington, D.C., p. 205 (1979).

4. A.W. Hussmann and G.W. Mayback, *SAE Trans.* 69, 563 (1961).

5. B.S. Haynes and H.G. Wagner, *Prog. Energy Combust. Sci.* 7, 229 (1981).

6. R.L. Schalla and G.E. McDonald, *Proc. Combust. Inst.* 5, 316 (1954).

7. K.P. Schug et al., *Combust. Sci. Tech.* 22, 235 (1980).

8. W.L. Flower and C.T. Bowman, *Proc.Combust. Inst.* 21, 1115 (1983).

9. P.B. Sunderland et al., *Combust. Flame* 96, 97 (1994).

10. D.L. Urban et al., *AIAA J.* 36, 1346 (1998).

11. G. Sugiyama, *Proc. Combust. Inst.* 25, 601 (1994).

12. J. Du et al., *Proc. Combust. Inst.* 22, 387 (1988).

13. J. Du and R.I. Axelbaum, *Combust. Flame* 100, 367 (1995).

14. K.T. Kang et al., *Combust. Flame* 109, 266 (1997).

15. K.-C. Lin and G.M. Faeth, *J. Prop. Power* 12, 10 (1996).

16. K.-C. Lin and G.M. Faeth, *Combust. Flame* 115, 468 (1999).

17. K.-C. Lin and G.M. Faeth, *J. Prop. Power* 12, 691 (1996).

18. C.H. Kaplan and K. Kailasanath, *Combust. Flame* 124, 275 (2001).

19. P.B. Sunderland et al., *Fifth International Microgravity Combustion Workshop*, NASA Report No. NASA/CP-1999-208917, Washington, D.C., p. 475 (1999).

20. K.-C. Lin and G.M. Faeth, *AIAA J.* 37, 759 (1999).

21. K.-C. Lin et al., *Combust. Flame* 116, 415 (1999).

22. Z. Dai and G.M. Faeth, *Proc. Combust. Inst.* 28, 2085 (2000).

23. D.L. Urban et al., *Proc. Combust. Inst.* 28, 1965 (2000).

24. F. Xu et al., *AIAA J.* 40, 2437 (2002).

25. S.P. Burke and T.E.W. Schumann, *Ind. Eng. Chem. Sci.* 20, 998 (1928).

26. T.H. Cochran and W.J. Masica, *Proc. Combust. Inst.* 13, 821 (1970).

27. J.B. Haggard, Jr. and T.H. Cochran, *Combust. Sci. Tech.* 5, 291 (1972).

28. R.B. Edelman et al., *Proc. Combust. Inst.* 14, 399 (1972).

29. R.B. Edelman and M.Y. Bahadori, *Acta Astro.* 13, 681 (1986).

30. M.Y. Bahadori et al., *AIAA J.* 28, 236 (1990).

31. M.Y. Bahadori et al., AIAA Paper 90-0691 (1990).

32. M.Y. Bahadori et al., AIAA Paper 91-0719 (1991).

33. M.Y. Bahadori et al., AIAA Paper 92-0243 (1992).

34. M.Y. Bahadori et al., *Modern Developments in Energy, Combustion and Spectroscopy* (F.A. Williams, ed.), Pergamon, New York, Chapt. 4, 1993.

35. P.B. Sunderland et al., *Combust. Flame* 116, 376 (1998).

36. P.B. Sunderland et al., *Combust. Flame* 100, 310 (1995).

37. W. Jost, *Explosion and Combustion Processes in Gases*, McGraw-Hill, New York, (1946).

38. F.G. Roper, *Combust. Flame* 29, 219 (1977).

39. D.B. Spalding, *Combustion and Mass Transfer*, Pergamon, New York, 185 (1979).

40. K.K. Kuo, *Principles of Combustion*, John Wiley & Sons, New York, 360 (1986).

41. M. Klajn and A.K. Oppenheim, *Proc. Combust. Inst.* 19, 223 (1982).

42. S.C. Li et al., *Combust. Sci. Tech.* 104, 75 (1995).

43. H. Ban et al., *J. Heat Trans.* 116, 954 (1994).

44. W.G. Braun et al., *Technical Data Book — Petroleum Refining*, 3rd ed., American Petroleum Institute, Washington, D.C., Chapts. 11 and 13 (1976).

45. F.A. Williams, *Combustion Theory*, 2nd ed., Benjamin/Cummings, Menlo Park, CA, p. 38 (1985).

46. S. Mahalingam et al., *Combust. Flame* 82, 231 (1990).

47. C.K. Law and G.M. Faeth, *Prog. Energy Combust. Sci.* 20, 65 (1994).

48. A. Hamins et al., *Combust. Sci. Tech.* 45, 309 (1986).

49. H. Schlichting, *Boundary Layer Theory*, 4th ed., McGraw-Hill, New York, p. 160 (1960).

Appendix A:

K.-C. Lin and G.M. Faeth, (1999) Shapes of nonbuoyant round luminous laminar jet diffusion flames in coflowing air. *AIAA J.* 37, 759-765.

AIAA JOURNAL
Vol. 37, No. 6, June 1999

Shapes of Nonbuoyant Round Luminous Laminar-Jet Diffusion Flames in Coflowing Air

K.-C. Lin* and G. M. Faeth†
University of Michigan, Ann Arbor, Michigan 48109-2140

The shapes (luminous flame boundaries) of steady nonbuoyant round luminous hydrocarbon-fueled laminar-jet diffusion flames burning in coflowing air were studied both experimentally and theoretically. Flame shapes were measured from photographs of flames burning at low pressures in order to minimize the effects of buoyancy. Test conditions involved acetylene-, propylene- and 1,3-butadiene-fueled flames having initial reactant temperatures of 300 K, ambient pressures of 19–50 kPa, jet-exit Reynolds numbers of 18–121, and initial air/fuel velocity ratios of 0.22–32.45 to yield luminous flame lengths of 21–166 mm. The present flames were close to the laminar smoke point but were not soot emitting. Simple expressions to estimate the shapes of nonbuoyant laminar-jet diffusion flames in coflow were found by extending an earlier analysis of Mahalingam et al. (Mahalingam, S., Ferziger, J. H., and Cantwell, B. J., "Self-Similar Diffusion Flames," *Combustion and Flame*, Vol. 82, No. 2, 1990, pp. 231–234). These formulas provided a good correlation of present measurements except near the burner exit where self-similar approximations used in the simplified analysis are no longer appropriate.

Nomenclature

C_f	= empirical flame length factor
D	= mass diffusivity
d	= jet-exit diameter
Fr_a, Fr_f	= air and fuel stream Froude numbers, $u_{a,o}^2/(2gL_f)$ and $u_{f,o}^2/(2gL_f)$
f	= mixture fraction
g	= acceleration of gravity
L_f	= distance from jet exit to luminous flame tip
L_o	= distance from jet exit to virtual origin
$\dot{m}$	= burner mass flow rate
p	= pressure
Re	= jet Reynolds number, $4\dot{m}/(\pi d\mu)$
r	= radial distance
Sc	= Schmidt number, ν/D
u	= streamwise velocity
u_d	= streamwise velocity defect; Eq. (1)
w	= luminous flame diameter
$w_{\frac{1}{2}}$	= luminous flame diameter at $\zeta = \frac{1}{2}$
x	= streamwise distance
Y_{FUEL}	= mass fraction of fuel
Y_{OXYGEN}	= mass fraction of oxygen
Z_{st}	= stoichiometric mixture fraction
ζ	= normalized streamwise distance; Eq. (12)
η	= dimensionless radial distance; Eq. (6)
μ	= dynamic viscosity
ν	= kinematic viscosity
ρ	= density
σ_i	= standard deviation of parameter i

Subscripts

a	= airstream property
f	= fuel-stream property
o	= burner exit-plane condition

Introduction

LAMINAR nonpremixed (diffusion) flames are of interest because they provide model flame systems that are far more tractable for analysis and experiments than more practical turbulent diffusion flames. Certainly understanding flame processes within laminar-jet diffusion flames must precede understanding these processes in more complex turbulent diffusion flames. In addition, many properties of laminar-jet diffusion flames are directly relevant to turbulent diffusion flames using laminar flamelet concepts.[1] Laminar-jet diffusion flame shapes (luminous flame boundaries) have been of particular interest since the classical study of Burke and Schumann[2] because they are a simple nonintrusive measurement that is convenient for evaluating flame-structure predictions. Motivated by these observations, the shapes of laminar diffusion flames were considered during the present investigation.

Nonbuoyant flames were emphasized during the present investigation to simplify interpretation and analysis of the measurements and increase the relevance of the results because most practical flames are not buoyant. Effects of buoyancy were minimized by observing flames having large flow velocities at small pressures.[3] Present methods were based on the study of the shapes of nonbuoyant round laminar-jet diffusion flames in still air due to Lin et al.,[4] who found that a simple analysis due to Refs. 5 and 6 yielded good predictions of the flame shapes reported by Urban et al.[7] and Sunderland et al.[8,9] The objective of the present study was to extend Ref. 4 to consider the shapes of nonbuoyant round laminar-jet diffusion flames in coflowing air, prompted by the widespread use of this configuration to study the structure and soot formation processes of laminar diffusion flames (see Refs. 10–19 and references cited therein). Similar to Ref. 4, a way to correlate flame-shape results was sought, convenient for use by others, based on simplified analysis of nonbuoyant laminar coflowing jet diffusion flames.

Most earlier studies of the shapes of nonbuoyant laminar-jet diffusion flames considered round hydrocarbon-fueled flames burning in still gases (generally air) (see Refs. 4–8, 20–33, and references cited therein). The results of these studies have raised several concerns: what conditions are needed to minimize effects of buoyancy when observations of nonbuoyant flames are sought at normal gravity, what is the effect of transient flame development on flame-shape measurements when nonbuoyant conditions are provided by ground-based facilities where available test times are limited, and what is the effect of soot luminosity on the flame-shape measurements of hydrocarbon-fueled flames?[7] With respect to minimizing effects of buoyancy at normal gravity, experiments at low pressures[3] and with very large flow velocities[33] have proven to be effective tactics that will be exploited during the present study. Transient flame development effects have been problematical using ground-based low-gravity facilities due to the limited test times of drop towers[24–27] and the flight-path disturbances of aircraft facilities.[7–9] Recent measurements from long-term low-gravity tests in space[7]

Received Aug. 20, 1998; revision received Dec. 15, 1998; accepted for publication Jan. 7, 1999.

*Research Associate, Department of Aerospace Engineering; currently Research Scientist, Taitech, Inc., Wright–Patterson Air Force Base, OH 45433-0630.

†A. B. Modine Professor, Department of Aerospace Engineering. Fellow AIAA.

and drop-tower tests at reduced pressures,[8] however, have minimized transient flame development problems and yielded results that could be correlated by simplified theories as mentioned earlier.

Effects of soot luminosity on the shapes of hydrocarbon-fueled laminar-jet diffusion flames in still air are more problematical than effects of buoyancy and transient flame development. The luminosity of hydrocarbon-fueled flames is caused mainly by glowing soot particles; therefore, the relationships between luminous flame dimensions and the location of the flame sheet (where the local mixture fraction is stoichiometic) are the main issues because the latter is generally associated with predictions of laminar flame shapes. Past measurements of the structure and soot properties of weakly buoyant and buoyant round laminar-jet diffusion flames burning in still or slowly moving air indicate that luminous/stoichiometric flame-length ratios are in the range 0.9–1.8, with the largest values observed as the laminar smoke point (the condition where the flame first begins to emit soot) is approached.[9,12–16] This behavior occurs because soot oxidation begins at slightly fuel-rich conditions and can continue in the fuel-lean region for a time before the soot is either consumed (for non-soot-emitting or nonsooting flames) or the soot oxidation reactions are quenched (for soot-emitting or sooting flames), with luminous flame lengths varying accordingly.[9] Finally, recent measurements of nonbuoyant laminar-jet diffusion flames in still air show that luminous flame lengths near laminar smoke-point conditions are roughly twice as long as those of soot-free (blue) flames at comparable conditions.[4,8] Fortunately, flame shapes at these two limiting conditions could still be correlated effectively based on the simplified Spalding[5] analysis, after defining an empirical factor to represent effects of soot luminosity.[4] Such empiricism is not desirable, but it is unavoidable at the present time because of limited understanding about soot reaction processes.

Even though the classic study of Burke and Schuman[2] addressed the shapes of laminar coflowing jet diffusion flames (for the limiting condition where initial fuel and oxidant velocities were the same), there has been relatively little subsequent consideration of this problem. Exceptions include the theoretical studies of Williams[34] and Mahalingam et al.,[35] which extended the Burke and Schumann[2] analysis to treat flames where the outer coflowing stream was unbounded. During the present study, the simple self-similar analysis of Mahalingam et al.[35] was further developed to provide a theoretical basis for correlating the shapes of nonbuoyant laminar-jet diffusion flames in coflowing air, analogous to the use of the simplified analysis of Spalding[5] to provide a theoretical basis for correlating the shape of nonbuoyant laminar-jet diffusion flames in still air by Lin et al.[4]

The preceding discussion suggests that significant progress has been made concerning the shapes of the hydrocarbon-fueled laminar-jet diffusion flames in still air but that corresponding information for flames in coflowing air is very limited in spite of the importance of this configuration for studies of soot processes in laminar-jet diffusion flames. With this status in mind, the present investigation considered nonbuoyant round luminous laminar-jet diffusion flames in coflowing air with the following specific objectives:

1) Measure the shapes (luminous flame boundaries) and associated properties such as laminar flame lengths and diameters for various fuel types, coflow velocities, jet-exit flow rates and ambient pressures.

2) Compare present measurements with earlier findings for similar flames in still air, e.g., the flames observed in Ref. 4, to help quantify effects of coflow on flame-shape properties.

3) Exploit the new measurements to develop a correlation for the shapes of coflowing laminar-jet diffusion flames, convenient for use by others, by extending the earlier analysis of Burke and Schumann[2] flames due to Mahalingam et al.[35]

Present observations were limited to soot-containing acetylene-, propylene- and 1,3-butadiene-fueled laminar-jet diffusion flames burning in coflowing air. Similar to Ref. 4, the measurements were limited to conditions near the laminar smoke point except for some preliminary observations to study the effect of approach to the laminar smoke point on flame shapes.

The following discussion begins with descriptions of experimental and theoretical methods. Results are then considered, treating flame appearance, luminous flame lengths, luminous flame diameters, and luminous flame shapes, in turn. Major conclusions are summarized at the end of the paper.

Experimental Methods

Experimental methods will be described only briefly (see Refs. 17–19 for more details). Effects of buoyancy were minimized by observing flames at relatively small pressures ($\leq$50 kPa) with either relatively large coflow velocities (air/fuel velocity ratios up to 32.45) or relatively large source Froude numbers when coflow velocities were small. The burner was placed within a windowed cylindrical chamber and directed vertically upward along its axis. The burner was a coaxial-tube arrangement with the fuel flowing from the inner port (6-mm inside diameter with the tube wall tapered to provide a negligible thickness at the tube exit) and air flowing from a concentric outer port (60-mm inside diameter). The inner port had sufficient length to provide fully developed laminar pipe flow at the burner exit. The outer port had several layers of beads and screens to provide a uniform velocity flow at the burner exit. Flame lengths were limited so that test conditions approximated flames in a uniform air coflow based on laser velocimetry measurements of flow velocity distributions.[17,19] The windowed chamber had a diameter of 300 mm and a length of 1200 mm. Optical access was provided by two pairs of opposing windows having diameters of 100 mm and centered on a horizontal plane located 500 mm above the base of the windowed chamber. The flames were positioned so that their full lengths could be observed and photographed through the windows.

Fuel was supplied to the inner port from commercial gas cylinders. Fuel flow rates were controlled and metered with critical flow orifices in conjunction with pressure regulators with this system calibrated with wet-test meters. Air was supplied from the room using critical flow orifices to control and meter air-flow rates. The exhaust products passed through a porous plate into a plenum chamber at the top of the windowed chamber to provide uniform flow conditions in the vicinity of the test flame. After dilution with air to reduce flow temperatures, the exhaust flow was removed using the laboratory vacuum pump system. The flames were ignited by a hot wire that could be manually moved out of the flowfield once flame stabilization was complete.

Dark field photographs of the flames were obtained using a 35-mm reflex camera. The photographs were subsequently printed using a 100 × 125 mm film format. The flames were measured directly from these prints, using photographs of objects of known size to calibrate vertical and horizontal distances on the prints. Experimental uncertainties (95% confidence) of luminous flame diameters and lengths were less than 2 and 5%, respectively.

Present test conditions are summarized in Table 1. Gas purities were greater than 99% for propylene and 1,3-butadiene but were only roughly 98% for acetylene due to contamination by acetone that is present in commercial acetylene gas cylinders for safety purposes. The effect of the acetone was evaluated by comparing observations with and without acetone vapor present, using the acetone purification system described by Hamins et al.[36] to create the acetone-free fuel stream. The effect of acetone on luminous flame shapes (and laminar smoke-point flame lengths[17,19]) was small compared with experimental uncertainties. Present test conditions included reactant

Table 1 Summary of test conditions[a]

Parameter	Acetylene	Propylene	1,3-Butadiene
Fuel flow rate, mg/s[b]	0.94–5.90	1.53–4.08	0.74–2.71
Re (–)	19–121	38–101	18–66
$u_{a,o}/u_{f,o}$ (–)	0.22–12.03	0.29–6.99	0.77–32.45
$\mu_{f,o}$, mg/s-m	10.3	8.61	8.66
L_f, mm	21–108	41–108	21–75
$w_{1/2}$, mm	3.5–9.5	5.9–13.1	4.3–10.0
Z_{st}	0.0704	0.0636	0.0667

[a]Fuel port inside diameter of 6 mm and concentric air port inside diameter of 60 mm with burner directed vertically upward. Reactant temperatures of roughly 300 K with ambient pressures of 19–50 kPa.

[b]Commercial grade gases in cylinders with purities as follows: greater than 98.0% for acetylene and greater than 99.0% for propylene and 1,3-butadiene.

temperatures of roughly 300 K, ambient pressures of 19–50 kPa, jet-exit Reynolds numbers of 18–121, and initial air/fuel velocity ratios of 0.22–32.45.

Theoretical Methods

The objective of the analysis was to develop a convenient way to help interpret and correlate flame-shape measurements for nonbuoyant laminar-jet diffusion flames in coflowing air, analogous to the approach used by Lin et al.[4] for the shapes of nonbuoyant laminar-jet diffusion flames in still air. Thus, a set of easily used equations was sought, along with recommendations for selecting the thermochemical and transport properties appearing in these equations, as opposed to more complete methods that would require numerical solutions on a computer. The approach used was to extend the analysis of Mahalingam et al.[35] (which considers the Burke and Schumann[2] problem in the self-similar regime far from the source when the outer reactant stream is unbounded) to treat the present problem. The following description of the analysis is brief. A more detailed example of this general approach, for somewhat different initial conditions and property assumptions, is provided by Mahalingam et al.[35]

Except for changed ambient flow properties, the major assumptions of the present flame-shape analysis are similar to those used earlier by Lin et al.[4] as follows: 1) Attention is limited to steady, axisymmetric laminar-jet diffusion flames burning at constant pressure in an unbounded coflowing gas having uniform properties; 2) effects of buoyancy and associated changes of potential energy are negligible; 3) the Mach number of the flow is small so that effects of viscous dissipation and changes of kinetic energy can be ignored; 4) the flame has a large aspect ratio so that diffusion of mass (species), momentum, and energy in the streamwise direction is small; 5) for the same reasons, the solution of the governing equations can be approximated by far-field conditions where the details of initial conditions can be replaced by integral invariants of the flow for the conservation of mass, momentum, and energy; 6) all chemical reactions occur in a thin-flame sheet with fast chemistry so that fuel and oxidant are never simultaneously present at finite concentrations; 7) the diffusivities of mass (of all species), momentum, and energy are all equal; 8) all thermophysical and transport properties are constant throughout the flame; and 9) effects of radiation are small. The first three assumptions are justified as conditions of the present experiments. The fourth and fifth assumptions are justified for most of the present measurements that have large aspect ratios, e.g., the present measurements summarized in Table 1 have flame aspect ratios $2L_f/w_{1/2}$ in the range 4–62 and burner aspect ratios $2L_f/d$ in the range 7–36. The sixth assumption, prescribing a thin-diffusion flame sheet, has a long history of effective use to find the shapes of laminar-jet diffusion flames, dating back to Burke and Schumann.[2] The remaining assumptions, however, are not satisfied by laminar-jet diffusion flames and were only adopted so that simple flame-shape formulas could be found, based on the past success of similar approximations to find the shapes of laminar-jet diffusion flames (see Refs. 4–8, 28–31, and references cited therein).

The flame configuration and notation used for the present analysis is sketched in Fig. 1. The approach is limited to self-similar behavior far from the source so that the details of source properties are not important; therefore, the source is represented by uniform average fuel- and air-stream velocities $u_{f,o}$ and $u_{a,o}$. The mixture fractions (defined as the fraction of mass at a point that originated from the source fuel stream) of the source fuel and air streams are $f_{f,o} = 1$ and $f_{a,o} = 0$ by definition. The enthalpy defect of the source can be defined in an analogous way, but this is not necessary because conservation of energy principles are not needed to find flame shapes under the present assumptions. The streamwise velocity defect is defined as follows:

$$u_d = u_{a,o} - u \tag{1}$$

noting that the airstream velocity approaches $u_{a,o}$ at large r for all distances from the source, based on assumption (1). In the far field, where self-similar behavior is approached, $|u_d|/u_{a,o} \ll 1$ (the absolute value is used to allow for values of $u_{f,o}$ both larger and smaller than $u_{a,o}$) and quadratic and higher terms in u_d can be neglected in the governing equations. Then, under the present approximations,

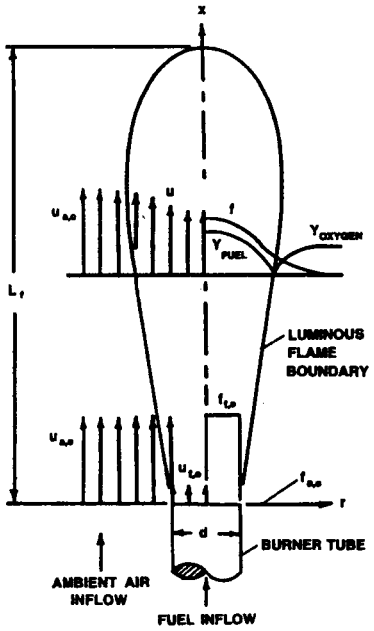

Fig. 1 Sketch of the coflowing laminar-jet diffusion flame configuration.

the governing equation for conservation of mixture fraction can be found in the same manner as the far-field formulation of laminar wake processes, as follows[37]:

$$u_{a,o}\frac{\partial f}{\partial x} = \frac{\nu}{r}\frac{\partial}{\partial r}\left(r\frac{\partial f}{\partial r}\right) \tag{2}$$

$$r = 0: \quad \frac{\partial f}{\partial r} = 0, \qquad r \to \infty: \quad f = 0 \tag{3}$$

The final condition of the analysis is conservation of the flow of fuel-stream mass in the streamwise direction, which can be written as follows in far field:

$$\int_0^\infty f r\, dr = \frac{d^2 u_{f,o}}{8u_{a,o}} \tag{4}$$

The solution of Eqs. (2–4) can be obtained using either conventional separation of variables or conversion into an ordinary differential equation by a suitable similarity transformation.[37] The resulting expression for the mixture fraction distribution in the self-similar regime is as follows:

$$f = u_{f,o}\, d^2 \exp(-\eta^2)/(16\nu x) \tag{5}$$

where

$$\eta = (r/2)[u_{a,o}/(\nu x)]^{\frac{1}{2}} \tag{6}$$

The location of the luminous flame boundary is assumed to coincide with the location of the thin flame sheet where the concentrations of fuel and oxidant are zero (see Fig. 1) and the stoichiometric mixture fraction is reached, $f = Z_{st}$ (see Table 1 for present values of Z_{st}). Introducing this mixture fraction into Eq. (5), for conditions along the flame axis, yields the following expression for luminous flame length:

$$\frac{L_f}{d} = \frac{Re}{16Z_{st}} \tag{7}$$

The corresponding expression for flame shape, providing the flame diameter as a function of streamwise distance, is as follows:

$$w/d = [(x/L_f)(u_{f,o}/u_{a,o})\ln(L_f/x)/Z_{st}]^{\frac{1}{2}} \tag{8}$$

Finally, a convenient measure of the flame diameter is its value at $x/L_f = \frac{1}{2}$, as follows:

$$w_{\frac{1}{2}}/d = [(u_{f,o}/u_{a,o})\,\ell n\{2\}/(2Z_{st})]^{\frac{1}{2}} \tag{9}$$

Correlation of the measurements was sought in the same manner as Lin et al.[4]: The equal diffusivity approximation was relaxed by introducing the Schmidt number into Eq. (7); the Schmidt number and viscosity used to compute the Reynolds number were taken from the properties of air at the average of the adiabatic flame temperature and the ambient temperature; the correlation of flame length was improved at small aspect ratios by introducing a virtual origin at a distance L_o from the jet exit; and the flame length correlation was fine-tuned for effects of soot luminosity, etc., by introducing an empirical coefficient C_f as discussed later. With these changes, Eq. (7) for the luminous flame length becomes

$$\frac{(L_f - L_o)}{d} = \frac{C_f ReSc}{16Z_{st}} \tag{10}$$

whereas Eq. (8) for the luminous flame diameter becomes

$$w/d = [-\zeta(u_{f,o}/u_{a,o})\,\ell n\{\zeta\}/Z_{st}]^{\frac{1}{2}} \tag{11}$$

where

$$\zeta = \frac{(x - L_o)}{(L_f - L_o)} \tag{12}$$

Equations (9–12) disclose some interesting properties of nonbuoyant laminar-jet diffusion flames in a coflowing and unbounded environment. First of all, the flame length from Eq. (10) is independent of the coflow velocity, which is surprising; nevertheless, flame lengths in still gases from Ref. 4 are a fixed ratio longer than in coflow (given similar values of C_f and L_o/d), e.g., the coefficients in the flame-length expressions for still and coflowing gases are $\frac{3}{32}$ and $\frac{1}{16}$, respectively. Diameters of flames in coflow vary with the ratio $u_{f,o}/u_{o,a}$; in contrast, diameters of flames in still gases are independent of reactant flow rates.[4] Flame-diameter properties in both coflowing and still gases, however, are only indirectly affected by assumed transport properties through the computation of flame-length from Eq. (10). Finally, the present analysis agrees with the results of Mahalingam et al.[35] at their limiting Burke and Schumann[2] condition of $u_{f,o} = u_{a,o}$, except for the presence of the virtual origin and the different treatment of transport properties. The corresponding agreement between the self-similar prediction and the more exact Burke and Schumann[2] analysis for $u_{f,o} = u_{a,o}$ as the diameter of the outer reactant stream becomes large also is quite good in the far field, as discussed by Mahalingam et al.[35]

Results and Discussion

Flame Appearance

Photographs of acetylene-, propylene- and 1,3-butadiene-fueled flames are illustrated in Fig. 2 for comparable flow conditions (Re of 62–66 and $u_{o,o}/u_{f,o}$ of 3.3–4.2). All three flames are close to their laminar smoke points, which can be arranged because flame shapes are relatively independent of the ambient pressure, whereas

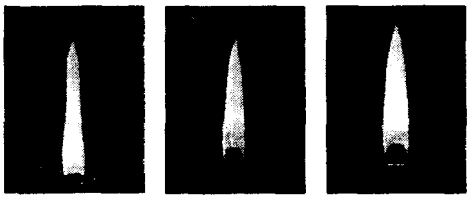

Fig. 2 Photographs of acetylene-, propylene-, and 1,3-butadiene-fueled laminar-jet diffusion flames burning in coflowing air at similar air/fuel velocity ratios.

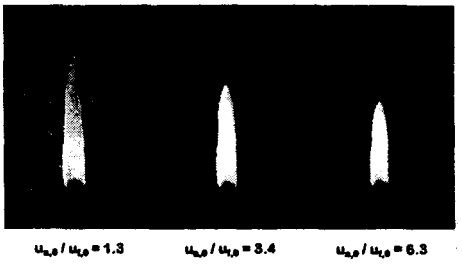

Fig. 3 Photographs of acetylene-fueled laminar-jet diffusion flames burning in coflowing air at various air/fuel velocity ratios.

laminar smoke-point flame lengths increase rapidly as the ambient pressure is decreased.[9] The 1,3-butadiene flame seems somewhat longer than the rest, but this is mainly because of the flame attachment farther downstream from the burner exit than the rest. Actually, all three flames have roughly the same length, which is consistent with Eq. (10) in view of the relatively small variation of Z_{st} for these fuels (see Table 1) and past experience concerning the effect of approach to the laminar smoke point on luminous flame shapes from Lin et al.[4] Observed flame diameters are somewhat larger for the 1,3-butadiene-fueled flame than the rest, rather than being nearly the same as anticipated from Eq. (9). This level of discrepancy between measured and predicted flame diameters is typical of observations over the test program and is similar to past experience for flames in still gases from Lin et al.[4] In view of the simplicity of the flame-shape analysis, and the fact that average properties and empirical factors cannot be chosen to fit predictions and measurements of flame diameters, it is rather remarkable that the trends of flame-diameter predictions are still reasonably good.

Photographs of acetylene-fueled flames at given fuel jet-exit conditions and ambient pressures (Re of 93 and ambient pressure of 19 kPa) are illustrated in Fig. 3 for various air/fuel velocity ratios. Contrary to the expectations of Eq. (10), where luminous flame lengths are independent of air/fuel velocity ratio, the flame lengths illustrated in Fig. 3 decrease significantly as the air/fuel velocity ratio is increased. This behavior follows because luminous flame lengths progressively increase relative to soot-free (blue) flames at comparable conditions as laminar smoke-point conditions are approached. For example, the luminous flame lengths at the laminar smoke point are roughly twice as long as corresponding blue flames for nonbuoyant laminar-jet diffusion flames in still air,[4] and similar behavior is quite reasonable for flames in coflowing air. In particular, increasing air/fuel velocity ratios tend to increase laminar smoke-point flame lengths based on measurements of Lin and Faeth.[19] Thus, for $u_{a,o}/u_{f,o} = 1.3$ in Fig. 3 the flame has nearly reached its laminar smoke-point flame length of 60 mm, but for $u_{a,o}/u_{f,o} = 3.4$ the luminous flame length is only 50 mm compared to a laminar smoke-point flame length of roughly 110 mm for this air/fuel velocity ratio, which implies a flame length between the length of a soot-free (blue) flame and the length at the laminar smoke point. In view of this effect of approach to the laminar smoke point, the following flame-shape measurements were obtained near laminar smoke-point conditions, and the corresponding lengths of soot-free (blue) flames are likely to be much shorter.

Flame Lengths

Luminous flame length is defined in the following as the streamwise distance between the burner exit and the farthest downstream plane normal to the flame axis that contacts a luminous region of the flame. For the present flames in coflowing air, this length was generally associated with the end of luminosity at the flame axis. For the flames of Lin et al.[4] in still air, however, this location was either along the axis or at an annular soot layer for the closed- and open-tip flames observed near laminar smoke-point conditions for nonbuoyant flames in still gases.[7]

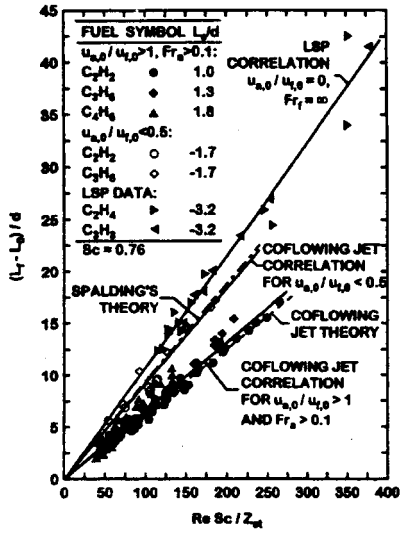

Fig. 4 Luminous flame lengths of hydrocarbon-fueled laminar-jet diffusion flames burning in coflowing air: correlation and measurements of Lin et al.[4] for $u_{a,o}/u_{f,o} = 0$, predictions of the Spalding[5] theory for $u_{a,o}/u_{f,o} = 0$, correlation and measurements of the present investigation for $0.22 \leq u_{a,o}/u_{f,o} < 0.5$, and correlation and measurements of the present investigation for coflowing jet theory.

Measured and predicted lengths of flames in coflowing and still air are plotted in Fig. 4. Present measurements have been divided into two groups: 1) $u_{a,o}/u_{f,o} < 0.5$, which roughly approximates nonbuoyant flames in still air; and 2) $u_{a,o}/u_{f,o} > 1$ for $Fr_a > 0.1$, which roughly approximates nonbuoyant flames in coflowing air. All of the measurements are presented as suggested by the simplified theories of flames in coflowing and still air, e.g., Eq. (10) for flames in coflowing air, with $(L_f - L_o)/d$ plotted as a function of $Re\,Sc/Z_{st}$. Values of Z_{st} used in the plots are as follows: 0.0704 for acetylene, 0.0636 for ethylene and propylene, 0.0667 for 1,3-butadiene and 0.0602 for propane. Clearly, as mentioned earlier, values of Z_{st} do not vary significantly over the present test range. All other properties were obtained from Braun et al.[38] Values of Sc were based on the properties of air at the mean temperatures of the flames; these values do not change significantly over the present test range so that a mean value of $Sc = 0.76$ was used for plotting all of the data. The values of μ used to find Re for the plots also was based on the properties of air at the mean flame temperature. Virtual origins were selected so that fits of the measurements for various fuels and ambient flow conditions passed through the origins of the plots; the resulting values of L_o/d are summarized in the legend of Fig. 4. Finally, plots of the various predictions for $C_f = 1.00$ (denoted theory) and for best-fit correlations of the various measurements (denoted correlation) are also shown on the figure. For convenience, the values of L_o/d and C_f for all of the flame-length plots considered here are summarized in Table 2.

The correlation of the flames in still gases according to the simple Spalding[5] analysis has already been discussed by Lin et al.[4] The results illustrated in Fig. 4 for flames in still gases represent near laminar smoke-point conditions and yield an excellent correlation having relatively little scatter with $C_f = 1.13$. As noted earlier, these luminous flame lengths for near laminar smoke-point conditions are roughly twice as long as the measurements of Sunderland et al.[8] for soot-free (blue) flames (Table 2). Present results for coflowing jet flames with $u_{a,o}/u_{f,o} > 1$ also yield a good correlation according to the simplified theory of Eq. (10), with $C_f = 1.05$ in this case. Thus, flame lengths for flames in still and coflowing gases have roughly the ratio discussed earlier in connection with Eq. (7), e.g., L_f (still air)/L_f (coflow) $\approx \frac{3}{2}$, with this ratio being relatively independent of $u_{a,o}/u_{f,o}$ and Re in accord with the simplified theories. Finally, present results for small coflow velocities $0.22 < u_{a,o}/u_{f,o} < 0.5$ yield a reasonably good correlation in terms of the theory for flames in still gases, e.g., $C_f = 0.98$ from Table 2. These results also are in reasonably good agreement with earlier measurements in still gases, with the somewhat shorter flame lengths in the presence of slow coflow being consistent with other effects of coflow seen in Fig. 4.

Table 2 Summary of flame-length correlations

Flame system	Source	L_o/d	C_f^a	σ_{Cf}
Nonbuoyant laminar-jet diffusion flame in coflowing air ($u_{a,o}/u_{f,o} > 1$, $Fr_a > 0.1$, soot-containing flames)	Present study	1.4[b]	1.05	0.12
Nonbuoyant laminar-jet diffusion flame in still air ($u_{a,o}/u_{f,o} = 0$, $Fr_f = \infty$, soot-containing flames)	Lin et al.[4]	−3.2	1.13	——
Nonbuoyant laminar-jet diffusion flame in slow-moving air ($0.22 \leq u_{a,o}/u_{f,o} < 0.5$, soot-containing flames)	Present study	−1.7	0.98	0.10
Nonbuoyant laminar-jet diffusion flame in still air ($u_{a,o}/u_{f,o} = 0$, $Fr_f = \infty$, soot-free, blue, flames)	Sunderland et al.[8]	2.7	0.56	——

[a] Empirical flame-length parameter based on Eq. (10) for flames in coflowing air and corresponding equations in Ref. 4 for flames in still or slow-moving ($u_{a,o}/u_{f,o} < 0.5$) air.
[b] Average of following individual values of L_o/d for particular hydrocarbon fuels: 1.0 for C_2H_2, 1.3 for C_3H_6, and 1.8 for C_4H_6.

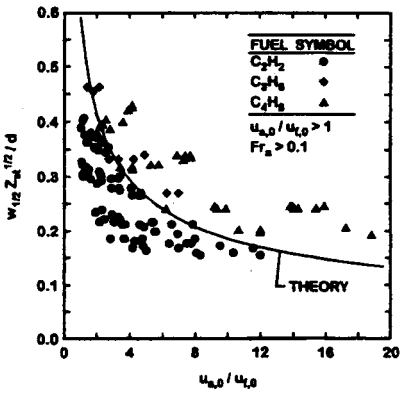

Fig. 5 Measured and predicted luminous flame diameters of hydrocarbon-fueled laminar-jet diffusion flames burning in coflowing air at various velocity ratios for $u_{a,o}/u_{f,o} > 1$ and $Fr_a > 0.1$.

Flame Diameters

The normalized characteristic flame diameter $w_{1/2}Z_{st}^{1/2}/d$ for coflowing jet diffusion flames is inversely proportional to the square root of the air/fuel velocity ratio and independent of flow transport properties, according to Eq. (9). This relationship, illustrated in Fig. 5, is based on present measurements for $u_{a,o}/u_{f,o} > 1$ and $Fr_a > 0.1$ along with the predictions of Eq. (9). The measurements follow the general trend of the predictions but are rather scattered. There also is a tendency for flame diameters to progressively increase as a function of fuel type in the order of acetylene, propylene, and 1,3-butadiene.

Insight concerning the scatter of the measurements in Fig. 5 was sought by plotting the entire argument of Eq. (9) as a function of normalized flame length, similar to the approach used for characteristic flame diameters for flames in still air by Lin et al.[4] These results are illustrated in Fig. 6 for the same range of test conditions as Fig. 5. The scatter about the predictions progressively decreases as the normalized flame length increases; therefore, small-flame aspect ratios appear to be mainly responsible for the scatter seen

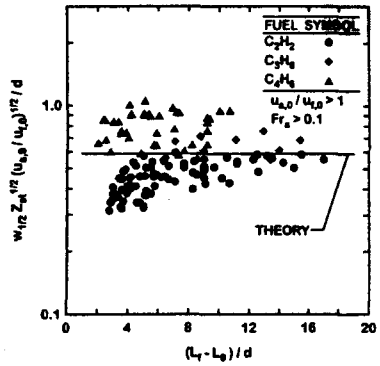

Fig. 6 Measured and predicted luminous flame diameters of hydrocarbon-fueled laminar-jet diffusion flames burning in coflowing air at various flame lengths for $u_{a,o}/u_{f,o} > 1$ and $Fr_a > 0.1$.

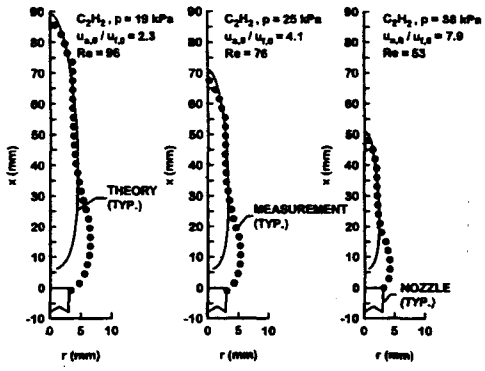

Fig. 8 Measured and predicted luminous flame shapes for acetylene-fueled laminar-jet diffusion flames burning in coflowing air at various fuel jet and coflow conditions.

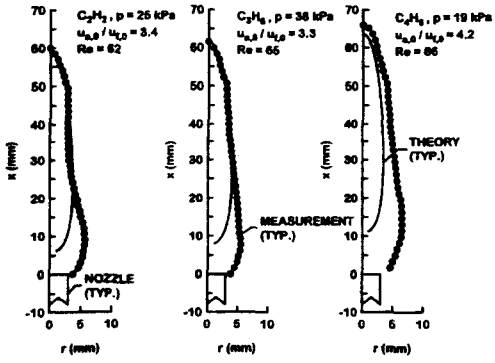

Fig. 7 Measured and predicted luminous flame shapes for acetylene-, propylene-, and 1,3-butadiene-fueled laminar-jet diffusion flames burning in coflowing air.

in Fig. 5. The normalized flame diameters illustrated in Fig. 6 also progressively increase as a function of fuel type in the order of acetylene, propylene, and 1,3-butadiene. Similar increases of normalized flame diameters also were observed when changing from ethylene- to propane-fueled flames in still gases.[4] The reasons for these fuel effects are not known, but fortunately the effects are not very large in view of the approximations of the simplified theories.

Flame Shapes

Measured and predicted luminous flame shapes are compared as the final step in the evaluation of the simplified flame-shape analysis leading to Eqs. (9–12) for flames in coflowing air. This comparison was carried out for relatively large flame lengths (or large aspect ratios) to reduce problems of flame-width predictions at small-flame aspect ratios discussed in connection with Figs. 5 and 6. Typical results for acetylene-, propylene-, and 1,3-butadiene-fueled flames at similar Reynolds numbers (Re of 62–66) and air/fuel velocity ratios ($u_{a,o}/u_{f,o}$ of 3.3–4.2) are illustrated in Fig. 7. Flame radius is plotted as a function of streamwise distance to illustrate directly the effectiveness of flame-shape predictions. The predictions clearly are quite good in the far field. A minor exception is a tendency for predictions to underestimate the radius of the 1,3-butadiene-fueled flame in the far field, similar to the results discussed in connection with Fig. 6. The far-field approximations of the analysis, however, break down near the nozzle exit where the predictions are not very satisfactory.

Effects of air/fuel velocity ratios and Reynolds numbers on discrepancies between measured and predicted flame shapes can be seen from the results plotted in Fig. 8. Conditions were selected for the plots to provide progressively shorter and narrower flames, e.g., acetylene-fueled flames having $u_{a,o}/u_{f,o} = 2.3$, 4.1, and 7.9 and $Re = 96$, 76, and 53, respectively. The approximate analysis is seen to provide good predictions of trends with respect to variations of air/fuel velocity ratios and Reynolds numbers in the far field. Predictions near the source, however, are not satisfactory because of the failure of the far-field approximations. Mahalingam et al.[35] observe similar trends where predictions are not satisfactory near the source when comparing their approximate self-similar analysis with the exact results of the Burke and Schumann[2] analysis for the property approximations and the uniform velocity flame conditions that they consider.

Conclusions

The luminous flame shapes of steady, nonbuoyant, round hydrocarbon-fueled laminar-jet diffusion flames burning in coflowing air were studied both experimentally and theoretically. Test conditions involved acetylene-, propylene-, and 1,3-butadiene-fueled flames having initial reactant temperatures of 300 K, ambient pressures of 19–50 kPa, jet-exit Reynolds numbers of 18–121, and initial air/fuel velocity ratios of 0.22–32.45 to yield luminous flame lengths of 21–108 mm. The present test flames usually were close to the laminar smoke point but were not soot emitting. The new measurements were used to evaluate predictions of luminous flame shapes based on simplified analysis due to Spalding[5] and Mahalingam et al.[35] The major conclusions of the study are as follows:

1) The present extension of the simplified analysis of nonbuoyant round laminar-jet diffusion flames in coflow due to Mahalingam et al.[35] provided reasonably good predictions of the luminous shapes of the present flames in the far field for $u_{a,o}/u_{f,o} > 1$ and $Fr_a > 0.1$ after appropriate selections of empirical flame-length parameters, e.g., L_o/d and C_f. The predictions were most satisfactory for large aspect ratio flames and tended to fail near the source where the far-field approximations used in the analysis were no longer valid.

2) The simplified analysis of nonbuoyant laminar-jet diffusion flames in still air due to Spalding,[5] developed by Lin et al.,[4] provided reasonably good predictions of the luminous shapes of the present flames in slow-moving coflow for $0.22 \leq u_{a,o}/u_{f,o} < 0.5$ after appropriate selections of empirical flame-length parameters, e.g., L_o/d and C_f. Present values of the flame lengths (or C_f) for slow coflow ($u_{a,o}/u_{f,o} < 0.5$) were 15% smaller than the earlier results of Lin et al.[4] with no coflow because of enhanced mixing rates caused by coflow.

3) Based on present correlations of the luminous flame boundaries of nonbuoyant laminar-jet diffusion flames in still and coflowing air, luminous flame lengths increase linearly with fuel flow rates but are relatively independent of jet-exit diameter, pressure, and air/fuel velocity ratio (for flames in coflow). Nevertheless flames in still air are roughly 50% longer than flames in significant coflow ($u_{a,o}/u_{f,o} > 1$) at comparable conditions, with this difference being

relatively independent of air/fuel velocity ratio and jet-exit Reynolds number.

4) Based on present correlations of the luminous flame boundaries of nonbuoyant laminar-jet diffusion flames in still and coflowing air, characteristic luminous flame diameters vary linearly with jet-exit diameter and are relatively independent of flow physical properties and jet-exit Reynolds numbers. For flames having significant levels of coflow ($u_{e,o}/u_{f,o} > 1$), however, characteristic luminous flame diameters are also inversely proportional to the square root of $u_{e,o}/u_{f,o}$. Thus, large aspect ratio flames can best be achieved using small injector diameters, large injector Reynolds numbers, and large air/fuel velocity ratios, subject to laminar smoke-point limitations if nonsooting flames are desired.

5) Progressive increases of luminous flame lengths at comparable conditions were observed as the laminar smoke point was approached for nonbuoyant laminar-jet diffusion flames in coflowing air. This behavior was similar to the observations of Lin et al.[4] that the luminous lengths of nonbuoyant laminar-jet diffusion flames in still air were roughly twice as long at near laminar smoke-point conditions as soot-free (blue) flames at comparable conditions. Whether quantitative effects of approach to the laminar smoke point are the same for flames in coflowing and still air, however, still must be established.

Finally, we recommend that the correlation of flame shapes for nonbuoyant laminar-jet diffusion flames in coflowing air [Eqs. (9–12)] be used with caution outside the present test range and until the results are definitively confirmed for long-term microgravity conditions where the intrusion of effects of transient flame development and buoyancy are absent. In particular, past observations of the shapes of steady nonbuoyant laminar-jet diffusion flames in still gases based on space-based observations in microgravity generally have been found to differ from earlier measurements obtained using ground-based facilities due to effects of transient flame development and disturbances due to buoyancy. The present conclusions concerning effects of burner diameter follow from the simplified theory; experimental evaluation of these trends is needed.

Acknowledgments

This research was supported by NASA Grants NAG3-1245 and NAG3-2048 under the technical management of David L. Urban of the NASA Lewis Research Center and by Office of Naval Research Grant N00016-95-0238 under the technical management of Gabriel D. Roy.

References

[1]Bilger, R. W., "Reaction Rates in Diffusion Flames," *Combustion and Flame*, Vol. 30, No. 3, 1977, pp. 277–284.

[2]Burke, S. P., and Schumann, T. E. W., "Diffusion Flames," *Industrial and Engineering Chemistry*, Vol. 20, No. 10, 1928, pp. 998–1004.

[3]Law, C. K., and Faeth, G. M., "Opportunities and Challenges of Combustion in Microgravity," *Progress in Energy and Combustion Sciences*, Vol. 20, No. 1, 1994, pp. 65–113.

[4]Lin, K.-C., Faeth, G. M., Sunderland, P. B., Urban, D. L., and Yuan, Z.-G., "Shapes of Nonbuoyant Round Luminous Hydrocarbon/Air Laminar Jet Diffusion Flames," *Combustion and Flame*, Vol. 116, No. 3, 1999, pp. 415–431.

[5]Spalding, D. B., *Combustion and Mass Transfer*, Pergamon, New York, 1979, pp. 185–195.

[6]Kuo, K. K., *Principles of Combustion*, Wiley, New York, 1986, pp. 360–370.

[7]Urban, D. L., Yuan, Z.-G., Sunderland, P. B., Linteris, G. T., Voss, J. E., Lin, K.-C., Dai, Z., Sun, K., and Faeth, G. M., "Structure and Soot Properties of Nonbuoyant Ethylene/Air Laminar Jet Diffusion Flames," *AIAA Journal*, Vol. 36, No. 8, 1998, pp. 1346–1360.

[8]Sunderland, P. B., Mendelson, B. J., Yuan, Z.-G., and Urban, D. L., "Shapes of Buoyant and Nonbuoyant Laminar Jet Diffusion Flames," *Combustion and Flame*, Vol. 116, No. 3, 1999, pp. 376–386.

[9]Sunderland, P. B., Mortazavi, S, Faeth, G. M., and Urban, D. L., "Laminar Smoke Points of Nonbuoyant Jet Diffusion Flames," *Combustion and Flame*, Vol. 96, No. 1, 1994, pp. 97–103.

[10]Schug, K. P., Manheimer-Timnat, Y., Yaccarino, P., and Glassman, I., "Sooting Behavior of Gaseous Hydrocarbon Diffusion Flames and the Influence of Additives," *Combustion Science and Technology*, Vol. 22, No. 5/6, 1980, pp. 235–250.

[11]Gomez, A., Sidebotham, G., and Glassman, I., "Sooting Behavior in Temperature-Controlled Laminar Diffusion Flames," *Combustion and Flame*, Vol. 58, No. 1, 1984, pp. 45–57.

[12]Mitchell, R. E., Sarofim, A. F., and Clomberg, L. A., "Experimental and Numerical Investigation of Confined Laminar Diffusion Flames," *Combustion and Flame*, Vol. 37, No. 3, 1980, pp. 227–244.

[13]Saito, K., Williams, F. A., and Gordon, A. S., "Structure of Laminar Coflow Methane-Air Diffusion Flames," *Journal of Heat Transfer*, Vol. 108, No. 3, 1986, pp. 640–648.

[14]Saito, K., Williams, F. A., and Gordon, A. S., "Effects of Oxygen on Soot Formation in Diffusion Flames," *Combustion Science and Technology*, Vol. 47, No. 3/4, 1986, pp. 117–138.

[15]Sunderland, P. B., "Soot Nucleation and Growth in Weakly Buoyant Laminar Jet Diffusion Flames," Ph.D. Dissertation, Dept. of Aerospace Engineering, Univ. of Michigan, Ann Arbor, MI, June 1995.

[16]Sunderland, P. B., Köylü, Ü. Ö., and Faeth, G. M., "Soot Formation in Weakly Buoyant Acetylene-Fueled Laminar Jet Diffusion Flames Burning in Air," *Combustion and Flame*, Vol. 100, No. 1/2, 1995, pp. 310–322.

[17]Lin, K.-C., "Hydrodynamic Effects on Soot Formation in Laminar Hydrocarbon-Fueled Diffusion Flames," Ph.D. Dissertation, Dept. of Aerospace Engineering, Univ. of Michigan, Ann Arbor, MI, June 1996.

[18]Lin, K.-C., Sunderland, P. B., and Faeth, G. M., "Soot Nucleation and Growth in Acetylene/Air Laminar Coflowing Jet Diffusion Flames," *Combustion and Flame*, Vol. 104, No. 3, 1996, pp. 369–375.

[19]Lin, K.-C., and Faeth, G. M., "Hydrodynamic Suppression of Soot Emissions in Laminar Diffusion Flames," *Journal of Propulsion and Power*, Vol. 12, No. 1, 1996, pp. 10–17.

[20]Cochran, T. H., and Masica, W. J., "An Investigation of Gravity Effects on Laminar Gas Jet Diffusion Flames," *Thirteenth Symposium (International) on Combustion*, Combustion Inst., Pittsburgh, PA, 1970, pp. 821–829.

[21]Haggard, J. B., Jr., and Cochran, T. H. "Stable Hydrocarbon Diffusion Flames in a Weightless Environment," *Combustion Science and Technology*, Vol. 5, No. 4–6, 1972, pp. 291–298.

[22]Edelman, R. B., Fortune, O. F., Weilerstein, G., Cochran, T. H., and Haggard, J. B., Jr., "An Analytical and Experimental Investigation of Gravity Effects upon Laminar Gas Jet-Diffusion Flames," *Fourteenth Symposium (International) on Combustion*, Combustion Inst., Pittsburgh, PA, 1972, pp. 399–412.

[23]Edelman, R. B., and Bahadori, M. Y., "Effects of Buoyancy on Gas-Jet Diffusion Flames: Experiment and Theory," *Acta Astronautica*, Vol. 13, No. 11/12, 1986, pp. 681–688.

[24]Bahadori, M. Y., Edelman, R. B., Stocker, D. P., and Olson, S. L., "Ignition and Behavior of Laminar Gas-Jet Diffusion Flames in Microgravity," *AIAA Journal*, Vol. 28, No. 2, 1990, pp. 236–244.

[25]Bahadori, M. Y., Stocker, D. P., and Edelman, R. B., "Effects of Pressure on Microgravity Hydrocarbon Diffusion Flames," AIAA Paper 90-0651, Jan. 1990.

[26]Bahadori, M. Y., Edelman, R. B., Sotos, R. G., and Stocker, D. P., "Radiation from Gas-Jet Diffusion Flames in Microgravity Environments," AIAA Paper 91-0719, Jan. 1991.

[27]Bahadori, M. Y., Edelman, R. B., Stocker, D. P., Sotos, R. G., and Vaughan, D. F., "Effects of Oxygen Concentration on Radiative Loss from Normal-Gravity and Microgravity Methane Diffusion Flames," AIAA Paper 92-0243, Jan. 1992.

[28]Jost, W., *Explosion and Combustion Processes in Gases*, McGraw–Hill, New York, 1946, Chap. 1.

[29]Roper, F. G., "Prediction of Laminar Jet Diffusion Flames; Part I: Theoretical Model," *Combustion and Flame*, Vol. 29, No. 3, 1977, pp. 219–226.

[30]Roper, F. G., Smith, C., and Cunningham, A. C., "The Predictions of Laminar Jet Diffusion Flame Sizes: Part II. Experimental Verification," *Combustion and Flame*, Vol. 29, No. 3, 1977, pp. 227–234.

[31]Klajn, M., and Oppenheim, A. K., "Influence of Exothermicity on the Shape of a Diffusion Flame," *Nineteenth Symposium (International) on Combustion*, Combustion Inst., Pittsburgh, PA, 1982, pp. 223–235.

[32]Li, S. C., Gordon, A. S., and Williams, F. A., "A Simplified Method for the Computation of Burke-Schumann Flames in Infinite Atmospheres," *Combustion Science and Technology*, Vol. 104, No. 1–3, 1995, pp. 75–91.

[33]Ban, H., Venkatesh, S., and Saito, K., "Convection-Diffusion Controlled Laminar Micro Flames," *Journal of Heat Transfer*, Vol. 116, No. 4, 1994, pp. 954–959.

[34]Williams, F. A., *Combustion Theory*, 2nd ed., Benjamin/Cummings Publishing, Menlo Park, CA, 1985, pp. 38–47.

[35]Mahalingam, S., Ferziger, J. H., and Cantwell, B. J., "Self-Similar Diffusion Flames," *Combustion and Flame*, Vol. 82, No. 2, 1990, pp. 231–234.

[36]Hamins, A., Gordon, A. S., Saito, K., and Seshadri, K., "Acetone Impurity in Acetylene from Tanks," *Combustion Science and Technology*, Vol. 45, No. 5, 1986, pp. 309–310.

[37]Schlichting, H., *Boundary Layer Theory*, 4th ed., McGraw–Hill, New York, 1960, pp. 160–164.

[38]Braun, W. G., Danner, R. P., and Daubert, T. E., *Technical Data Book—Petroleum Refining*, 3rd ed., American Petroleum Inst., Washington, DC, 1976, Chaps. 11 and 13.

S. K. Aggarwal
Associate Editor

Appendix B:

K.-C. Lin, G.M. Faeth, P.B. Sunderland, D.L. Urban, and Z.-G. Yuan (1999) Shapes of nonbuoyant round luminous hydrocarbon/air laminar jet diffusion flames. *Combust. Flame* 116, 415-431.

Shapes of Nonbuoyant Round Luminous Hydrocarbon/Air Laminar Jet Diffusion Flames

K.-C. LIN, G. M. FAETH*
The University of Michigan, Ann Arbor, Michigan 48109

P. B. SUNDERLAND, D. L. URBAN, and Z.-G. YUAN
NASA Lewis Research Center, Cleveland, Ohio 44135

The shapes (luminous flame boundaries) of round luminous nonbuoyant soot-containing hydrocarbon/air laminar jet diffusion flames at microgravity were found from color video images obtained on orbit in the Space Shuttle Columbia. Test conditions included ethylene- and propane-fueled flames burning in still air at an ambient temperature of 300 K, ambient pressures of 35–130 kPa, initial jet diameters of 1.6 and 2.7 mm, and jet exit Reynolds numbers of 45–170. Present test times were 100–200 s and yielded steady axisymmetric flames that were close to the laminar smoke point (including flames both emitting and not emitting soot) with luminous flame lengths of 15–63 mm. The present soot-containing flames had larger luminous flame lengths than earlier ground-based observations having similar burner configurations: 40% larger than the luminous flame lengths of soot-containing low gravity flames observed using an aircraft (KC-135) facility due to reduced effects of accelerative disturbances and unsteadiness; roughly twice as large as the luminous flame lengths of soot-containing normal gravity flames due to the absence of effects of buoyant mixing and roughly twice as large as the luminous flame lengths of soot-free low gravity flames observed using drop tower facilities due to the presence of soot luminosity and possible reduced effects of unsteadiness. Simplified expressions to estimate the luminous flame boundaries of round nonbuoyant laminar jet diffusion flames were obtained from the classical analysis of Spalding (1979); this approach provided successful correlations of flame shapes for both soot-free and soot-containing flames, except when the soot-containing flames were in the opened-tip configuration that is reached at fuel flow rates near and greater than the laminar smoke point fuel flow rate.

NOMENCLATURE

C_f	empirical flame length parameter
d	jet exit diameter
D	mass diffusivity
L_o	distance from jet exit to virtual origin
L_f	distance from jet exit to luminous flame tip
$\dot{m}$	burner mass flow rate
p	pressure
Re	jet Reynolds number, $4\,\dot{m}/(\pi d\mu)$
r	radial distance
Sc	Schmidt number, ν/D
t_{ch}	characteristic residence time, $2L_f/u_o$
u_o	mean burner exit velocity, $4\,\dot{m}/(\pi\rho_o d^2)$
w	luminous flame diameter
w_{MAX}	maximum luminous flame diameter
$w_{1/2}$	luminous flame diameter at $\zeta = 1/2$.
Z_{st}	stoichiometric mixture fraction
z	streamwise distance
ζ	normalized streamwise distance, Eq. 6
μ	dynamic viscosity
ν	kinematic viscosity
ρ	density

Subscripts

o	burner exit condition

INTRODUCTION

Observations of nonbuoyant laminar diffusion flames are described which were obtained at microgravity on board the orbiting Space Shuttle Columbia. Laminar diffusion flames are of interest because they provide model flame systems that are far more tractable for theoretical and experimental studies than more practical turbulent diffusion flames. Laminar diffusion flames also merit study because understanding their transport and chemical reaction processes is a necessary precursor to understanding these processes in turbulent diffusion flames. In addi-

*Corresponding author. E-mail: gmfaeth@umich.edu

COMBUSTION AND FLAME 116:415–431 (1999)

Published by Elsevier Science Inc.

0010-2180/99/$19.00
PII S0010-2180(98)00100-X

tion, many aspects of laminar diffusion flames have direct relevance to turbulent diffusion flames by application of the laminar flamelet concept of turbulent diffusion flames [1]. The present study specifically considered the shapes (the luminous flame boundaries) of laminar diffusion flames, which is a flame property that has attracted numerous investigations since the classical study of Burke and Schumann [2]. This interest follows because simple nonintrusive measurements yield flame shapes, which can be used to evaluate theories of laminar flame processes and predictions of laminar flame structure. A concern about measurements of the shapes of laminar diffusion flames at normal gravity, however, involves the intrusion of disturbances due to buoyancy because they are not relevant to practical diffusion flames, which generally are not buoyant due to their large velocities. These buoyant disturbances also tend to obscure important properties of the nonbuoyant flames that are of the greatest interest [3]. Thus, the present investigation sought measurements of the shapes of classical steady nonbuoyant round laminar jet diffusion flames by exploiting the long-term microgravity environment of an orbiting space shuttle. The objectives of this paper are to document these measurements and to develop a summary of the results, convenient for use by others, based on simplified analysis of nonbuoyant laminar jet diffusion flames.

Past measurements of the shapes of nonbuoyant laminar jet diffusion flames have been carried out using either drop towers to provide microgravity environments [4–13] or aircraft facilities [14] to provide low-gravity environments. The earliest work along these lines was a series of studies of hydrocarbon-fueled laminar jet diffusion flames using a 2.2 s free-fall (drop) tower due to Cochran and co-workers [4–6]. They ignited the flames before putting the experiment package into free-fall and observed an immediate reduction of the luminous flame length when the flame was exposed to the low gravity environment. The subsequent transient development of the flame shape, combined with the relatively short duration of the microgravity environment, raised concerns about the results due to potential effects of unsteady flame development. Another problem with measurements of the shapes of hydrocarbon-fueled flames is that the luminosity of these flames is mainly caused by glowing soot particles, particularly along the flame axis where luminous flame lengths are normally measured. Thus, the relationship between luminous flame dimensions and the location of the flame sheet (where the local mixture fraction is stoichiometric) is an issue because the latter generally is associated with predictions of laminar flame shapes. Past measurements of the flame structure and soot properties of weakly buoyant and buoyant round laminar jet diffusion flames burning in still or slowly moving air provide some information about luminous and stoichiometric flame lengths [15–18]. These observations indicate that ratios of luminous- to stoichiometric-flame lengths are in the range 0.9–1.8, with these ratios increasing as the laminar smoke point flame length is approached [15–18]. This behavior comes about because soot oxidation begins at slightly fuel-rich conditions and can continue in the fuel-lean region for a time before either the soot is consumed (non-soot-emitting flames), or the soot oxidation reactions are quenched (soot-emitting flames), with luminous flame lengths varying accordingly [15].

Studies following the work of Cochran and coworkers [4–6] due to Bahadori and coworkers [7–12] sought to resolve potential effects of transient flame development and soot luminosity on measurements of the shape of nonbuoyant round laminar jet diffusion flames using both 2.2 s and 5.2 s drop towers. In order to minimize problems of transient behavior, they ignited the flames shortly after the experimental package was released and observed nearly steady flame shapes near the end of free fall. Nevertheless, temperature fields and radiation emissions of the flames were still changing at the end of the 5.2s free-fall periods for the flame conditions that they considered, implying that transient effects had still not fully relaxed during the available microgravity test time.

Sunderland et al. [14] considered the luminous flame lengths of nonbuoyant soot-containing round laminar jet diffusion flames as part of a study of the laminar smoke point properties of nonbuoyant laminar diffusion flames. These experiments were carried out in a KC-135 aircraft facility that provided roughly 20 s at low gravity

by flying parabolic trajectories. It was hoped that these long low-gravity test times would minimize effects of transient flame development on observed flame shapes. These flames all approached laminar smoke point conditions and should be representative of long luminous flame lengths discussed earlier. Unfortunately, the KC-135 aircraft facility provided a rather disturbed low-gravity environment (with significant g-jitter) with the accompanying unsteady effects influencing both flame shapes and laminar smoke point properties [14].

In spite of potential effects of unsteadiness for the ground-based studies of nonbuoyant laminar jet diffusion flames, however, Cochran and co-workers [4–6], Bahadori and co-workers [7–12], and Sunderland et al. [14] all observed a linear correlation between luminous flame lengths and fuel flow rates, independent of jet exit diameter, for each fuel burning in air. This behavior also is typical of the luminous flame lengths of buoyant round laminar jet diffusion flames [19]. Thus, to the extent that this linear relationship is retained for truly steady and nonbuoyant laminar jet diffusion flames, it offers an important characteristic useful for testing flame shape predictions.

Most recently, Sunderland et al. [13] sought to avoid problems of both unsteadiness and soot luminosity by measuring the shape of soot-free laminar jet diffusion flames using a 2.2 s drop tower facility. Ambient pressures, jet exit diameters and fuel flow rates were controlled to provide soot-free (blue) laminar jet diffusion flames having relatively small characteristic flame residence times so that unsteady effects were potentially minimized. These results for soot-free flames exhibit generally shorter flame lengths than corresponding soot-containing flames but the limited flame development period at microgravity still introduces uncertainties in the flame shape measurements due to potential effects of transient flame development.

The shapes of laminar jet diffusion flames also have attracted significant theoretical attention. Measured flame lengths for both soot-free and soot-containing flames have been used to develop empirical models and to evaluate theoretical predictions for a range of buoyant conditions. The most well-known empirical model for laminar diffusion flames is the linear correlation between the luminous flame length and the corresponding fuel flow rate [19] that was mentioned earlier. Several laminar diffusion flame models of varying complexity also have been proposed [20–26] that successfully predict the linear correlation between stoichiometric flame lengths and the fuel flow rates (or equivalently between the stoichiometric flame length normalized by the jet exit diameter and the jet exit Reynolds number). Among these, the analysis of Spalding [22] (which is described in some detail by Kuo [23]) offers a potentially simple and robust method for estimating the shapes of steady nonbuoyant round laminar jet diffusion flames. Nevertheless, modifications of this approach to deal with soot-containing flames (as opposed to soot-free flames), the capabilities of this approach to estimate (or correlate) all flame shape properties (as opposed to simply luminous flame lengths), and the performance of this approach for truly steady and nonbuoyant round laminar jet diffusion flames, are all issues that need to be addressed.

Based on the previous discussion of the literature, several aspects of the shape of nonbuoyant round laminar jet diffusion flames need to be resolved, as follows: to what extent have past observations using ground-based microgravity facilities been affected by transient development or disturbances of the flames, to what extent have differences between stoichiometric conditions and the limits of visible luminosity from soot affected estimates of flame shapes, and to what extent can flame shape data be predicted (correlated) by simplified analysis? These issues were addressed during the present investigation based on observations of nonbuoyant round laminar jet diffusion flames at long-duration microgravity conditions on board the orbiting Space Shuttle Columbia, and by evaluation of simplified analysis of flame structure using these observations, with the following specific objectives:

1. Measure the shapes (luminous flame boundaries), and associated properties such as luminous flame lengths and diameters, for various fuel types, jet exit diameters, jet exit flow rates (Reynolds numbers), and ambient pressures.

2. Compare the present measurements with earlier ground-based observations having similar burner conditions in order to help quantify effects of transient flame development, flow disturbances (g-jitter), soot luminosity, and buoyancy on flame shape properties.
3. Exploit the measurements in order to evaluate the simple flame shape analysis of Spalding [22] and develop this approach to provide convenient correlations of flame shape measurements for use by others.

Present observations were limited to soot-containing ethylene- and propane-fueled flames burning in still dry air, at conditions near the laminar smoke point.

The following description of the study begins with consideration of experimental methods, test conditions, and theoretical methods. Results are then discussed, considering luminous flame lengths, luminous flame diameters, and luminous flame shapes, in turn. Major conclusions are summarized at the end of the article.

EXPERIMENTAL METHODS

Experimental methods will be only briefly described; see Urban et al. [27] for more details. The laminar jet diffusion flames were stabilized at the exit of round fuel nozzles located along the axis of a windowed cylindrical chamber. The chamber had a diameter of 400 mm, a maximum length of 740 mm, an internal volume of 0.082 m^3, and was operated at pressures of 35–130 kPa. The chamber was filled with oxygen/nitrogen mixtures to provide the nominal composition of dry air (21 ± 1% oxygen by volume). The pressure, temperature, and composition of the gas surrounding the test flames all varied slightly over the flame burning periods due to the limited amount of air within the closed chamber. The greatest change involved the composition of gas within the chamber but even this was controlled so that the maximum oxygen consumption never exceeded 2% by volume during any flame test. These conditions were maintained by venting the chamber to space and adding fresh dry air (as needed) prior to each test.

Two fuel nozzles, consisting of constant diameter cylindrical stainless steel tubes having inside diameters of 1.6 and 2.7 mm, wall thicknesses of 0.28 mm, and lengths of 148 mm from the inlet plenum, were used. The inlets of these nozzles had flow straighteners while the overall length-to-diameter ratios of the passages were greater than 55:1, which was sufficient to yield fully developed laminar pipe flow at the nozzle exit for the present test conditions ($172 \geq Re_o \geq 46$). The test fuels were stored in cylinders and were delivered to the nozzles through solenoid valves and a mass flow rate controller and sensor. The flames were ignited by a hot wire coil that was retracted from the nozzle exit once ignition was successful.

Several measurements were made to monitor flame operation as follows: fuel flow rate with an accuracy of 0.8%, fuel temperature at the nozzle inlet with an accuracy of ±1.5 K, chamber pressure with an accuracy of 1.2%, and chamber gas temperature (far from flames) with an accuracy of ±1 K. These measurements were recorded at a rate of approximately 1 Hz.

Flame shapes (luminous flame boundaries) were measured from images obtained using a standard color CCD video camera (Hitachi, Model KP-C553). The camera had a 125 × 164 mm field of view and a depth of field of 25 mm centered on the flame axis. The spatial resolution of the recorded images was better than 0.3 mm. It was not possible to adjust image brightness on orbit; therefore, it was necessary to select camera settings so that the flames having the smallest levels of luminosity (found from ground-based tests at microgravity using a free-fall facility) could still be observed. This implied that the flame images were generally overexposed although they still provided sharp images of luminous flame boundaries. Flame images were recorded at a rate of 30 images/s. The flames were unusually symmetric; nevertheless, the shapes reported here represent average positions for the two sides.

TEST CONDITIONS

The test conditions of the present flames are summarized in Table 1. A total of 21 flames were observed, yielding the following ranges of test properties: ethylene- and propane-fueled

TABLE 1

Summary of Test Conditions

Test[a]	p (kPa)	$\dot{m}$ (mg/s)	u_o[b] (mm/s)	Re_o (−)	t_{ch} (ms)	L_f (mm)	w_{MAX} (mm)
C_2H_4/air flames, d = 1.6 mm, Z_{st} = 0.0636:							
01E*	100	1.84	820	138	121	49.3	13.7
03E*	50	1.84	1630	138	77	63.0	14.2
01E	100	0.71	320	54	130	20.6	12.6
02E	50	0.76	670	57	53	17.7	13.1
03E	50	1.29	1140	97	64	36.5	13.8
04E	65	0.91	620	68	86	26.5	13.1
14E	80	0.67	370	50	97	18.0	12.9
15E	100	0.61	270	46	109	14.7	11.5
16E	65	0.74	510	56	75	19.0	13.4
17E	35	1.34	1690	100	40	34.0	14.7
C_2H_4/air flames, d = 2.7 mm, Z_{st} = 0.0636:							
05E	65	1.14	270	51	215	29.1	21.4
06E	80	1.16	230	51	269	30.3	20.9
07E	100	1.08	170	48	302	25.5	19.6
08E	50	1.38	430	62	173	37.3	21.4
C_3H_8/air flames, d = 1.6 mm, Z_{st} = 0.0602:							
09P	130	0.78	170	73	277	23.3	17.4
10P	50	1.82	1020	172	120	61.4	18.8
11P	65	1.22	530	116	144	38.1	17.4
12P	100	0.88	250	83	218	27.1	16.6
13P	80	1.04	370	99	177	32.4	17.2
18P	80	0.82	290	78	164	23.9	16.9
19P	100	0.71	200	67	191	19.0	16.1

[a] 01E* and 03E* were carried out on flight STS-83, all other tests were carried out on flight STS-94. Only tests 01E*, 03E*, and 01E involved soot-emitting flames in the period when flame shape observations were made.

[b] Mean velocity based on fuel density at jet exit (nominal pressure and 300 K).

[c] Mean Reynolds number based on fuel viscosities at jet exit (300 K), i.e., 10.6 mg/(sm) for ethylene and 8.4 mg/(sm) for propane.

flames in burning dry air, ambient temperatures and pressures of 300 K and 35–130 kPa, jet exit diameters of 1.6 and 2.7 mm, jet exit velocities of 170–1630 mm/s, jet exit Reynolds numbers of 46–172, characteristic residence times (defined as $2L_f/u_o$) of 40–302 ms, and luminous flame lengths of 15–63 mm.

For convenience, the test numbers have the suffixes E and P to denote ethylene- and propane-fueled flames, respectively. Asterisks are used to denote the two tests completed during flight STS-83. It should be noted that the characteristic residence times of the present flames are large (40–302 ms) compared to most practical applications where characteristic residence times are typically less than 10 ms. As mentioned earlier, present flames were generally relatively close to laminar smoke point conditions with test flames 01E*, 03E*, and 01E actually emitting soot in the period when flame shape observations were made. The remaining flames all contained soot but were not emitting soot.

THEORETICAL METHODS

The goal of the analysis was to develop a convenient method to help interpret and correlate the present flame shape measurements. A set of easily used equations was sought, along with recommendations for selecting the thermochemical and transport properties appearing in these equations, as opposed to more complete methods that would require numerical solutions on a computer. Thus, the basis for this approach was the simplified analysis of nonbuoyant round laminar jet diffusion flames due to Spalding

[22]. The following description of the analysis is brief and concentrates on the present application of the approach; see Spalding [22] and Kuo [23] for more details.

The major assumptions of the flame shape analysis of Spalding [22] are as follows: (1) attention is limited to steady, axisymmetric laminar jet diffusion flames burning at constant pressure in still environments; (2) effects of buoyancy and associated changes of potential energy are negligible; (3) the Mach number of the flow is small so that effects of viscous dissipation and changes of kinetic energy can be ignored; (4) the flame has a large aspect ratio so that diffusion of mass (species), momentum, and energy in the streamwise direction is small; (5) for the same reasons, the solution of the governing equations can be approximated by far-field conditions where the details of initial conditions at the jet exit can be replaced by jet invariants for the conservation of mass (elements), momentum, and energy in the integral sense; (6) all chemical reactions occur in a thin flame sheet with fast chemistry so that fuel and oxidant are never simultaneously present at finite concentrations; (7) the diffusivities of mass (of all species), momentum and energy are all equal; (8) all thermophysical and transport properties are constant throughout the flame; and (9) effects of radiation are small. The first three assumptions are justified as conditions of the present experiments. The fourth and fifth assumptions are justified for at least the portion of the present measurements that have large aspect ratios (e.g., present measurements summarized in Table 1 involve flame aspect ratios, $2L_f/w_{MAX}$, in the range 2–9, and burner aspect ratios, L_f/d, roughly four times larger). The sixth assumption prescribing a thin diffusion flame sheet has a long history of effective application to find the shape of laminar diffusion flames, extending back to the classical work of Burke and Schumann [2]. The remaining assumptions, however, are not satisfied by laminar jet diffusion flames and were only adopted here so that a simple formula for flame shapes could be found, and due to past success of similar approximations for analysis of the shapes of laminar diffusion flames [20–24].

Solution of the governing equations using the present assumptions, after associating the location of the luminous flame boundary with the location of the thin flame sheet where the stoichiometric mixture fraction is reached, yields the following expression for the luminous flame length [22, 23]:

$$L_f/d = (3/32)Re/Z_{st}. \quad (1)$$

The value of Z_{st} in Eq. 1 can be found simply as the mass fraction of burner exit fluid (fuel in the present case) in a stoichiometric mixture of burner-exit fluid and ambient fluid (air in the present case); these values are summarized in Table 1 for the present test conditions. The variation of Z_{st} is not large for combustion of hydrocarbon/air mixtures; thus, while the variation of Z_{st} is small for present experiments, the values considered are relevant to many practical applications. The corresponding expression for the flame shape, yielding the flame diameter as a function of streamwise distance, is as follows:

$$wZ_{st}/d = 3^{1/2}(z/L_f)[(L_f/z)^{1/2} - 1]^{1/2}. \quad (2)$$

Differentiating Eq. 2, and setting the result equal to zero, provides expressions for the maximum flame diameter and the streamwise distance where this maximum diameter is reached, as follows:

$$w_{MAX}Z_{st}/d = 9/16 \quad \text{at} \quad z/L_f = 9/16. \quad (3)$$

Correlation of the measurements was sought by selecting conditions to find mean transport properties and introducing some empirical parameters to match measurements and predictions. First of all, the equal diffusivity approximation was relaxed by introducing the Schmidt number into Eq. 1 because the flame sheet is mainly affected by mass transport properties represented by the Schmidt number. Transport properties affect Eqs. 1–3 through the Schmidt number and the viscosity used to compute the Reynolds number. It was found that a reasonable correlation of luminous flame lengths could be obtained by approximating these properties by the properties of air at the average of the adiabatic flame temperature and the ambient temperature. This selection seems reasonable because air-like gases dominate the composition of the present flames. The properties needed to find the Schmidt number and the mean gas viscosity were taken from Braun et al.

[28]. The range of the flame shape correlations was extended to flames having small aspect ratios by introducing a virtual origin at a distance L_o from the jet exit, which is a conventional step for properties like luminous flame lengths. The flame length expression was then fine-tuned by introducing an empirical coefficient, C_f, as discussed later. With these changes, Eq. 1 for the luminous flame length becomes:

$$(L_f - L_o)/d = (3C_f/32)ReSc/Z_{st}, \quad (4)$$

while Eq. 2 for the luminous flame diameter becomes

$$wZ_{st}/d = 3^{1/2}\zeta(\zeta^{-1/2} - 1)^{1/2}, \quad (5)$$

where

$$\zeta = (z - L_o)/(L_f - L_o). \quad (6)$$

Thus, the flame radius properties are only indirectly affected by assumed transport properties, through the computation of the flame length of Eq. 4.

RESULTS AND DISCUSSION

Flame Appearance

Ignition conditions were established during ground-based tests at microgravity using a free-fall facility and involved fuel flow rates greater than the values used during the present flame tests. Thus, after ignition was confirmed, fuel flow rates were reduced to conditions near but generally smaller than the laminar smoke point fuel flow rates. Exceptions to this practice where tests 01E*, 03E*, and 01E, that were soot emitting.

After the fuel flow rate was set, an additional 5–10 s was required for disturbances to decay away. The flames were then observed during an 80–180 s quasi-steady burning period where flame shapes and colors changed slowly due to the modest variations of oxygen concentrations, pressures and temperatures of the gas within the test chamber, see Urban et al. [27] for typical records of chamber gas properties as a function of time during the experiments. Video records used for the present flame shape measurements were obtained near the start of the quasi-burning period; therefore, the test conditions correspond to the nominal conditions summarized in Table 1 within experimental uncertainties.

Typical of many past observations of soot-containing nonbuoyant laminar jet diffusion flames [8–14], present flame shapes could be grouped into closed-tip and opened-tip configurations, which were observed for fuel flow rates smaller and larger than the laminar smoke point fuel flow rates, respectively. In fact, the tip-opening phenomenon provided a convenient indicator of laminar smoke points for present test conditions because the associated dramatic change of the shape of the flame tip invariably corresponded to the first observations of soot emissions.

Some typical video records of the present closed-tip laminar nonbuoyant jet diffusion flames are illustrated in Fig. 1. The test numbers, corresponding to the test numbers of Table 1, are marked below each image. The flames illustrated include both ethylene- and propane-fueled flames for jet exit diameters of 1.6 mm. The jet exits, which are visible only in the images of tests 02E, 03E, 16E, and 17E, are on the same side of each image as the test number. As noted earlier, fixed camera settings imply that images of some strongly-luminous flames are overexposed. Thus, while the images provide a general indication of regions of the flames that have different colors, they do not provide an accurate representation of actual flame colors. In spite of this limitation, however, luminous flame shapes and corresponding flame shape parameters (e.g., luminous flame lengths and diameters) can still be identified from the video images. In addition to the brightly luminous region caused by the presence of glowing soot velocities, blue luminosity can be seen near the jet exit and just beyond the edge of the brightly luminous region, particularly near the base of the flame. The blue region was never resolved clearly, however, and was not visible at all near the flame tip due to the presence of the brightly luminous region. Finally, as the laminar smoke point fuel flow rate was approached, the flames tended to become blunt as a precursor to the tip-opening phenomena; thus, the images of tests 02E, 16E, and 18P are typical of blunt closed-tip flames.

The present measurements of flame shapes

were based on the boundary of the brightly luminous region caused by visible radiation from soot because this was the most obvious indication of luminous flame shape. The stoichiometric flame sheet (the flame sheet based on the location of the stoichiometric mixture fraction) also is of great interest but this condition could not be resolved, as already discussed. Thus, the relationship between the luminous flame boundaries and the position of the stoichiometric flame sheet is important for interpreting the present measurements. Soot concentration and temperature records suggest that the present luminous flame boundaries lie just inside the stoichiometric flame sheet along the sides of the flame, not too near the flame tip; see Urban et al. [27] for some typical examples. The same evidence suggests that the present luminous flame boundaries extend beyond the stoichiometric flame sheet in the streamwise direction near the flame tip, due to soot burnout in the lean portions of the flames because present test conditions were close to laminar smoke points. Unfortunately, the extent of the streamwise overlap cannot be quantified directly because local mixture fractions are not known for the present flames. As discussed earlier, past measurements in laminar jet diffusion flames suggest that the luminous flame length might be as much as twice the flame length based on the location of the stoichiometric conditions along the axis for conditions near the laminar smoke point [15–18]. Thus, in order to help quantify differences between luminous and stoichiometric flame lengths, the flame lengths of both soot-containing and soot-free nonbuoyant laminar jet diffusion flames for similar burner and buoyancy conditions will be compared in the following.

Some typical video records of opened-tip nonbuoyant laminar jet diffusion flames are illustrated in Fig. 2. The identification of test conditions and the location of the burner exit are the same as Fig. 1. The flames illustrated include ethylene-fueled flames for a jet exit diameter of 2.7 mm and propane-fueled flames for a jet exit diameter of 1.6 mm. The dramatic difference between the shape of the tips of closed- and opened-tipped flames is clearly evident by comparing the flame images of Figs. 1 and 2. Measurements of the structure of opened-tipped flames show that soot is mainly confined to an annular region, and that little soot is present along the flame axis [27]. Thus, soot luminosity from the annular-soot containing region, combined with small levels of soot luminosity along the axis, is responsible for the blunt or even cusp-like luminous shape of the tip of these flames when viewed from the side as projections. The flames illustrated in Fig. 2 have fuel flow rates slightly smaller than the laminar smoke point fuel flow rates. Video images of opened-tip flames that are emitting soot, tests 01E* and 03E*, appear in Urban et al. [27]; however, they are qualitatively similar to the opened-tip flames illustrated in Fig. 2.

Flame Lengths

The luminous flame length of laminar jet diffusion flames is a widely reported property that is used to both characterize flame shapes and to summarize soot emission properties (as laminar smoke point flame lengths). The luminous flame lengths reported here are the streamwise distances between the burner exit and the farthest downstream plane normal to the flame axis that contacts a luminous region of the flame [either along the axis for closed-tip (non-soot-emitting or nonsooting) flames or at the annular soot layer for opened-tip (nonsooting and soot-emitting or sooting) flames]. It is well known that L_f/d can be correlated as a linear function of the jet exit Reynolds numbers, Re, for buoyant laminar jet diffusion flames for a given fuel and ambient environment, however, each fuel has its own individual correlation curve [19–24]. Thus, the performance of similar correlations will be considered for the present nonbuoyant laminar jet diffusion flames, based on the simple classical theory of Spalding [22] as discussed earlier, seeking a general correlation capable of treating various fuels, burner diameters, and ambient environments (pressures, temperatures, oxygen concentrations, etc.).

Measured and predicted luminous flame lengths of the present nonbuoyant laminar jet diffusion flames are illustrated in Fig. 3. These results are presented as suggested by the modified Spalding [22] analysis, Eq. 4, with $(L_f - L_o)/d$ plotted as a function of $ReSc/Z_{st}$. Measured luminous flame lengths are shown for all

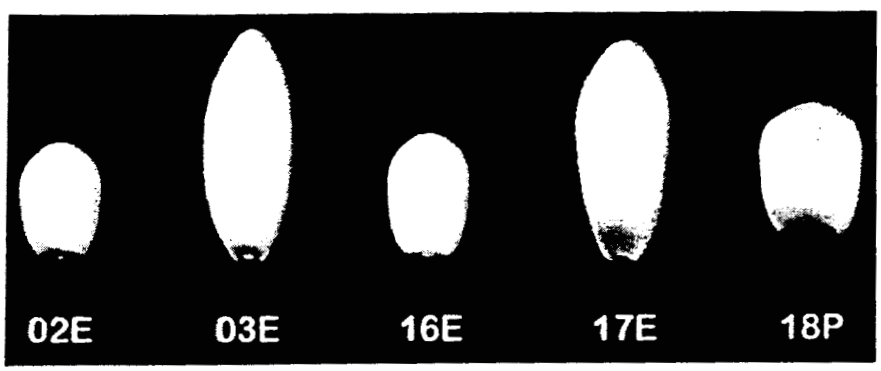

Fig. 1. Video images of typical closed-tip luminous hydrocarbon/air laminar jet diffusion flames (Tests 02E, 03E, 16E, 17E, and 18P).

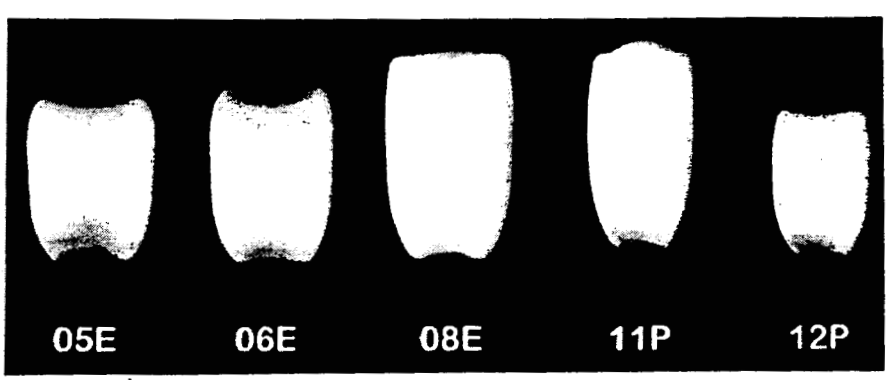

Fig. 2. Video images of typical opened-tip luminous hydrocarbon/air laminar jet diffusion flames (Tests 05E, 06E, 08E, 11P, and 12P).

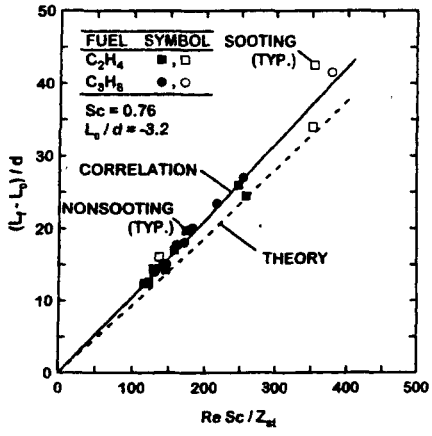

Fig. 3. Measured and predicted luminous flame lengths of nonbuoyant hydrocarbon/air laminar jet diffusion flames as a function of $ReSc/Z_{st}$; measurements from present space-based experiments.

the test conditions summarized in Table 1, with non-sooting and sooting flames denoted by closed and open symbols, respectively. The values of Z_{st} used for the ethylene-fueled and propane-fueled flames are summarized in Table 1; other properties were taken from Braun et al. [28]. Values of Sc were based on the properties of air at the mean temperature of the flames; these values do not vary significantly over the present test range so that a mean value of $Sc = 0.76$ was adopted for all the predictions. The value of μ used to find the Re in Eq. 4 was also based on the properties of air at the mean flame temperature. A virtual origin at $L_o/d = -3.2$ was selected so that the fit of present data passed through the origin of the plot. This type of initial flame displacement seems quite reasonable because the flames generally attached somewhat below the jet exit; see Figs. 1 and 2. Furthermore, this empirical displacement of the origin should hold for other flames at similar conditions. In addition, this displacement of the virtual origin, $L_o/d = -3.2$, is relatively small compared to the present normalized flame lengths (L_f/d in the range 9–39), which is typical of conventional use of virtual origins to extend large aspect ratio correlations to modest aspect ratio conditions. Finally, plots of Eq. 4 for the $C_f = 1.00$ (denoted theory) and a best-fit correlation for the present data for $C_f = 1.13$ (denoted correlation) are also shown on the figures for comparison with present measurements. For convenience, values of the virtual origin and C_f for all the flame length correlations considered here are summarized in Table 2.

The unprecedented steadiness of the present nonbuoyant laminar jet diffusion flames at microgravity minimized measurement uncertainties and yielded the remarkably unscattered correlation of luminous flame lengths illustrated in Fig. 3. The results for closed-tip and opened-tip flames are illustrated but there is little to choose between the two because tip opening does not modify luminous flame lengths significantly. This is somewhat surprising because the end of luminosity in soot-emitting flames is caused by soot particles cooling below a level where they can be observed rather than by soot burnout which is the case for the other flames. Nevertheless, these different mechanisms for

TABLE 2

Summary of Flame Length Correlations

Flame system	Source	L_o/d	C_f^b
Space-based, soot-containing and nonbuoyant	Present study	−3.2	1.13
KC-135, soot-containing and nonbuoyant	Sunderland et al. [14][a]	0.4	0.80
1-g, soot-containing and buoyant	Urban et al. [26]	−1.0	0.57
Drop tower, soot-free and nonbuoyant	Sunderland et al. [13]	2.7	0.56

[a] Previously unpublished measurements obtained during the course of the cited study.

[b] The slope of the flame length correlations in Figs. 3 and 4 can be found by multiplying the C_f by 3/32, following Eq. 4.

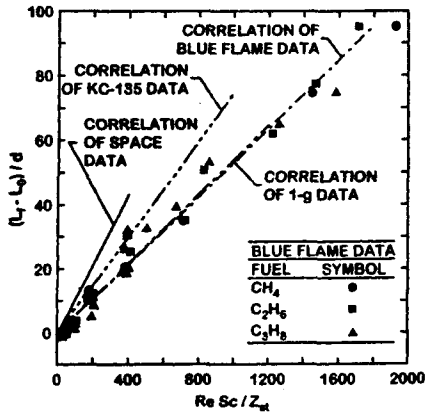

Fig. 4. Luminous flame lengths of hydrocarbon/air laminar jet diffusion flames as a function of $ReSc/Z_{st}$; correlation of measurements of soot-free (blue) flames from Sunderland et al. [13], correlation of measurements of KC-135 flames obtained during the study reported by Sunderland et al. [14], measurements (symbols) and correlation of 1-g flames reported by Urban et al. [26] and correlation of measurements of the present space-based flames. Note that the various correlations are terminated at the upper end of their corresponding data range.

ending flame luminosity do not have a large effect, with the luminous flame length correlations of the nonsooting and sooting flames being essentially the same; therefore, both sets of data are included in the present correlation according to Eq. 4.

The present selections of mean transport properties in Eq. 4 yield results that are in surprisingly good agreement with the measurements. In particular, the best fit value of C_f is only 13% larger than unity. This behavior is somewhat fortuitous, however, because the luminous flame length corresponds to the end of the soot-containing region at near laminar smoke point conditions, which generally is downstream from the position of the stoichiometric flame sheet, as discussed earlier.

Several additional experimental determinations of luminous flame lengths are plotted along with the present measurements in Fig. 4 in order to gain insight about effects of unsteadiness, buoyancy, and soot luminosity on luminous flame lengths. In order to provide a unified basis for comparison, all these results are based on experiments with laminar jet diffusion flames in still air having burner exit and test chamber configurations similar to the present space-based experiments and are plotted according to the Spalding [22] analysis. The resulting best fit values of L_o/d and C_f for each of these sets of data are summarized in Table 2. All the measurements illustrated in Fig. 4 correlated quite nicely according to Eq. 4, and have relatively small virtual origins as summarized in Table 2. On the other hand, flame lengths differ considerably for the various test conditions with present space-based flames clearly longer than the rest; this behavior is quantified by the values of C_f summarized in Table 2. Reasons for this behavior are discussed next.

The results closest to the present measurements in Fig. 4 are based on a correlation of earlier measurements of luminous flame lengths of nonbuoyant soot-containing flames for test conditions similar to the present measurements except carried out at low gravity using the KC-135 aircraft facility [14]. These low-gravity tests were completed to assist the development of the present space-based microgravity experiments so that burner properties were the same and laminar smoke point conditions were approached. Finally, available times at low gravity were relatively long, roughly 20 s, to minimize potential effects of unsteadiness. Thus, these test conditions provided reasonably close simulations of the present space-based microgravity experiments. Nevertheless, the best-fit correlations of the two sets of measurements indicate that the space-based flames are consistently longer, by roughly 40%, than the flames observed using the KC-135 facility. These differences are attributed to well-known effects of disturbances of the gravitational field when using aircraft facilities (g-jitter) with enhanced mixing due to these disturbances tending to reduce luminous flame lengths.

The results next closest to the present measurements in Fig. 4 are based on a correlation of earlier measurements of luminous flame lengths of buoyant soot-containing flames for test conditions similar to the present experiments except carried out at normal gravity [26]. These tests were completed to assist development of the present space-based experiments so that burner properties were the same and laminar

smoke point conditions were approached. Similar to other observations of buoyant soot-containing laminar jet diffusion flames [19], these flames provide the linear correlation between luminous flame lengths and fuel flow rates mentioned earlier. Nevertheless, the present space-based flames are roughly twice as long as the buoyant flames, due to the absence of enhanced mixing caused by convection effects resulting from buoyant motion.

The last series of luminous flame lengths illustrated in Fig. 4 are due to Sunderland et al. [13] and yield a laminar flame length correlation very similar to the results for buoyant flames but for very different reasons. The luminous flame length measurements of Sunderland et al. [13] involved nonbuoyant soot-free (blue) methane-, ethane-, and propane-fueled round laminar jet diffusion flames burning in still air at microgravity using a 2.2 s drop tower facility. The burner properties were similar to the present space-based experiments. As noted earlier, burner diameters, fuel flow rates and ambient pressures were manipulated in order to eliminate the presence of soot so that blue flames were observed whose location could be associated with the position of the stoichiometric flame sheet. These same tactics also reduced characteristic flame residence times to minimize effects of transient flame development. The luminous flame lengths of Sunderland et al. [13] exhibit somewhat greater scatter than the present space-based laminar flame lengths (see Fig. 3) when correlated according to Eq. 4; this behavior is probably due to ignition disturbances and flame development effects caused by the limited available test time at microgravity. Nevertheless, a reasonably good correlation between predictions and measurements is achieved. (Note that Sunderland et al. [13] also compare their luminous flame lengths to predictions from Burke and Schumann [2], Roper [21] and Klajn and Oppenheim [24].). The luminous flame lengths of the present space-based flames, however, are roughly twice as long as the nonbuoyant soot-free flames; this difference is felt to be mainly due to the different locations of the luminous flame length and the stoichiometric flame sheet as the laminar smoke point is approached, as discussed earlier. Notably, Sunderland and co-workers [15, 16] find similar differences between these two locations along the axis of their weakly-buoyant flames as the laminar smoke point is approached for similar fuels, which tends to support this conclusion.

Flame Diameters

The normalized maximum flame diameter, $w_{MAX}Z_{st}/d$, is simply a constant value, 0.563, according to Eq. 3. This implies that maximum flame diameters for nonbuoyant laminar jet diffusion flames burning in still air are only functions of the jet exit diameter and the stoichiometry, and are remarkably independent of parameters associated with fuel flow rates and transport properties, such as Re and Sc. Another parameter of interest is the flame diameter at the mid-point of the flame, $\zeta = 1/2$. This parameter can be readily found from Eq. 5, as follows:

$$w_{1/2}Z_{st}/d = 0.557 \quad \text{at} \quad \zeta = 1/2. \tag{7}$$

Thus, w_{MAX} and $w_{1/2}$ are essentially the same, mainly because the streamwise locations of these positions are not very different. Thus, flame diameter results will be presented in the following as w_{MAX} in order to avoid cluttering the plots.

As noted earlier, the blue stoichiometric boundaries could not be identified for the present test flames due to the adjustment limitations of the color video camera. Thus, the maximum luminous flame diameter was found from the luminous boundaries of the soot-containing region, similar to the present luminous flame lengths. Measurements of radial temperature distributions in the vicinity of the maximum flame diameter (see Urban et al. [27] for some typical examples) suggest that the stoichiometric flame sheet was just outside these boundaries.

Measured and predicted normalized maximum flame diameters, $w_{MAX}Z_{st}/d$, are plotted as a function of normalized luminous flame lengths in Fig. 5. Present measurements for both ethylene- and propane-fueled flames are shown. The predicted correlation of Eq. 3, along with the best-fit values of the measurements for the ethylene- and propane-fueled flames are also shown on the plot.

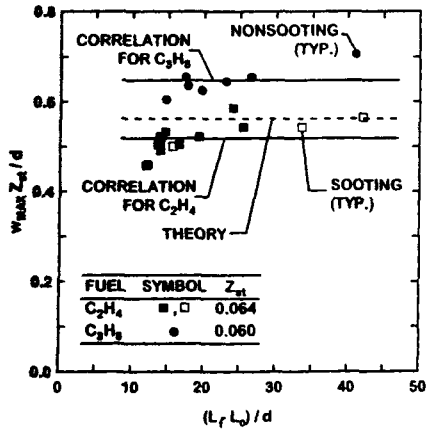

Fig. 5. Measured and predicted luminous flame diameters of nonbuoyant hydrocarbon/air laminar jet diffusion flames; measurements from present space-based experiments.

The experimental results illustrated in Fig. 5 are in remarkably good agreement with the predictions. There is a slight tendency for w_{MAX} to increase with increasing luminous flame lengths but present flames are relatively long, $(L_f - L_o)/d > 10$, and maximum flame diameters are essentially independent of flame length, agreeing with the trend predicted by the theory. The measured normalized maximum luminous flame diameters are slightly scattered about the prediction, with the best fit values of 0.518 and 0.647 for the ethylene- and propane-fueled flames, respectively, compared with the theoretical prediction of 0.563. The locations of the normalized maximum flame diameters for closed-tip flames also correspond reasonably well to estimates from Eq. 3, i.e., they are observed at roughly the mid-point of the flame; see Test 03E illustrated in Fig. 1. The maximum flame diameters for the blunt-tipped and opened-tip flames are observed beyond the mid-point toward the tip of the flames, see the flames illustrated in Fig. 2. This may help explain why the average values of $w_{MAX}Z_{st}/d$ for the present propane-fueled flames is larger than the value of this parameter for the ethylene-fueled flames, because most of the propane-fueled flames have the opened-tip configuration; see Fig. 2. Thus, based on the rather effective predictions of flame widths from Eq. 2, it becomes clear that the larger jet exit diameter is mainly responsible for the larger flame diameters, and smaller flame aspect ratios, for the luminous flame boundaries of Tests 05E, 06E, and 08E illustrated in Fig. 2 (see Table 1). Finally, the effectiveness of the predictions of Eq. 3 are somewhat startling because the results cannot be fitted to the measurements by appropriately selecting a condition to estimate mean transport properties in the same manner as the *luminous flame length correlation.*

Flame Shapes

Present predicted and measured luminous flame shapes are compared in the following as a final step in the evaluation of the effectiveness of Eq. 4 due to Spalding [22] for correlating luminous flame shape data. This comparison is illustrated in Fig. 6 for some typical closed-tip flames, with the radial position of the luminous flame boundary plotted directly as a function of streamwise distance. The predictions shown in the figure were computed as described in connection with Figs. 3–5, using the best fit values of C_f and L_o/d given in Table 2. The agreement between measurements and predictions is seen to be excellent for Tests 03E and 16E in spite of the complexity of the flame processes that define the location of the luminous flame boundaries and the simplicity of the Spalding [22] theory. The comparison between measurements and predictions is not quite as good for Test 18P in the region near the flame tip, however, because this is a relatively blunt closed-tip flame as discussed in connection with Fig. 5.

Measured and predicted luminous flame boundaries for opened-tip ethylene- and propane-fueled flames are plotted in Figs. 7 and 8, respectively. It is evident that the flame length predictions remain reasonably good for these opened-tip flames but the shapes of the tips of the flames are not predicted very well. Such behavior is certainly not surprising because the theory does not consider processes of flame extinction along the axis and the formation of an annular soot layer. Nevertheless, the fortuitous qualitative agreement between measurements and predictions should still be helpful for estimating the flame-containing region of non-

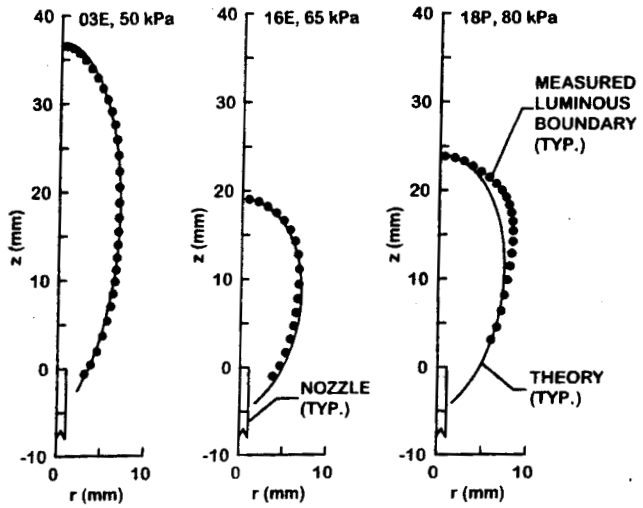

Fig. 6. Measured and predicted luminous flame shapes for typical closed-tip nonbuoyant hydrocarbon/air laminar jet diffusion flames; measurements from present space-based experiments (Tests 03E, 16E, and 18P).

buoyant laminar jet diffusion flames when imaging systems are designed for nonintrusive measurements of flame properties, if this finding proves to be robust for reasonable ranges of test conditions.

Measured and predicted luminous flame shapes for the present nonbuoyant laminar jet diffusion flames are plotted according to the normalized variables of Eq. 4 in Figs. 9 and 10 for selected closed-tip and opened-tip flames, respectively. Predictions shown on these plots were obtained as described in connection with Figs. 3 and 5. As expected from the results discussed thus far, the agreement between mea-

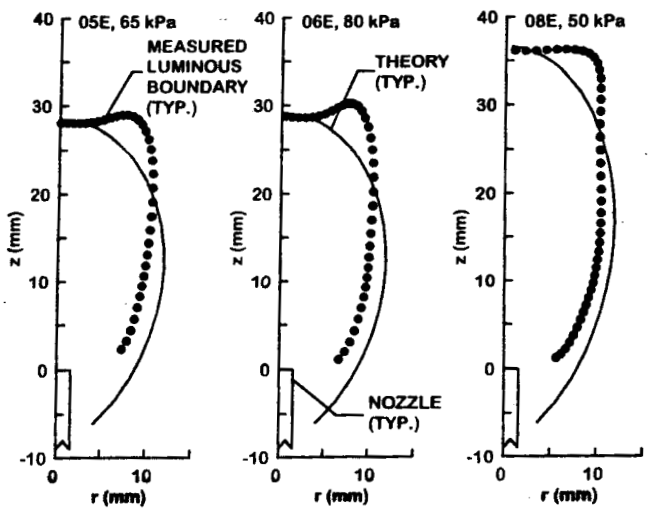

Fig. 7. Measured and predicted luminous flame shapes for typical opened-tip nonbuoyant ethylene/air laminar jet diffusion flames; measurements from present space-based experiments (Tests 05E, 06E, and 08E).

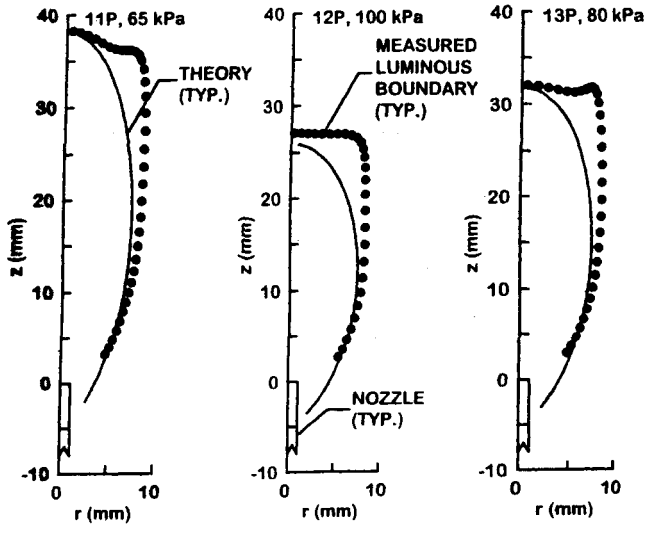

Fig. 8. Measured and predicted luminous flame shapes for typical opened-tip nonbuoyant propane/air laminar jet diffusion flames; measurements from present space-based experiments (Tests 11P, 12P, and 13P).

surements and predictions is excellent for the closed-tip flames in Fig. 9, except for the blunt-tipped flames that are seen as the laminar smoke point fuel flow rate is approached. The opened-tip luminous flame shapes are not predicted as well, with significant discrepancies observed between measurements and predictions as the flame tip is approached. In addition, the tendency for opened-tip flames to be broadest near the flame tip, as opposed to the midpoint as indicated by theory, is evident. Nevertheless, the qualitative agreement between

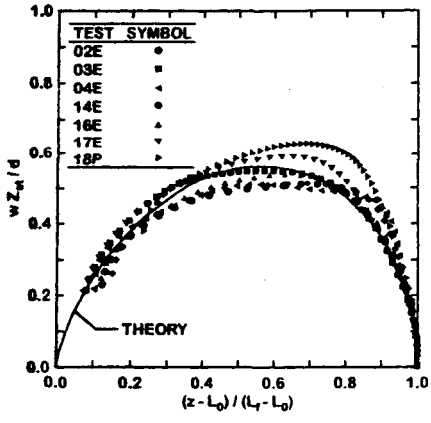

Fig. 9. Measured and predicted normalized luminous flame shapes for closed-tip nonbuoyant hydrocarbon/air laminar jet diffusion flames; measurements from present space-based experiments.

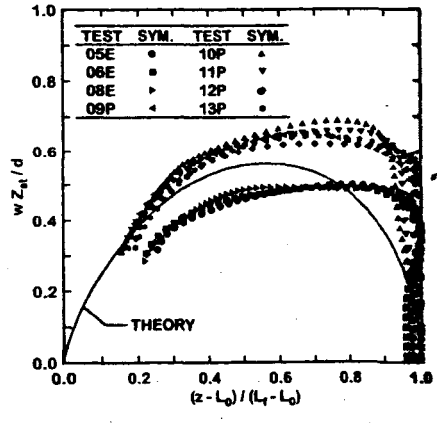

Fig. 10. Measured and predicted normalized luminous flame shapes for opened-tip nonbuoyant hydrocarbon/air laminar jet diffusion flames; measurements from present space-based experiments.

measurements and predictions, even for opened-tip flames, is quite good considering the simplicity of the model.

CONCLUSIONS

The luminous flame shapes of steady, nonbuoyant, round laminar jet diffusion flames were studied at microgravity during long-term tests carried out in an orbiting space shuttle. Test conditions involved ethylene- and propane-fueled flames burning in still air at ambient temperatures of 300 K, ambient pressures of 35–130 kPa, initial jet diameters of 1.6 and 2.7 mm, and jet exit Reynolds numbers of 45–170 to yield luminous flame lengths of 15–63 mm. These test conditions involved soot-containing luminous flames near laminar smoke point conditions, and included both nonsooting and sooting flames. The new measurements were used to evaluate predictions of luminous flame shapes based on the simple classical theory of nonbuoyant laminar jet diffusion flames due to Spalding [22]. The major conclusions of the study are as follows:

1. The present soot-containing luminous flames had larger luminous flame lengths than earlier ground-based observations: 40% larger than the luminous flame lengths of soot-containing nonbuoyant flames observed using an aircraft (KC-135) facility due to reduced effects of gravitational disturbances (g-jitter), roughly twice as large as the luminous flame lengths of soot-containing buoyant flames at normal gravity due to the absence of effects of buoyant mixing, and roughly twice as large as the luminous flame lengths of soot-free nonbuoyant flames observed by Sunderland et al. [13] using drop tower facilities due to the presence of soot luminosity and possible reduced effects of unsteadiness.
2. Similar to earlier observations of soot-containing nonbuoyant laminar jet diffusion flames [7–12, 14], present luminous flame shapes could be grouped into closed-tip and opened-tip configurations, which were observed for fuel flow rates smaller and larger than the laminar smoke point fuel flow rate, respectively. Blunt-tipped flames were also observed as fuel flow rates approached the tip-opening condition.
3. The simplified theoretical analysis of nonbuoyant laminar jet diffusion flames due to Spalding [22] yielded excellent correlations of the luminous flame shapes of closed-tip soot-containing and soot-free flames upon adjusting an empirical flame length parameter to account for the fact that flame luminosity ends at the location of soot consumption and at the location of the stoichiometric flame sheet along the axis of soot-containing and soot-free flames, respectively. Nevertheless, the slopes of the flame length correlations in Fig. 4 differed by roughly a factor of 2 for nonbuoyant soot-free (blue) and soot-containing (near the laminar smoke point limit) flames. This difference is consistent, however, with the ratios between luminous flame lengths and stoichiometric lengths for soot-containing flames reported previously [15–18].
4. Remarkably, the simplified theoretical analysis of nonbuoyant laminar jet diffusion flames due to Spalding [22] fortuitously still yields reasonably good predictions of luminous flame shapes for soot-containing nonbuoyant opened-tip flames as well as for conventional buoyant flames, after appropriate selections of empirical flame length parameters. Thus, taken together, the simple formulation of Eq. 4 exhibits encouraging potential to correlate the luminous flame boundaries of laminar jet diffusion flames that should be useful for designing imaging systems for nonintrusive measurements of flame properties.
5. Based on the present correlations of luminous flame boundaries for nonbuoyant laminar jet diffusion flames, luminous flame lengths increase linearly with fuel flow rate but are relatively independent of jet exit diameter and pressure, while maximum luminous flame diameters increase linearly with jet exit diameter but are relatively independent of fuel flow rate and pressure. Both dimensions, however, are proportional to the stoichiometric mixture fraction, although this parameter was not varied sufficiently during the present experiments to test predictions of this trend.

The correlation of Eq. 4 from Spalding [22] should be used with caution outside the present test range. Additional experiments are needed to evaluate this expression during long-term space-based tests at microgravity, emphasizing evaluation of effects of approach to the laminar smoke point and the relationship between the locations of the luminous flame boundaries due to the presence of soot and the location of the stoichiometric flame sheet.

This research was supported by NASA grant nos. NAG3-1245 and NAG3-2048 under the overall technical management of Howard B. Ross of the NASA Lewis Research Center. The authors would like to acknowledge the contributions of R. Hager, A. Over, R. Chucksa, and their associates at NASA LeRC to the development and operation of the test apparatus; to G. T. Linteris, J. E. Voss, and R. Crouch of the NASA Johnson Space Center who carried out the assembly of the test apparatus and the execution of the experiments on orbit; and to Z. Dai of The University of Michigan who helped with the collection of the data.

REFERENCES

1. Bilger, R. W., *Prog. Energy Combust. Sci.* 1:87 (1976).
2. Burke, S. P., and Schumann, T. E. W., *Ind. Eng. Chem.* 20:998 (1928).
3. Law, C. K., and Faeth, G. M., *Prog. Energy Combust. Sci.* 20:65 (1994).
4. Cochran, T. H., and Masica, W. J., *Thirteenth Symposium (International) on Combustion*, The Combustion Institute, Pittsburgh, 1970, p. 821.
5. Haggard, J. B., Jr., and Cochran, T. H., *Combust. Sci. Tech.* 5:291 (1972).
6. Edelman, R. B., Fortune, O. F., Weilerstein, G., Cochran, T. H., and Haggard, J. B., Jr., *Fourteenth Symposium (International) on Combustion*, The Combustion Institute, Pittsburgh, 1972, p. 399.
7. Edelman, R. B., and Bahadori, M. Y., *Acta Astronautica* 13:681 (1986).
8. Bahadori, M. Y., Edelman, R. B., Stocker, D. P., and Olson, S. L., *AIAA J.* 28:236 (1990).
9. Bahadori, M. Y., Stocker, D. P., and Edelman, R. B., AIAA Paper No. 90-0691, 1990.
10. Bahadori, M. Y., Edelman, R. B., Sotos, R. G., and Stocker, D. P., AIAA Paper No. 91-0719, 1991.
11. Bahadori, M. Y., Edelman, R. B., Stocker, D. P., Sotos, R. G., and Vaughan, D. F., AIAA Paper No. 92-0243, 1992.
12. Bahadori, M. Y., Stocker, D. P., Vaughan, D. F., Zhou, L., and Edelman, R. B., in *Modern Developments in Energy, Combustion and Spectroscopy* (F. A. Williams et al., eds.), Pergamon, New York, 1993, Chapt. 4.
13. Sunderland, P. B., Mendelson, B. J., Yuan, Z.-G., and Urban, D. L., *Combust. Flame* 116:376–386 (1998).
14. Sunderland, P. B., Mortazavi, S., Faeth, G. M., and Urban, D. L., *Combust. Flame* 96:97 (1994).
15. Sunderland, P. B., Köylü, Ü. Ö., and Faeth, G. M., *Combust. Flame* 100:310 (1995).
16. Sunderland, P. B., Ph.D. thesis, The University of Michigan, Ann Arbor, Michigan, 1995.
17. Mitchell, R. E., Sarofim, A. F., and Clomburg, L. A., *Combust. Flame* 37:227 (1980).
18. Saito, K., Williams, F. A., and Gordon, A. S., *Combust. Sci. Tech.* 47:117 (1986).
19. Schug, K. P., Manheimer-Timnat, Y., Yaccarino, P., and Glassman, I., *Combust. Sci. Tech.* 22:235 (1980).
20. Jost, W., *Explosion and Combustion Processes in Gases*, McGraw-Hill, New York, 1946.
21. Roper, F. G., *Combust. Flame* 29:219 (1977).
22. Spalding, D. B., *Combustion and Mass Transfer*, Pergamon, New York, 1979, p. 185.
23. Kuo, K. K., *Principles of Combustion*, John Wiley & Sons, New York, 1986, p. 360.
24. Klajn, M., and Oppenheim, A. K., *Nineteenth Symposium (International) on Combustion*, The Combustion Institute, Pittsburgh, 1982, p. 223.
25. Li, S. C., Gordon, A. S., and Williams, F. A., *Combust. Sci. Tech.* 104:75 (1995).
26. Ban, H., Venkatesh, S., and Saito, K., *J. Heat Trans.* 116:954 (1994).
27. Urban, D. L., Yuang, Z.-G., Sunderland, P. B., Linteris, G. T., Voss, J. E., Lin, K.-C., Dai, Z., Sun, K., and Faeth, G. M., *AIAA J.* 36:1346 (1998).
28. Braun, W. G., Danner, R. P., and Daubert, T. E., *Technical Data Book—Petroleum Refining*, 3rd ed., American Petroleum Institute, Washington, 1976, Chapters 11 and 13.

Received 6 May 1998; revised 22 June 1998; accepted 25 June 1998.

Appendix C:

Z. Dai and G.M. Faeth, Hydrodynamic suppression of soot formation in laminar coflowing jet diffusion flames. *Proc. Combust. Inst.* 28, 2085-2092.

Proceedings of the Combustion Institute, Volume 28, 2000/pp. 2085–2092

HYDRODYNAMIC SUPPRESSION OF SOOT FORMATION IN LAMINAR COFLOWING JET DIFFUSION FLAMES

Z. DAI AND G. M. FAETH
Department of Aerospace Engineering
University of Michigan
Ann Arbor, MI 48109-2140, USA

Effects of flow (hydrodynamic) properties on limiting conditions for soot-free laminar non-premixed hydrocarbon/air flames (called laminar soot-point conditions) were studied, emphasizing non-buoyant laminar coflowing jet diffusion flames. Effects of air/fuel-stream velocity ratios were of particular interest; therefore, the experiments were carried out at reduced pressures to minimize effects of flow acceleration due to the intrusion of buoyancy. Test conditions included reactant temperatures of 300 K; ambient pressures of 3.7–49.8 kPa; methane-, acetylene-, ethylene-, propane-, and methane-fueled flames burning in coflowing air with fuel-port diameters of 1.7, 3.2, and 6.4 mm; fuel jet Reynolds numbers of 18–121; air coflow velocities of 0–6 m/s; and air/fuel-stream velocity ratios of 0.003–70. Measurements included laminar soot-point flame lengths, laminar soot-point fuel flow rates, and laminar liftoff conditions. The measurements show that laminar soot-point flame lengths and fuel flow rates can be increased, broadening the range of fuel flow rates where the flames remain soot free, by increasing air/fuel-stream velocity ratios. The mechanism of this effect involves the magnitude and direction of flow velocities relative to the flame sheet where increased air/fuel-stream velocity ratios cause progressive reduction of flame residence times in the fuel-rich soot-formation region. The range of soot-free conditions is limited by both liftoff, particularly at low pressures, and the intrusion of effects of buoyancy on effective air/fuel-stream velocity ratios, particularly at high pressures. Effective correlations of laminar soot- and smoke-point flame lengths were also found in terms of a corrected fuel flow rate parameter, based on simplified analysis of laminar jet diffusion flame structure. The results show that laminar smoke-point flame lengths in coflowing air environments are roughly twice as long as soot-free (blue) flames under comparable conditions due to the presence of luminous soot particles under fuel-lean conditions when smoke-point conditions are approached. This is very similar to earlier findings concerning differences between laminar smoke- and soot-point flame lengths in still environments.

Introduction

Motivated by technological and public health problems, several methods have been developed to control the soot content and emissions of hydrocarbon-fueled flames. Among these, soot-control methods based on fast mixing for non-premixed (diffusion) flames are of interest because they avoid the operational problems of additives and premixed combustion [1–3]. The objective of fast mixing is to minimize residence times of fuel and fuel-decomposition products at fuel-rich conditions so that few soot particles develop and they can be readily consumed in the soot-oxidation regions of the flame. The present investigation seeks improved understanding of fast mixing concepts based on experimental observations of laminar coflowing jet diffusion flames. Laminar diffusion flames were studied because they provide relatively tractable models of mixing and reaction within more practical but relatively intractable turbulent diffusion flames. Another advantage of the laminar coflowing jet diffusion flame configuration is that it has been widely used to study the soot-formation properties of diffusion flames (see Refs. [4–8]).

While fast mixing reduces soot formation within diffusion flames, past studies of both laminar opposed and coflowing jet diffusion flames show that the way that mixing is carried out is important as well [9–17]. In fact, existing evidence from both laminar and turbulent jet diffusion flames, and from empirical industrial practice, suggests that soot reductions can be achieved most effectively by ensuring that velocities normal to the flame sheet are directed from the fuel-rich toward the fuel-lean side. This configuration, called "soot-formation-oxidation flame conditions" by Kang et al. [13], tends to reduce the residence times of soot precursors and soot at fuel-rich soot-formation conditions by drawing these materials directly through the flame sheet toward fuel-lean oxidation conditions. In contrast, when velocities normal to the flame sheet are directed from the fuel-lean toward the fuel-rich side, called "soot-formation flame conditions" by Kang et al. [13], residence times of soot precursors and soot at fuel-rich

soot-formation conditions are enhanced, making oxidation of these materials more problematic when oxidation conditions are finally reached.

Studies of effects of velocities normal to the flame sheet on soot formation have been carried out in laminar opposed and coflowing jet diffusion flames [9–17]. During most of these studies [9–15], velocities normal to the flame sheet were varied by varying the compositions of the oxidant- and fuel-carrying streams. For example, diluting the fuel stream with an inert gas (e.g., nitrogen) while enriching the oxidant stream by removing existing diluent (e.g., removing nitrogen from air) promotes increased velocities normal to the flame sheet directed from the fuel-rich toward the fuel-lean side and yields reduced soot concentrations in the flame [9–14]. As pointed out by Sunderland et al. [12], however, these composition changes alone are sufficient to retard soot formation and enhance soot oxidation, which tends to reduce soot concentrations, obscuring the effect of hydrodynamics on soot control. In addition, the practical utility of varying reactant-stream compositions to control soot formation in diffusion flames is relatively limited.

The present investigation sought a direct evaluation of effects of velocities normal to the flame sheet on soot formation in diffusion flames by considering pure air and fuel reactant streams for laminar coflowing jet diffusion flames. In this configuration, enhanced (retarded) airstream velocities provide entrainment velocities normal to the flame sheet directed from the fuel-rich (fuel-lean) to the fuel-lean (fuel-rich) sides of the flame, which should reduce (increase) both soot concentrations within the flame and the tendency to emit soot from the flame. This behavior has been observed, with enhanced airstream velocities yielding significant increases of laminar smoke-point flame lengths—particularly for low-pressure flames, in which disturbances of the velocity field due to the intrusion of effects of buoyancy become relatively small [16]. Recent numerical simulations from Kaplan and Kailasanath [17] exhibit similar tendencies for soot concentrations within laminar coflowing jet diffusion flames to decrease for locally enhanced airstream velocities. Finally, air atomization, which is widely used for soot control in aircraft gas turbine combustors, corresponds to an enhanced airstream velocity flame configuration, which may explain this soot-control mechanism.

Prompted by these observations, the present investigation considered effects of enhanced airstream velocities on laminar soot-point properties—that is, the condition where soot is first observed in laminar diffusion flames. The main issue was to learn whether gas-phase processes (dominated by both diffusive and convective transport) could be controlled to yield soot-free flames by manipulating air/fuel velocity ratios in the same way that gas/solid processes (dominated by convective transport alone) can be controlled to eliminate soot emissions. Associated flame properties such as luminous flame lengths and flame liftoff conditions were also observed. Finally, present results define conditions where detailed numerical simulations of flame structure can be evaluated without the complications associated with soot chemistry [18–20].

Experimental Methods

Measurements were carried out at subatmospheric pressures to control the effects of buoyancy [21]. The test burner was a vertical coaxial tube arrangement with the fuel flowing from an inner port with inside diameters of 1.7, 3.2, and 6.4 mm and the air flowing from an outer port with an inside diameter of 60 mm. The air passage used beads and screens to provide a uniform velocity distribution at the burner exit; the fuel passage provided fully developed laminar flow at its exit. The exit of the fuel port was 10 mm above the exit of the air port to provide an undisturbed region for flame attachment. The air-port diameter was sufficiently large so that the mixing layer between the air coflow and the ambient air in the vacuum chamber did not disturb the flame. The burner was operated within a windowed vacuum chamber with an inside diameter and length of 300 and 1200 mm, respectively.

Acetylene-, ethylene-, propane-, and methane-fueled laminar jet diffusion flames in coflowing air were considered with gas purities in excess of 99%, except for acetylene, which had a purity of only 98% due to contamination by the acetone that is present in commercial acetylene cylinders for safety purposes. Past work has shown, however, that effects of acetone contamination of acetylene on luminous flame shapes and laminar smoke-point flame lengths are small compared with experimental uncertainties [16]. In addition to the variations of burner-port diameters and fuels mentioned earlier, test conditions included reactant temperatures of roughly 100 K; ambient pressures of 3.7–49.8 kPa; fuel jet exit Reynolds numbers, *Re*, of 18–121; air coflow velocities of 0–6 m/s; and air/fuel-stream velocity ratios of 0.003–70. Transition to turbulent flames was never observed during the present experiments, whereas characteristic flame residence times were small so that effects of radiative heat losses from the flames were negligible [8,22].

Results and Discussion

Flame Appearance

Photographs of typical soot-free (blue) and soot-containing ethylene/air flames at identical fuel-port

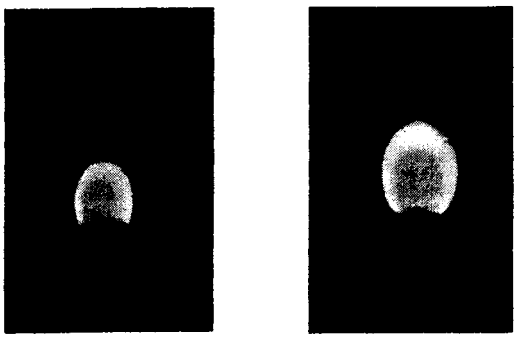

FIG. 1. Photographs of ethylene/air diffusion flames for a fixed burner diameter (3.2 mm), pressure (10.2 kPa), and fuel flow rate (1.3 mg/s): left image at the laminar soot point at the largest possible air/fuel-stream velocity ratio, $u_a/u_f = 0.2$, at this condition; right image for a soot-containing flame at a relatively small air/fuel-stream velocity ratio, $u_a/u_f = 0.004$, at this condition.

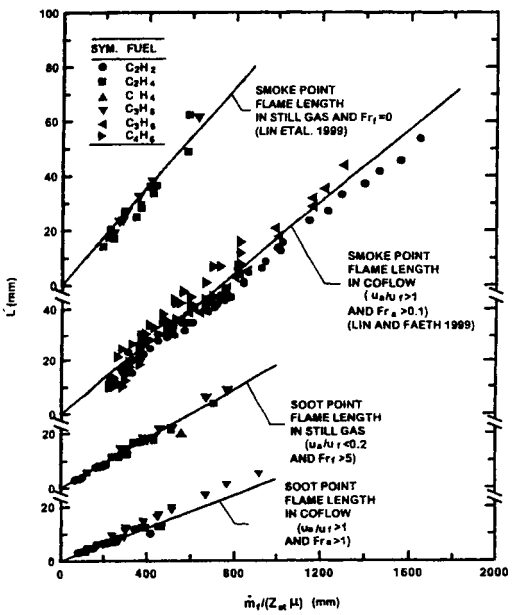

FIG. 2. Correlations between laminar soot- and smoke-point flame lengths and corrected fuel flow rates for coflowing laminar jet diffusion flames fueled with acetylene, ethylene, methane, propane, propylene, and 1-3-butadiene and burning in air based on the simplified flame shape analysis of Lin et al. [22] and Lin and Faeth [23]. Laminar smoke-point flame length correlations also are from Refs. [22] and [23].

exit conditions are illustrated in Fig. 1. Effects of buoyancy are relatively small at this low-pressure condition (10.2 kPa), so that flame properties approximate the non-buoyant behavior of greatest interest for practical applications. The flame on the left is at its laminar soot-point condition at the largest air/fuel-stream velocity ratio, $u_a/u_f = 0.2$, that could be used without liftoff at this jet exit condition. The flame on the right illustrates the effect of reducing the air/fuel-stream velocity ratio from the soot-point condition to a relatively small value, $u_a/u_f = 0.004$, while keeping all other flame properties the same. The reduced entrainment from the airstream at small u_a/u_f increases flame residence times at conditions where soot formation is favored, which causes soot to appear, as evidenced by a region of yellow flame luminosity near the flame tip.

Flame Length Correlations

Similar to the observations of luminous flame lengths at laminar smoke points by Schug et al. [5] and Lin and Faeth [14], the present luminous flame lengths at laminar soot points were closely associated with the fuel flow rate. Measurements establishing this behavior and a brief discussion of a simplified theory that helps explain the experimental findings are considered in the following.

Laminar soot- and smoke-point luminous flame lengths are plotted in Fig. 2 as a function of a corrected fuel flow rate suggested by simplified theories of flame shapes for non-buoyant laminar jet diffusion flames in still and coflowing gases [22,23] developed by extending earlier analyses [24–26]. The laminar soot-point measurement conditions from the present investigation were summarized earlier. The measured laminar smoke-point correlations are from Lin and Faeth [14] for acetylene-, propylene-, and 1-3-butadiene-fueled flames burning in air at pressures of 19–51 kPa, a burner diameter of 6 mm, and air/fuel-stream velocity ratios of 0.4–6.7. Two sets of correlations (each) are illustrated for the laminar soot- and smoke-point luminous flame lengths in Fig. 2: one for small u_a/u_f based on analysis of laminar jet diffusion flames in still air [22] and one for large u_a/u_f based on analysis of laminar jet diffusion flames in coflowing air [23]. There are good correlations between measured luminous flame lengths and the corrected fuel flow rates for both laminar soot- and smoke-point conditions (see Ref. [23] for the latter). As a result, laminar soot-point properties are represented by the laminar soot-point fuel flow rate in the following, similar to past work [14]. It is also evident that the correlation for laminar smoke-point flame lengths is roughly twice as long as that for laminar soot-point flame lengths at both large and small u_a/u_f limits.

An explanation of the flame length behavior observed in Fig. 2 can be obtained from the flame

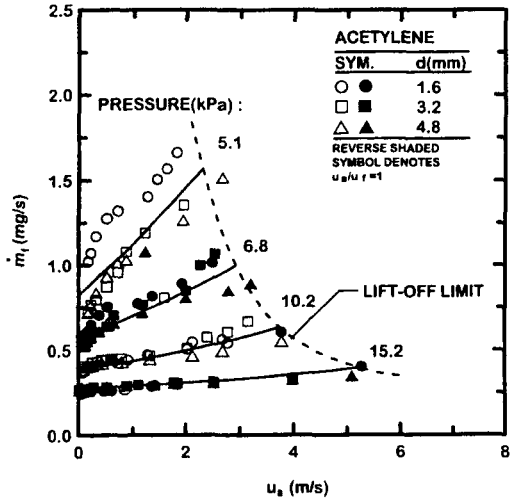

FIG. 3. Fuel flow rates at laminar soot-point and liftoff conditions as a function of air coflow velocities, fuel-port diameter, and pressure for acetylene/air flames.

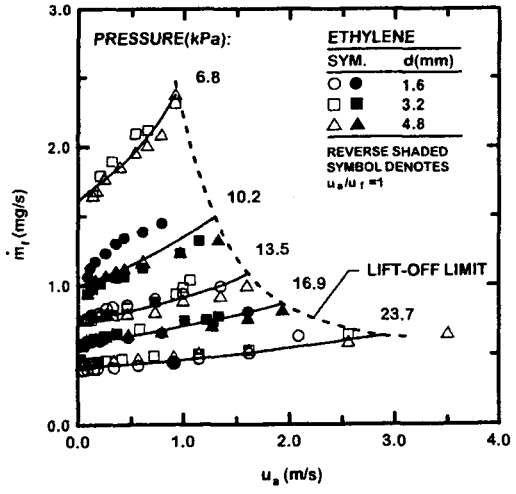

FIG. 4. Fuel flow rates at laminar soot-point and liftoff conditions as a function of air coflow velocities, fuel-port diameter, and pressure for ethylene/air flames.

shape correlations based on the simplified analyses of Refs. [22] and [23]. Ignoring small effects of virtual origins, both these correlations can be written to yield the luminous flame length as a function of the corrected flow rate parameter used in Fig. 2, as follows:

$$L = (C_n C_f Sc/(8\pi))\, \dot{m}_f/(Z_{st}\mu) \qquad (1)$$

Following Refs. [22] and [23], a simple correlation of equation 1 was fitted to measurements of flames in air environments by using values of the Schmidt number and viscosity for air at the average of the adiabatic flame temperature and the ambient temperature. Similarly, $C_n = 3$ for non-buoyant flames in still gases, whereas $C_n = 2$ for non-buoyant flames in coflowing gases [23]. The measurements of Refs. [27] and [28] yield $C_f \approx 0.5$ for soot-free blue flames and $C_f \approx 1.0$ for flames at the laminar smoke point for flames in still air [22]. These assignments provide the good correlations of the present results in coflowing air seen in Fig. 2, as well as an explanation of the increased luminous flame lengths caused by reduced air coflow velocities and the presence of soot near the flame tip for these conditions seen in Fig. 1.

Laminar Soot-Point Properties

Both laminar soot-point and liftoff properties were measured during the present experiments. The tests were conducted by varying the pressure range for each fuel based on its propensity to soot, so that effects of reasonable variations of air/fuel-stream velocity ratios could be measured for flames fueled with each fuel in spite of limitations due to effects of liftoff and the intrusion of buoyancy.

In the following, effects of air coflow on laminar soot-point and liftoff properties are presented as plots of laminar soot-point fuel flow rates as a function of air coflow velocities because this approach provides a compact presentation of the measurements. Effects of air coflow velocities on laminar soot-point fuel flow rates were qualitatively similar for the four fuels that were considered. This can be seen from the plots of fuel mass flow rate at soot-point conditions as a function of air coflow velocities for the various pressures and fuel-port diameters that are illustrated in Figs. 3–6. To indicate the transition between soot-formation and soot-formation-oxidation configurations at the base of the test flames, the condition of $u_a/u_f = 1$ is denoted by reverse-shaded symbols on the plots (note that the soot-formation and soot-formation-oxidation configurations occur for test conditions in the left and right of the reverse-shaded symbols, respectively). Liftoff conditions are denoted by the symbol at the highest air flow rate for each pressure and fuel-port diameter, with the extreme liftoff limit denoted by a dashed line.

The measurements illustrated in Figs. 3–6 show that increased air coflow velocities increase laminar soot-point fuel rates. Notably, this behavior is observed for air/fuel-stream velocity ratios both smaller and larger than unity. Increasing pressures generally reduce allowable fuel mass flow rates and flame lengths for soot-free flames due to increased soot-formation rates and flame residence times for a given flame length. The relative enhancement of laminar soot-point fuel flow rates between small and

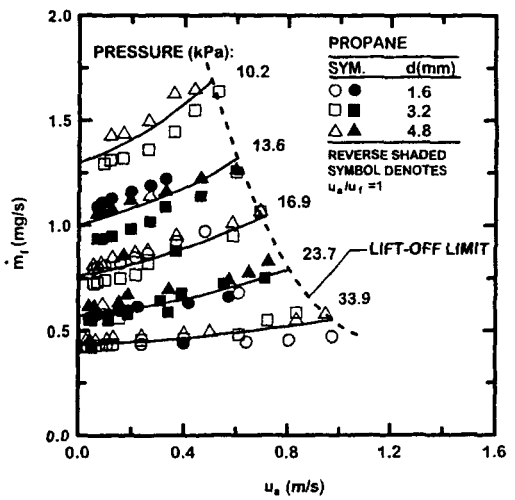

FIG. 5. Fuel flow rates at laminar soot-point and liftoff conditions as a function of air coflow velocities, fuel-port diameter, and pressure for propane/air flames.

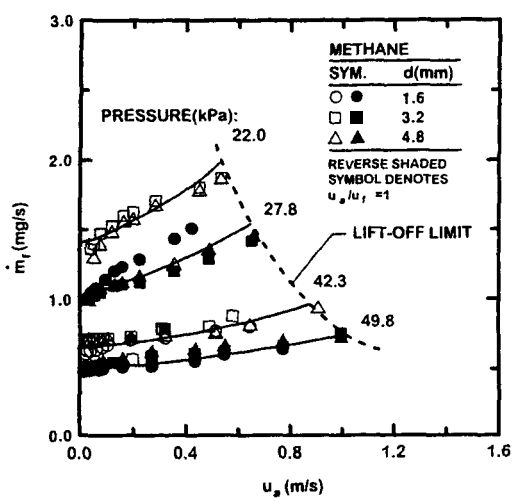

FIG. 6. Fuel flow rates at laminar soot-point and liftoff conditions as a function of air coflow velocities, fuel-port diameter, and pressure for methane/air flames.

maximum allowable values of air coflow velocities before liftoff, however, tends to be relatively independent of the pressure for a particular fuel. This behavior comes about because generally more intense reaction rates at elevated pressures accommodate large air coflow velocities before liftoff, which tends to compensate for faster soot reaction rates at elevated pressures. Taken together, it is clear that sufficiently large air coflow velocities are capable of completely suppressing the formation of particulate soot for these conditions, supporting the soot-suppression argument discussed in the introduction. The resulting soot-free flames also provide potentially useful conditions for evaluating detailed models of diffusion flame chemistry and transport at the computationally tractable limit of soot-free laminar diffusion flames for light hydrocarbons.

For the present tests, the propensity of a fuel to soot can be associated with the pressure range for observing soot-free flames. On this basis, the present tests indicate that the propensity to form and emit soot progressively decreases in the order acetylene, ethylene, propane, and methane. This finding agrees with conventional determinations of laminar smoke-point properties based on observations of buoyant laminar jet diffusion flames [4–8]. In addition, the general behavior of the laminar soot-point properties in Figs. 3–6 is qualitatively similar to earlier observations of laminar smoke-point properties as a function of air coflow velocities in Ref. [16].

An important issue concerning the results illustrated in Figs. 3–6 is the mechanism for increased resistance to soot formation as the air coflow velocity increases for a particular fuel, fuel-port diameter, and pressure. Consider the simplest case, when the flame is in the soot-formation-oxidation condition for air/fuel-stream velocity ratios greater than unity, which generally involves conditions in which buoyancy does not significantly affect flame velocities. The results discussed in connection with Fig. 2 then indicate that the flame shape (length) is largely controlled by the fuel flow rate and is relatively independent of fuel velocity at the burner exit (or the burner-port diameter). In contrast, the characteristic flame residence time, t_a, is proportional to the flame length divided by the air coflow velocity [23]. Thus, given a critical residence time for the appearance of soot for a particular fuel and pressure, the fuel flow rate at the laminar soot-point limit progressively increases with increasing air coflow velocity, relatively independent of fuel-port diameter, which is typical of the behavior seen in Figs. 3–6 for reasonably large air/fuel-stream velocity ratios.

The mechanism of increased resistance to soot formation as the air coflow velocity increases for a particular fuel, fuel-port diameter, and pressure is more complex when the flame is in the soot-formation configuration (at least near the flame base). This generally involves conditions in which buoyancy affects flame velocities and air/fuel-stream velocity ratios are less than unity. For such conditions, increasing the air coflow velocity causes the flame to shift from the soot-formation toward the soot-formation-oxidation configuration, which reduces the proportion of the flame residence time spent at soot-formation conditions compared with soot-oxidation conditions and thus tendencies for soot formation. Behavior of this nature can be observed from the soot-concentration measurements near laminar

smoke-point conditions in Ref. [16], where variations of soot concentrations as a function of residence time become path independent as the soot-formation-oxidation condition is approached. Similarly, this effect is not uniform for all soot precursor paths through the present flames, whereas all paths are affected to some extent by reduced flame residence times as air coflow velocities are increased. These effects, and the intrusion of buoyancy, introduce greater effects of fuel-port diameter on laminar soot-point conditions for these flames for the simple soot-formation-oxidation flame configuration discussed earlier, as seen in Figs. 3–6. Nevertheless, in spite of variations of flame behavior depending on the range of air/fuel-stream velocity ratios and effects of the intrusion of buoyancy, the general capability of increased air coflow velocities to reduce the content and emissions of soot for the present flames is evident.

Flame Stability Properties

Limiting conditions for flame liftoff are plotted in Figs. 3–6 as a function of pressure for each fuel. At high pressures, fuel-port velocities are small at liftoff conditions, and this limit correlates quite nicely as a function of coflow velocity and pressure, relatively independent of fuel-port diameter. At low pressures, however, fuel-port velocities become relatively large and also begin to affect liftoff conditions, with small fuel-port diameters (which yield the largest fuel-port velocities) generally contributing to reduced flame stability.

Conclusions

The present experimental investigation considered the effect of air/fuel-stream velocity ratios on soot processes within laminar coflowing jet diffusion flames for the experimental conditions summarized earlier. Major conclusions of the study are as follows:

1. Laminar soot-point flame lengths and fuel flow rates were increased with increasing air/fuel-stream velocity ratios; these effects were most pronounced at low pressures, where effects of buoyancy were minimized, and initial air/fuel-stream velocity ratios are reasonably representative of the entire visible portion of the flame for the present test conditions. These results are qualitatively similar to earlier measurements of laminar smoke-point properties, as well as recent predictions of soot-concentration properties [17], for similar flame conditions.
2. Laminar soot-point flame lengths were conveniently correlated in terms of a corrected fuel flow rate parameter based on an earlier simplified analysis of the structure of non-buoyant laminar coflowing jet diffusion flames [23]. It was found that laminar smoke-point flame lengths in both coflowing and still air environments are roughly twice as long as soot-free (blue) flames under comparable conditions due to the presence of luminous soot particles under fuel-lean conditions as laminar smoke-point conditions are approached.
3. The mechanism of increased resistance to soot formation with increasing air/fuel-stream velocity ratios at low pressures (where buoyancy does not significantly affect flame velocities) and large air/fuel-stream velocity ratios (where the flame is in the soot-formation-oxidation configuration) involves progressive reduction of flame residence times for soot production, eventually reaching the soot-free (blue) flame limit. Given a critical residence time for the appearance of soot for a particular fuel and pressure, this behavior is consistent with present measurements and the simplified analysis of the shape of non-buoyant laminar jet diffusion flames in coflowing air [23]. Notably, the shape (length) of these flames is largely controlled by the fuel flow rate, while the characteristic residence time is proportional to the flame length divided by the air coflow velocity. Then, laminar soot-point fuel flow rates should increase with increasing air coflow velocities for a given fuel and pressure, relatively independent of fuel-port diameter, as observed at low pressures and large air coflow velocities in Figs. 3–6.
4. The mechanism of increased resistance to soot formation with increasing air/fuel-stream velocity ratios is more complex at high pressures (where buoyancy significantly affects flame velocities) and at small air/fuel-stream velocity ratios (where the flame is in the soot-formation configuration). Then, increasing air/fuel-stream velocity ratios causes the flame to shift from the soot-formation toward the soot-formation-oxidation configuration, which reduces the proportion of the flame residence time spent at soot-formation conditions compared with soot-oxidation conditions, reducing tendencies for soot formation accordingly. However, this effect is not uniform for all soot precursor paths through the flame, whereas all paths are affected to some degree by reduced flame residence times with increasing air/fuel-stream velocity ratios, as discussed in conclusion 3 above.

Other effects observed during the present investigation generally are consistent with earlier findings concerning the propensity of diffusion flames to form and emit soot [7–8]: laminar soot-point fuel flow rates and flame lengths tend to progressively increase with decreasing pressure, and the propensity to form and emit soot with variations of fuel type

progressively decreases in the order acetylene, ethylene, propane, and methane. Finally, in spite of limitations due to the intrusion of buoyancy, the results of the present investigation support the earlier findings of Ref. [16] that effects of enhanced air/fuel-stream velocity ratios contribute to the mechanism of reduced sooting tendencies for non-premixed flames using air atomization techniques. Nevertheless, more work is needed to resolve the specific contributions of enhanced air/fuel-stream velocity ratios and improved atomization to reducing the sooting tendencies of practical spray flames.

Nomenclature

C_f	flame length empirical parameter
C_n	flame length configuration parameter
d	fuel-port diameter
D	mass diffusivity
Fr_a, Fr_f	air- and fuel-stream Froude numbers, $(u_a^2$ or $u_s^2)/(2gL)$
g	acceleration of gravity
L	laminar smoke- and soot-point flame lengths
$\dot{m}_f$	fuel mass flow rate
p	pressure
Re	Reynolds number, $4\,\dot{m}/(\pi d\mu)$
Sc	Schmidt number, ν/D
t_t	characteristic residence time, L/u_a
u	streamwise velocity
Z_{st}	stoichiometric mixture fraction
μ	dynamic viscosity
ν	kinematic viscosity

Subscripts

a	initial property of airstream
f	initial property of fuel stream

Acknowledgments

This research was supported by NASA grants NCC3-661, NAG3-1878, and NAG3-2048 under the technical management of D. L. Urban and Z.-G. Yuan of the NASA Glenn Research Center.

REFERENCES

1. Bahr, D. W., in *Gas Turbine Combustion Design Problems* (A. H. Lefevre, ed.), Hemisphere, Washington, DC, 1979, pp. 205–223.
2. Hussman, A. W., and Maybach, G. W., *SAE Trans.* 69:563–574 (1961).
3. Haynes, B. S., and Wagner, H. G., *Prog. Energy Combust. Sci.* 7:229–273 (1981).
4. Schalla, R. L., and McDonald, G. E., *Proc. Combust. Inst.* 5:316–324 (1954).
5. Schug, K. P., Manheimer-Timnat, Y., Yaccarino, P., and Glassman, I., *Combust. Sci. Technol.* 22:235–250 (1980).
6. Flower, W. L., and Bowman, C. T., *Proc. Combust. Inst.* 21:1115–1124 (1983).
7. Sunderland, P. B., Mortazavi, S., Faeth, G. M., and Urban, D. L., *Combust. Flame* 96:97–103 (1994).
8. Urban, D. L., Yuan, Z.-G., Sunderland, P. B., Linteris, G. T., Voss, J. E., Lin, K.-C., Dai, Z., Sun, K., and Faeth, G. M., *AIAA J.* 36:1346–1360 (1998).
9. Sugiyama, G., *Proc. Combust. Inst.* 25:601–608 (1994).
10. Du, J., Axelbaum, R. L., and Law, C. K., *Proc. Combust. Inst.* 22:387–394 (1988).
11. Du, J., and Axelbaum, R. L., *Combust. Flame* 100:367–375 (1995).
12. Sunderland, P. B., Axelbaum, R. L., and Urban, D. L., in *Fifth International Microgravity Combustion Workshop*, report NASA/CP-1999-208917, NASA, Washington, DC, 1999, pp. 475–478.
13. Kang, K. T., Hwang, J. Y., Chung, S. M., and Lee, W., *Combust. Flame* 109:266–281 (1997).
14. Lin, K.-C., and Faeth, G. M., *J. Prop. Power* 12:691–698 (1996).
15. Lin, K.-C., and Faeth, G. M., *Combust. Flame* 115:468–480 (1998).
16. Lin, K.-C., and Faeth, G. M., *J. Prop. Power* 12:10–17 (1996).
17. Kaplan, C. R., and Kailasanath, K., *Combust. Flame*, in press (2000).
18. Markatou, P., Wang, H., and Frenklach, M., *Combust. Flame* 93:467–482 (1993).
19. Sun, C. J., Sung, C. J., Wang, H., and Law, C. K., *Combust. Flame* 107:321–335 (1996).
20. Lin, K.-C., and Faeth, G. M., *Environ. Combust. Technol.* 1:53 (2000).
21. Law, C. K., and Faeth, G. M., *Prog. Energy Combust. Sci.* 20:65–113 (1994).
22. Lin, K.-C., Faeth, G. M., Sunderland, P. B., Urban, D. L., and Yuan, Z. G., *Combust. Flame* 116:415–431 (1999).
23. Lin, K.-C., and Faeth, G. M., *AIAA J.* 37:759–765 (1999).
24. Spalding, D. B., in *Combustion and Mass Transfer*, Pergamon Press, New York, 1979, pp. 185–195.
25. Schlichting, H., *Boundary Layer Theory, 4th ed.*, McGraw-Hill, New York, 1960, pp. 160–164.
26. Mahalingam, S., Ferziger, J. H., and Cantwell, B. J., *Combust. Flame* 82:231–234 (1990).
27. Sunderland, P. B., Köylü, Ü. Ö., and Faeth, G. M., *Combust. Flame* 100:310–322 (1995).
28. Sunderland, P. B., and Faeth, G. M., *Combust. Flame* 105:132–146 (1996).

COMMENTS

C. H. Priddin, Rolls Royce, UK. In the 80s-style fuel atomizers you showed, the overall AFRs are of the order 4–6, that is, still overall rich. Do you think your analysis still applies in this situation, or is the flame somewhere else?

Author's Reply. The general success of air atomization to reduce soot emissions from aircraft gas turbine engines for a variety of fuel atomizer AFRs [Ref. 1 in paper] suggests that effects of increasing air/fuel velocity ratios persist even when AFRs are small. We believe that this is reasonable based on present findings because small fuel stream velocities should generally provide conditions where air stream velocities are larger than fuel stream velocities throughout the combustion process, leading to generally desirable soot emissions properties, e.g., soot-formation-oxidation conditions as defined by Kang [Ref. 13 in paper]. Direct demonstration of this conjecture, however, would be desirable.

•

Cary Presser, NIST, USA. Please describe your thoughts regarding the use of different gases in place of air. Is the propensity to soot purely an aerodynamic effect (and thus other gases may be used) or is the pressure of oxygen required to assist in the oxidation of soot? It is assumed that ambient (or secondary) air is present to sustain a stable flame.

Author's Reply. For the same reasons discussed in the reply to C. H. Pridden, we believe that the nature of the atomizing gas used in the fuel atomizer is not the most critical aspect of soot control using air atomization. It seems to us that the crucial elements are relatively good atomization with relatively small fuel momentum (velocities). This should generally yield desirable air/fuel stream velocity ratio properties when the region of the flame sheet is approached, e.g., soot-formation-oxidation conditions as defined by Kang (Ref. [13] in paper). Direct assessment of the conjecture, however, would also be desirable.

Appendix D:

D.L. Urban, Z.-G. Yuan, P.B. Sunderland, K.-C. Lin, Z. Dai and G.M. Faeth (2000) Smoke-point properties of nonbuoyant round laminar jet diffusion flames. *Proc. Combust. Inst.* 28, 1965-1972.

Proceedings of the Combustion Institute, Volume 28, 2000/pp. 1965–1972

SMOKE-POINT PROPERTIES OF NON-BUOYANT ROUND LAMINAR JET DIFFUSION FLAMES

D. L. URBAN,[1] Z.-G. YUAN,[1] P. B. SUNDERLAND,[1] K.-C. LIN,[2] Z. DAI[2] AND G. M. FAETH[2]
[1]*NASA Glenn Research Center*
Cleveland, OH 44135, USA
[2]*University of Michigan*
Ann Arbor, MI 48109, USA

The laminar smoke-point properties of non-buoyant round laminar jet diffusion flames were studied emphasizing results from long-duration (100–230 s) experiments at microgravity carried out in orbit aboard the space shuttle Columbia. Experimental conditions included ethylene- and propane-fueled flames burning in still air at an ambient temperature of 300 K, pressures of 35–130 kPa, jet exit diameters of 1.6 and 2.7 mm, jet exit velocities of 170–690 mm/s, jet exit Reynolds numbers of 46–172, characteristic flame residence times of 40–302 ms, and luminous flame lengths of 15–63 mm. Contrary to the normal-gravity laminar smoke point, in microgravity, the onset of laminar smoke-point conditions involved two flame configurations: closed-tip flames with soot emissions along the flame axis and open-tip flames with soot emissions from an annular ring about the flame axis. Open-tip flames were observed at large characteristic flame residence times with the onset of soot emissions associated with radiative quenching near the flame tip: nevertheless, unified correlations of laminar smoke-point properties were obtained that included both flame configurations. Flame lengths at laminar smoke-point conditions were well correlated in terms of a corrected fuel flow rate suggested by a simplified analysis of flame shape. The present steady and non-buoyant flames emitted soot more readily than non-buoyant flames in earlier tests using ground-based microgravity facilities and than buoyant flames at normal gravity, as a result of reduced effects of unsteadiness, flame disturbances, and buoyant motion. For example, present measurements of laminar smoke-point flame lengths at comparable conditions were up to 2.3 times shorter than ground-based microgravity measurements and up to 6.4 times shorter than buoyant flame measurements. Finally, present laminar smoke-point flame lengths were roughly inversely proportional to pressure to a degree that is a somewhat smaller than observed during earlier tests both at microgravity (using ground-based facilities) and at normal gravity.

Introduction

The laminar smoke-point properties of jet diffusion flames (the luminous flame length, fuel flow rate, characteristic residence time, etc., at the onset of soot emissions) are useful observable soot properties of non-premixed flames. For example, these measures provide a means to rate several aspects of flame sooting properties: the relative propensity of various fuels to produce soot in flames [1–4]; the relative effects of fuel structure, fuel dilution, flame temperature, and ambient pressure on the soot emission properties of flames [5–14]; the relative levels of continuum radiation from soot in flames [15–17]; and effects of the intrusion of gravity (buoyancy) on emissions of soot from flames [18–26]. Laminar smoke-point properties generally are measured using buoyant round laminar jet diffusion flames, surrounded by co-flowing air in order to prevent pulsations characteristic of buoyant jet diffusion flames in still environments. Laminar smoke-point properties found using this configuration are relatively independent of burner diameter and co-flow velocities, which tends to enhance their value as global measures of soot properties [9,10]. Recent studies, however, suggest that the laminar smoke-point properties of buoyant and non-buoyant laminar jet diffusion flames are fundamentally different [19–26]. Thus, the overall objective of the present investigation was to measure the laminar smoke-point properties of non-buoyant flames, because of the relevance of non-buoyant flames to most practical industrial processes where effects of buoyancy are small.

The potential differences between the laminar smoke properties of buoyant and non-buoyant flames can be attributed mainly to the different hydrodynamic properties of these flames [24–27]. In particular, soot particles are too large to diffuse like gas molecules so that they are convected at gas velocities, aside from minor effects of Brownian motion and thermophoresis [24]. In non-buoyant flames, the streamlines diverge from the nozzle axis, whereas in buoyant flames the streamlines (and the entrained flow) converge toward the nozzle axis. As

a result, flow acceleration due to gravitational forces in buoyant round laminar jet diffusion flames implies that soot mainly nucleates near the flame sheet and then is drawn toward fuel-rich conditions nearer to the flame axis, promoting soot growth for an extended residence time before the soot finally crosses the flame sheet within an annular soot layer near the flame tip to reach soot oxidation conditions. This type of soot path, termed *soot-formation flame conditions* by Kang et al. [27], tends to promote soot growth and inhibit soot oxidation, enhancing the tendency of the flame to emit soot. On the other hand, flow deceleration in non-buoyant round laminar jet diffusion flames implies that soot mainly nucleates in the cool core of the flame at fuel-rich conditions and then is drawn directly toward and through the flame sheet, so that soot tends to leave the flame over a relatively extended region. This type of soot path, termed *soot-formation-oxidation conditions* by Kang et al. [27], tends to inhibit soot growth and enhance soot oxidation compared to buoyant flames that have similar characteristic residence times, reducing the tendency of the flame to emit soot. Thus, the soot nucleation, growth, and oxidation environments of buoyant and non-buoyant laminar jet diffusion flames are quite different, providing significant potential for different laminar smoke-point properties as well.

Several studies of the laminar smoke-point properties of non-buoyant laminar jet diffusion flames have been reported, motivated by the potential effects of buoyancy on soot processes in flames (see Refs. [18–25] and references cited therein). Most of these studies used ground-based microgravity facilities to observe non-buoyant flames and showed that laminar smoke-point flame lengths were significantly smaller and laminar smoke-point characteristic residence times were significantly larger for non-buoyant than buoyant flames. These differences generally have been attributed to the different soot paths in buoyant and non-buoyant flames that were just discussed, as well as increased effects of radiative quenching in non-buoyant flames due to their increased characteristic residence times compared to buoyant flames. A concern about these results, however, is that limited testing using space-based microgravity facilities yielded significantly different results than those observed using ground-based microgravity facilities [25]. Thus, the objective of the present study was to more completely assess these differences by measuring laminar smoke-point properties during long-term experiments (100–230 s) at microgravity carried out on orbit in the space shuttle Columbia (flights STS-83 and STS-94 in 1997). The scope of the study was limited to round ethylene- and propane-fueled laminar jet diffusion flames burning in still and slightly vitiated air at pressures of 35–130 kPa.

Experimental Methods

Experimental methods are described only briefly, see Urban et al. [25] for details about the apparatus and instrumentation and Lin et al. [28] for a tabulation of test conditions. The laminar jet diffusion flames were stabilized at the exit of round fuel nozzles located along the axis of a windowed chamber having a diameter and length of 400 mm and 740 mm, respectively. The chamber was filled with oxygen/nitrogen mixtures to provide the nominal composition of dry air (21 ± 1% oxygen by volume). The properties of the gas surrounding the flames varied slightly over the present relatively long test times because the test chamber was closed. The greatest change involved the gas composition, but even this change was modest, with maximum oxygen consumptions never exceeding 0.02 mol fraction during any test. These conditions were maintained by periodically venting the chamber to space and adding fresh dry air in the period between tests. Present flames typically required 10 s times to approach steady behavior as exemplified by constant flame lengths after a disturbance [25].

Stainless steel fuel nozzles having inside diameters of 1.6 mm and 2.7 mm, lengths of 148 mm, and inlet flow straighteners yielded nonswirling fully developed laminar flow at the jet exit. The test fuels were stored in cylinders and delivered to the nozzles through solenoid valves and a mass flow rate controller and sensor. The flames were ignited with a hot wire coil that was retracted from the nozzle exit once the flame was stabilized.

Monitoring measurements included the fuel flow rate, the fuel inlet temperature, the chamber pressure, and the chamber gas temperature [25,28]. The flames were observed using a color CCD video camera (Hitachi, Model KP-C553) with a 125 × 164 mm field of view and a 25 mm depth of field centered on the flame axis. Flame images were recorded at a rate of 30 images/s and could be measured with a spatial resolution better than 0.3 mm. Initial fuel flow rates were set in excess of laminar smoke-point flow rates and could be adjusted up to ±30% in 5% steps to achieve the desired final conditions near (within 5%), but generally smaller than, laminar smoke-point fuel flow rates. Three tests were exceptions in which initial excessively large fuel flow rates prevented final flame lengths from being shorter than laminar smoke-point conditions, as noted by Lin et al. [28].

A total of 21 flames were observed, yielding the following ranges of test properties: ethylene- and propane-fueled flames, ambient air temperatures and pressures of 300 K and 35–130 kPa, respectively, jet exit velocities and Reynolds numbers of 170–1690 mm/s and 46–172, respectively, characteristic residence times of 40–302 ms, and luminous flame lengths of 15–63 mm. Characteristic residence times

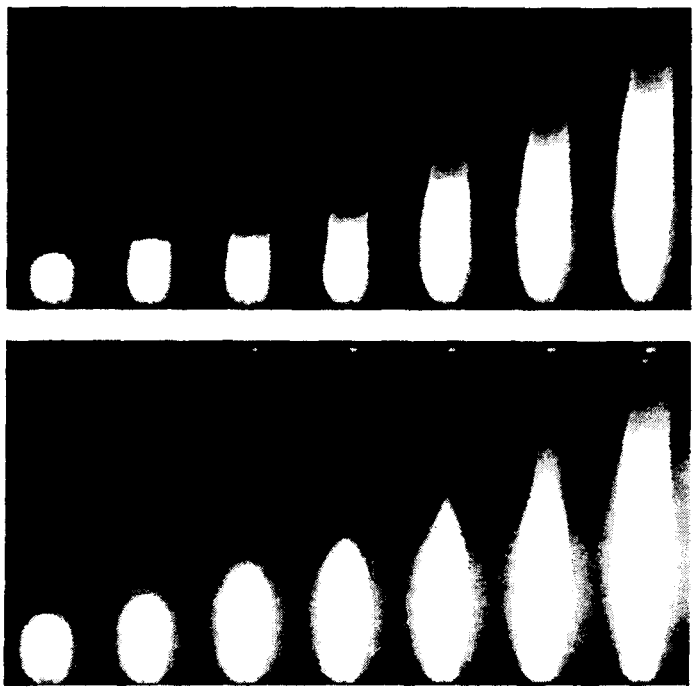

FIG. 1. Photographs of round non-buoyant laminar jet diffusion flames in still air as the fuel flow rate is increased in the transition region where the laminar smoke-point is approached and exceeded for ethylene-fueled flames with a 1.6 mm jet exit diameter. Upper series of photographs shows open-tip smoke-point behavior at 100 kPa, with the third flame from the left just beyond the smoke-point condition; lower series of photographs shows closed-tip smoke-point behavior at 50 kPa, with the fifth flame from the left just beyond the smoke-point condition.

are reported elsewhere [29] and are taken to be $2L/u_o$.

Results and Discussion

Flow Visualization

Typical of many past observations of non-buoyant round laminar jet diffusion flames [18–22,24,25,28], the present flames could be grouped into closed-tip and open-tip configurations. The difference between these two configurations was particularly noticeable in the vicinity of the laminar smoke-point, as illustrated by the images in Fig. 1. These photographs show the flame appearance as the fuel flow rate is increased in the transition region where the laminar smoke-point is approached and exceeded for ethylene-fueled flames having 1.6 mm jet exit diameters. The upper series of photographs shows the behavior of large characteristic residence time flames (larger than 80 ms) where the flame tips were blunt (open-tip) throughout the transition to soot emitting conditions, and the first emission of soot was associated with an annular region surrounding the flame axis and having a diameter comparable to the maximum flame diameter. The lower series of photographs shows the behavior of small characteristic residence time flames (smaller than 80 ms) where the flame tips were rounded (closed-tip) and the first emission of soot was along the flame axis. Even these latter flames, however, eventually exhibited open-tip behavior as fuel flow rates increased beyond the laminar smoke-point condition (see the last image of the lower series of photographs in Fig. 1). Thus, tip opening generally is closely associated with laminar smoke-point conditions for non-buoyant flames, which has also been observed by several other investigators (see Refs. [18–22] and references cited therein).

Measurements of soot concentrations in the present flames using deconvoluted laser extinction show that soot is contained within a narrow annular ring and that no soot is present at the flame axis for open-tip conditions [25]. Corresponding soot temperatures using deconvoluted multiline emission measurements show that soot temperatures progressively decrease with increasing streamwise distances in open-tip flames and reach values of roughly 1000 K near the flame tip [25]. Low reaction rates at such conditions are consistent with quenching of soot oxidation, allowing soot to escape from the flame. The main mechanism causing this progressive reduction of temperature is continuum radiation from soot. This radiative heat loss becomes more significant with increasing streamwise distance due to the progressive reduction of flow velocities, which involves a corresponding reduction of transport and thus reaction rates at the flame sheet. The corresponding reduced chemical energy release rates, combined with progressively increasing radiative heat losses due to increasing soot concentrations,

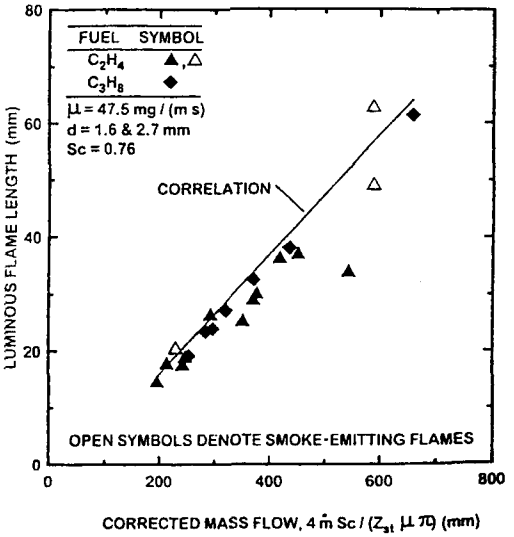

FIG. 2. Luminous flame lengths as a function of corrected fuel flow rate for round non-buoyant laminar jet diffusion flames in still air at the laminar smoke point. Correlation based on simplified analysis of Lin et al. [28].

provide ample potential for quenching, and thus tip-opening, and corresponding emissions of soot. In contrast, buoyant diffusion flames have progressively increasing velocities and thus increasing transport rates with increasing streamwise distance, due to effects of buoyancy, so that soot emissions occur because of rapid mixing and residence times that are insufficient to complete soot oxidation, rather than because of radiative quenching [25]. Finally, this latter condition is approached by non-buoyant flames at short residence times where effects of radiative quenching are reduced, which tends to produce the closed-tip laminar smoke-point behavior illustrated in the lower series of photographs of Fig. 1.

Luminous Flame Lengths

Similar to the observations of luminous flame lengths at the smoke-points of buoyant round laminar jet diffusion flames as described by Schug et al. [5], the present luminous flame lengths at the smoke points of non-buoyant round laminar jet diffusion flames were closely associated with the fuel flow rate, as suggested by the simplified analysis of Lin et al. [28]. This behavior is illustrated in Fig. 2, where present measurements of laminar smoke-point luminous flame lengths are plotted as a function of the corrected fuel flow rate based on the results of the simplified flame shape theory for non-buoyant laminar jet diffusion flames of Ref. [28]. The open symbols on this plot denote the three test conditions in which soot-emitting flames just beyond the laminar smoke-point conditions were measured; nevertheless, these measurements are very similar to the remaining results which are from flames at the laminar smoke point but which were not emitting soot. The one data point remote from the rest resulted at at the lowest pressure tested, 35 kPa, at which luminous flame lengths and the onset of soot-emitting conditions were more difficult to observe due to relatively small maximum soot concentrations (less than 1 ppm based on multiline emission measurements). Except for the one outlier, the correlation between luminous flame lengths and corrected fuel mass flow rates at laminar smoke-point conditions is seen to be quite good; therefore, laminar smoke-point properties will be represented by luminous flame lengths alone to simplify the comparison between present measurements and the earlier findings in Refs. [5,16,24].

An explanation of the luminous flame length behavior observed in Fig. 2 can be obtained from the flame shape correlations of Lin et al. [28] for non-buoyant round laminar jet diffusion flames in still air. These results are based on a simplified analysis (Spalding [29]) for this flame configuration. Ignoring small effects of the virtual origin, this correlation can be written to yield the luminous flame length as a function of the corrected fuel flow rate parameter used in Fig. 2, as follows:

$$L = (3C_f/32)(4\dot{m}\ Sc/(Z_{st}\ \mu\pi)) \qquad (1)$$

where the empirical parameter C_f is used to account for the presence or absence of soot within the flame. Following Ref. [28], a simple correlation of equation 1 was fitted to the measurements of flames in air environments using values of Sc and μ for air at roughly the average of the adiabatic flame temperature and the ambient temperature (the values used are summarized on the plot). The correlation shown in the figure is for $C_f = 1$ for flames at the laminar smoke point from Lin et al. [28], in contrast to $C_f = 0.5$ for soot-free blue flames from Sunderland et al. [30]. The longer soot-containing flames are consistent with luminosity due to the presence of soot at fuel-lean conditions for flames at the transition to soot emissions [28]. Finally, it is evident that equation 1 provides a surprisingly good correlation between luminous flame lengths and the corrected mass flow rate for present observations of non-buoyant round laminar jet diffusion flames in spite of the approximate nature of the Spalding [29] analysis.

Laminar Smoke Points

In view of the different mechanisms leading to the onset of soot emissions for buoyant and non-buoyant laminar jet diffusion flames, it is not surprising that they have substantially different laminar smoke-point properties. This behavior is illustrated in Figs. 3 and 4 by plots of laminar smoke-point flame

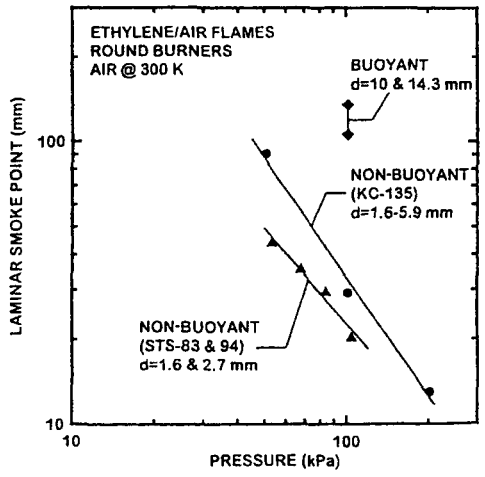

FIG. 3. Laminar smoke-point flame lengths of ethylene-fueled round non-buoyant and buoyant laminar jet diffusion flames burning in air as a function of pressure. Non-buoyant KC-135 results from Sunderland et al. [24], buoyant results from Schug et al. [5] and Sivathanu and Faeth [16].

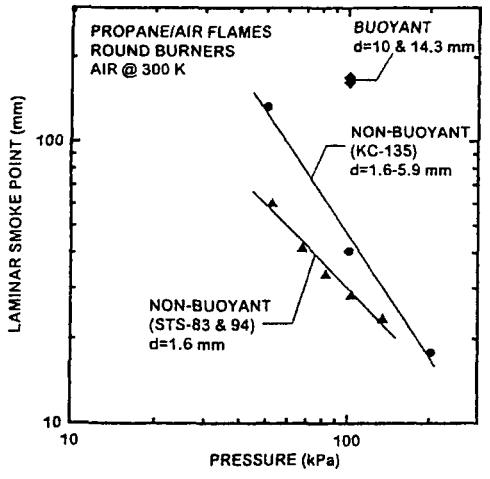

FIG. 4. Laminar smoke-point flame lengths of propane-fueled round non-buoyant and buoyant laminar jet diffusion flames burning in air as a function of pressure. Non-buoyant KC-135 results from Sunderland et al. [24], buoyant results from Schug et al. [5] and Sivathanu and Faeth [16].

lengths as a function of pressure for ethylene- and propane-fueled flames. Measurements illustrated in the figures include results for non-buoyant flames having jet exit diameters of 1.6 and 2.7 mm from the present space-based experiments, results for non-buoyant flames having jet exit diameters of 1.6, 2.7 and 5.6 mm from Sunderland et al. [24] using ground-based microgravity facilities, and results for buoyant flames having jet exit diameters of 10.0 mm from Schug et al. [5] and 14.3 mm from Sivathanu and Faeth [16].

There are several interesting features about the measurements illustrated in Figs. 3 and 4. First of all, an obvious feature of these results is that the present laminar smoke-point flame lengths of the non-buoyant flames are significantly smaller than those of the buoyant flames. For example, the laminar smoke-point flame lengths of the buoyant flames are up to 6.4 times larger than the present non-buoyant flames at comparable conditions. This behavior comes about because the present non-buoyant flames have much larger characteristic residence times (up to 300 ms [28]) than the buoyant flames (only up to 50 ms [24]), which is due to buoyancy-induced motion, in spite of the greater length of the buoyant flames. This provides greater potential for radiative heat losses for the non-buoyant flames, leading to the radiative quenching mechanism of soot emissions discussed in connection with tip openings (Fig. 1).

Another important feature of the laminar smoke-point flame lengths illustrated in Figs. 3 and 4 is that the present non-buoyant flames are significantly smaller than those of nonbuoyant flames in ground-based microgravity facilities (which typically have gravity of 10^{-2} g) up to a factor of 2.3 at comparable conditions. This behavior is caused by the closer approach to steady, non-buoyant flame properties by the long-term space-based experiments compared to the relatively unsteady and disturbed microgravity environment of ground-based microgravity facilities. Flow velocities are very small near the flame tip of non-buoyant laminar jet diffusion flames [24] and can be disturbed by small levels of g-jitter resulting enhanced mixing, which defers radiative quenching. This behavior is exacerbated by the relatively slow development of non-buoyant flames for the relatively large jet exit diameters considered during the ground-based microgravity tests, so flame response times were generally longer than periods when the test apparatus was free of disturbances [25]. Further evidence of enhanced mixing in the ground-based microgravity tests compared to the space-based tests is provided by the observations of generally shorter luminous flame lengths at comparable conditions for the ground-based results (e.g., 30% shorter as discussed by Lin et al. [28]).

Another difference between the laminar smoke-point properties of non-buoyant flames from ground- and space-based microgravity facilities involves the pressure dependence. In particular, the present long-term microgravity experiments yield laminar smoke-point flame lengths that are roughly inversely proportional to pressure. This effect of pressure comes about because increased pressures tend to increase rates of soot formation [11–14], and

because of residence times available for soot growth for given burner conditions and flame lengths: both these effects imply smaller flame lengths for onset of soot emissions as pressures increase. In contrast, the more disturbed microgravity environment of the ground-based facilities yields laminar smoke-point flame lengths that are inversely proportional to pressure to the 1.4 power. This latter behavior is a stronger pressure variation than that observed for buoyant flames. Flower and Bowman [11–14] report laminar smoke-point flame lengths inversely proportional to pressure to the 1.3 power. These variations of the pressure dependence of laminar smoke-point flame lengths due to the intrusion of disturbances and gravitational forces are not surprising, however, because flame response to these effects varies with pressure. Differences of these magnitudes are of interest for gaining a better understanding of soot formation in diffusion flames (see Glassman [10]), which highlights the importance of achieving truly steady and non-buoyant diffusion flame conditions for reliable experimental results.

Other properties of the laminar smoke-point flame lengths plotted in Figs. 3 and 4 are qualitatively similar for non-buoyant space-based flames, non-buoyant ground-based flames, and buoyant flames. For example, effects of jet exit diameter on laminar smoke-point flame lengths are small in all three cases, which agrees with the well-known behavior of buoyant flames (see Glassman [9,10]). This behavior is expected for buoyant flames because their flame heights and characteristic residence times are both independent of jet exit diameter, with the latter being largely a function of flame height [16]. This behavior is not expected for non-buoyant flames, however, because while their flame lengths are independent of jet exit diameter, as discussed in connection with Fig. 2, their characteristic residence times decrease with decreasing jet exit diameter [24], which should contribute to corresponding increases of laminar smoke-point flame lengths. Such increases are not observed, and this behavior merits further study. Finally, the laminar smoke-point flame lengths of ethylene-fueled flames are smaller than those of propane-fueled flames for all three flame conditions considered in Figs. 3 and 4. This behavior agrees with past observations of the greater propensity to soot of ethylene-fueled compared to propane-fueled laminar jet diffusion flames [5,15,16].

Conclusions

The smoke-point properties of nonbuoyant round laminar jet diffusion flames were observed during long-term (100–230 s) experiments at microgravity using space-based facilities. Measurements included ethylene- and propane-fueled flames burning in still air at an ambient temperature of 300 K, pressures of 35–130 kPa, jet exit diameters of 1.6 and 2.7 mm, jet exit velocities of 170–1690 mm/s, jet exit Reynolds numbers of 46–172, characteristic flame residence times of 40–302 ms, and luminous flame lengths of 15–63 mm. The major conclusions of the study are as follows:

1. The onset of laminar smoke-point conditions in microgravity involved either a closed-tip configuration with first soot emissions along the flame axis, or an open-tip configuration with first soot emissions from an annular ring about the flame axis and having a diameter comparable to the maximum flame diameter. Closed- and open-tip flames were observed at small and large characteristic flame residence times, respectively, supporting earlier observations that open-tip behavior is caused by radiative quenching of soot oxidation near the flame tip.
2. Luminous flame lengths at laminar smoke-point conditions were equally well correlated for both closed- and open-tipped flame configurations in terms of a corrected fuel flow rate, independent of the jet exit diameter, as suggested by the simplified flame shape analysis of Lin et al. [28]. These laminar smoke-point flame lengths were roughly 30% longer than those measured using ground-based microgravity facilities because of decreased effects of unsteadiness and g-jitter.
3. The present steady and non-buoyant flames emitted soot more readily than other non-buoyant flames at microgravity in ground-based facilities and than buoyant flames at normal gravity. For example, the laminar smoke-point flame lengths of non-buoyant flames from ground-based microgravity facilities were up to 2.3 times longer than the present measurements at comparable conditions because of effects of unsteadiness and g-jitter; similarly, the laminar smoke-point flame lengths of buoyant flames were up to 6.4 times longer than the present measurements at comparable conditions because of effects of buoyancy-induced motion.
4. Laminar smoke-point flame lengths as a function of pressure were identical for both closed- and open-tipped flames and were roughly inversely proportional to pressure and relatively independent of jet exit diameter for the present non-buoyant flames. In contrast, the laminar smoke-point flame lengths of non-buoyant flames in ground-based microgravity facilities and buoyant flames at normal gravity were inversely proportional to pressure to the 1.4 and 1.3 powers, respectively, because of effects of unsteadiness, g-jitter, and buoyancy-induced motion. All flame conditions considered, however, indicated that laminar smoke-point flame lengths are generally smaller for ethylene than for propane, reflecting the greater propensity to soot of ethylene compared to propane.

Nomenclature

C_f	flame length parameter
d	fuel port diameter
D	mass diffusivity
L	laminar smoke-point flame length
$\dot{m}$	fuel mass flow rate
p	pressure
Re	flame Reynolds number, $4\,\dot{m}/(\pi d\mu)$
Re_o	jet exit Reynolds number, $4\,\dot{m}/(\pi d\mu_o)$
Sc	Schmidt number, υ/D
u	streamwise velocity
Z_{st}	stoichiometric mixture fraction
μ	dynamic viscosity
ν	kinematic viscosity
ρ	density

Subscript

o	burner exit condition

Acknowledgments

This research was supported by NASA Grants NCC3-661, NAG3-1878, and NAG3-2048 of the Office of Life and Microgravity Sciences under the overall technical management of H. D. Ross of the Glenn Research Center. The authors acknowledge the efforts R. Crouch, G. T. Linteris, and J. E. Voss, who actually carried out the experiments in orbit, and A. Over and her associates at the Glenn Research Center for development and operation of the test apparatus.

REFERENCES

1. Clarke, A. E., Hunter, T. C., and Garner, F. H., *J. Inst. Petrol.* 32:627–642 (1946).
2. Schalla, R. L., Clark, T. P., and McDonald, G. E., NACA report 1186, 1954.
3. Schalla, R. L., and McDonald, G. E., *Proc. Combust. Inst.* 5:316–324 (1954).
4. Schalla, R. L., and Hubbard, R. R., NACA report 1300, 1959.
5. Schug, K. P., Manheimer-Timnat, Y., Yaccarino, P., and Glassman, I., *Combust. Sci. Technol.* 22:235–250 (1980).
6. Glassman, I., and Yaccarino, P., *Proc. Combust. Inst.* 18:1175–1183 (1980).
7. Glassman, I., and Yaccarino, P., *Combust. Sci. Technol.* 24:107–114 (1980).
8. Gomez, A., Sidebotham, G., and Glassman, I., *Combust. Flame* 58:45–57 (1984).
9. Glassman, I., *Proc. Combust. Inst.* 22:295–311 (1988).
10. Glassman, I., *Proc. Combust. Inst.* 27:1589–1596 (1998).
11. Flower, W. L., and Bowman, C. T., *Combust. Sci. Technol.* 37:93–97 (1984).
12. Flower, W. L., and Bowman, C.T., *Proc. Combust. Inst.* 20:1035–1044 (1984).
13. Flower, W. L., and Bowman, C. T., *Proc. Combust. Inst.* 21:1115–1129 (1986).
14. Flower, W. L., and Bowman, C. T., *Combust. Sci. Technol.* 53:217–224 (1987).
15. Markstein, G. H., *Proc. Combust. Inst.* 22:363–370 (1988).
16. Sivathanu, Y. R., and Faeth, G. M., *Combust. Flame* 81:133–149 (1990).
17. Köylü, Ü. Ö., and Faeth, G. M., *Combust. Flame* 87:61–76 (1991).
18. Ito, H., Fujita, A., and Ito, K., *Combust. Flame* 99:363–370 (1994).
19. Ku, J. C., Griffin, D. W., Greenberg, P. S., and Roma, J., *Combust. Flame* 102:216–218 (1995).
20. Megaridis, C. M., Griffin, D. W., and Konsur, K., *Proc. Combust. Inst.* 26:1291–1299 (1996).
21. Konsur, B., Megaridis, C. M., and Griffin, D. W., *Combust. Flame* 116:334–347 (1998).
22. Konsur, B., Megaridis, C. M., and Griffin, D. W., *Combust. Flame* 118:509–520 (1999).
23. Atreya, A., and Agrawal, S., *Combust. Flame* 115:372–382 (1998).
24. Sunderland, P. B., Mortazavi, S., Faeth, G. M., and Urban, D. L., *Combust. Flame* 96:97–103 (1994).
25. Urban, D. L., Yuan, Z.-G., Sunderland, P. B., Linteris, G. T., Voss, J. E., Lin, K.-C., Dai, Z., Sun, K., and Faeth, G. M., *AIAA J.* 36:1346–1360 (1998).
26. Law, C. K., and Faeth, G. M., *Prog. Energy Combust. Sci.* 20:65–113 (1994).
27. Kang, K. T., Hwang, J. Y., Chung, S. M., and Lee, W., *Combust. Flame* 109:266–281 (1997).
28. Lin, K.-C., Faeth, G. M., Sunderland, P. B., Urban, D. L., and Yuan, Z.-G., *Combust. Flame* 116:415–431 (1998).
29. Spalding, D. B., *Combustion and Mass Transfer*, Pergamon Press, New York, 1979, pp. 185–195.
30. Sunderland, P. B., Mendelson, B. J., Yuan, Z.-G., and Urban, D. L., *Combust. Flame* 116:376–386 (1999).

COMMENTS

John L. de Ris, Factory Mutual Research, USA. Your instrumentation includes a radiometer. One wonders whether the total radiative fraction from the flame at its smoke point at zero-gravity takes on the same value of 30% as is found for normal buoyant flames at their smoke-point. For normal buoyant flames, this radiant fraction is independent of fuel type. You also measured the flame tip temperature of flames at their smoke-point condition. How does this temperature compare to the 1400 K value found for smoke-point flames for normal gravity?

Author's Reply. The total radiative fraction from the flames we studied was between 40% and 60%. Since most of our flames were very near the smoke height, the limited data set studied here did not show evidence of a correlation between radiative emission and smoke height as reported for normal-gravity flames.

As reported (Ref. [25] in paper), the extrapolated temperatures (from the multiline emission measurements) at the flame tip (at the smoke point) were approximately 1000 K. This is substantially lower than the 1400 K value reported by other workers for normal-gravity flames.

•

Fletcher J. Miller, National Center for Microgravity Research, USA. Since the laminar smoke points are so dependent on residence time, how might the presence of a co-flow in the 1g experiments versus the absence of a co-flow in the μg experiments affect the comparison between the two gravitational levels? Would μg experiments with a co-flow be valuable to provide an independent way to alter residence times?

Author's Reply. Co-flow flames are used in 1g smoke-point studies to eliminate buoyancy induced flicker. In 1g, the co-flow has a very limited effect on the flame residence time (and likewise on the smoke point) which are dominated by the buoyant acceleration. In low gravity, the situation is quite different: the flow diverges from the nozzle; consequently, the velocity at the flame tip can be quite small and is therefore easily influenced (increased) by the co-flow. We agree with the suggestion that testing with co-flow in low gravity should provide interesting results, and this is part of a planned future experiment.

Appendix E:

F. Xu, Z. Dai, and G.M. Faeth, Flame and soot boundaries of laminar jet diffusion flames. *AIAA J.* 40, 2437-2446.

AIAA JOURNAL
Vol. 40, No. 12, December 2002

Flame and Soot Boundaries of Laminar Jet Diffusion Flames

F. Xu,* Z. Dai,† and G. M. Faeth‡
University of Michigan, Ann Arbor, Michigan 48109-2140

The shapes (flame-sheet and luminous-flame boundaries) of steady weakly buoyant round hydrocarbon-fueled laminar-jet diffusion flames in still and coflowing air were studied both experimentally and theoretically. Flame-sheet shapes were measured from photographs using a CH optical filter to distinguish flame-sheet boundaries in the presence of blue CO_2 and OH emissions and yellow continuum radiation from soot. Present experimental conditions included acetylene-, methane-, propane-, and ethylene-fueled flames having initial reactant temperatures of 300 K, ambient pressures of 4–50 kPa, jet-exit Reynolds numbers of 3–54, initial air/fuel velocity ratios of 0–9, and luminous flame lengths of 5–55 mm; earlier measurements for propylene- and 1,3-butadiene-fueled flames for similar conditions were considered as well. Nonbuoyant flames in still air were observed at microgravity conditions; essentially nonbuoyant flames in coflowing air were observed at small pressures to control effects of buoyancy. Predictions of luminous flame boundaries from soot luminosity were limited to laminar smoke-point conditions, whereas predictions of flame-sheet boundaries ranged from soot-free to smoke-point conditions. Flame-shape predictions were based on simplified analyses using the boundary-layer approximations along with empirical parameters to distinguish flame-sheet and luminous-flame (at the laminar smoke point) boundaries. The comparison between measurements and predictions was remarkably good and showed that both flame-sheet and luminous-flame lengths are primarily controlled by fuel flow rates with lengths in coflowing air approaching $\frac{2}{3}$ of the lengths in still air as coflowing air velocities are increased. Finally, luminous flame lengths at laminar smoke-point conditions were roughly twice as long as flame-sheet lengths at comparable conditions because of the presence of luminous soot particles in the fuel-lean region of the flames.

Nomenclature

C_f	=	empirical soot factor
C_u	=	empirical coflow factor
D	=	mass diffusivity
d	=	jet-exit diameter
Fr_a, Fr_f	=	air- and fuel-stream Froude numbers, $u_{ao}^2/(2gL_f)$ and $u_{fo}^2/(2gL_f)$
g	=	acceleration of gravity
L_f	=	distance from jet exit to either flame-sheet or luminous-flame tip
L_o	=	distance from jet exit to virtual origin
$\dot{m}$	=	burner mass flow rate
$\dot{m}_f$	=	burner fuel mass flow rate
p	=	pressure
Re	=	jet Reynolds number, $4\dot{m}/(\pi d\mu)$
r	=	radial distance
Sc	=	Schmidt number, ν/D
u	=	streamwise velocity
w	=	luminous flame diameter
$w_{1/2}$	=	luminous flame diameter at $\zeta = \frac{1}{2}$
x	=	streamwise distance
Z_{st}	=	stoichiometric mixture fraction
ζ	=	normalized streamwise distance; Eq. (4)
μ	=	dynamic viscosity
ν	=	kinematic viscosity

Subscripts

a	=	airstream property
f	=	fuel-stream property
MAX	=	maximum value
o	=	burner exit plane or virtual origin condition

Introduction

LAMINAR nonpremixed (diffusion) flames are of interest because they provide model flame systems that are far more tractable for analysis and experiments than practical turbulent diffusion flames. Clearly, an understanding of laminar diffusion flames must precede an understanding of more complex turbulent diffusion flames. In addition, many properties of laminar diffusion flames are directly relevant to turbulent diffusion flames using laminar flamelet concepts. Finally, laminar diffusion flame shapes have been of interest since the classical study of Burke and Schumann[1] because they involve a simple nonintrusive measurement that is convenient for evaluating flame structure predictions. Motivated by these observations, the shapes of round laminar-jet diffusion flames were considered both experimentally and theoretically during the present investigation. The study was limited to flames where effects of buoyancy were either nonexistent or small, however, in order to minimize parameters and because most practical flames are not buoyant.

Most earlier studies of the shapes of hydrocarbon-fueled nonbuoyant laminar-jet diffusion flames have considered combustion in still air (see Refs. 2–6 and references cited therein). These studies have shown that soot-containing flames at the laminar smoke point (flames at the condition of onset of soot emissions) have luminous flame lengths roughly twice as long as the length of flame sheet (the position where fuel and oxidant combine in roughly stoichiometric proportions generally within a thin reaction zone) and have developed simple but effective ways to estimate their shapes.[4,5] Corresponding studies of hydrocarbon-fueled nearly nonbuoyant (weakly buoyant) laminar-jet diffusion flames burning in coflowing air have also been reported (see Refs. 1, 7–9, and references cited therein). These studies were limited to soot-containing flames at laminar smoke-point conditions and also developed simple but effective ways to estimate their shapes; however, the corresponding behavior of the flame sheet for these conditions [in either soot-free

Received 15 September 2000; revision received 25 June 2002; accepted for publication 8 July 2002.

*Research Associate, Department of Aerospace Engineering; currently Assistant Professor, Mechanical Engineering Department, Central Florida University, Orlando, FL 32816.

†Research Associate, Department of Aerospace Engineering; currently Lead Engineer, G.E. Aircraft Engines, Cincinnati, OH 45215.

‡A.B.M. Modine Professor, Department of Aerospace Engineering. Fellow AIAA.

(blue) flames or soot-containing flames] has not been addressed. This is unfortunate because hydrodynamic effects to reduce soot concentrations in diffusion flames are of great interest.[10-19] In addition, soot-free hydrocarbon-fueled flames are fundamentally important because they have enhanced computational tractability compared to soot-containing flames as a result of the absence of the complexities of soot chemistry, and they provide results useful for evaluating detailed models of hydrocarbon-fueled flame chemistry and transport.

The ability to achieve soot-free laminar diffusion flames by subjecting the fuel stream to higher momentum (velocity) oxidant streams (e.g., by strong coflows), similar to the behavior of air atomization processes,[11,18,19] is discussed by Lin and Faeth[18] and Dai and Faeth.[19] The effect of enhanced coflow comes about because the position of the flame sheet tends to be fixed by the fuel flow rate independent of the coflow velocity at large coflow velocities,[9] which implies that characteristic residence times for soot formation are inversely proportional to the coflow velocity.[18,19] Thus, increasing the coflow velocity inhibits soot emissions and eventually leads to completely soot-free (blue) flames as long as flame liftoff conditions are not exceeded. This tactic was exploited during the present study in order to provide conditions where the shapes of the flame sheet of hydrocarbon-fueled laminar-jet diffusion flames in coflowing air could be observed.

Thus, the objectives of the present investigation were to observe the flame-sheet shapes of weakly buoyant laminar-jet diffusion flames in coflowing air considering both soot-free and soot-containing flames and to use these results to develop a simplified model of flame-sheet shape for these conditions. Corresponding results for laminar-jet diffusion flames in nearly still air are also considered in order to highlight effects of coflow on flame structure, soot formation, and soot emission properties. Finally, luminous flame shapes at the laminar smoke point, in both still and coflowing air, are also considered for completeness, exploiting earlier measurements in the literature.[5,9]

Experimental Methods

Test Apparatus

Experimental methods were similar to Lin et al.,[5] Lin and Faeth,[9] and Lin[17] and will be described only briefly. Effects of buoyancy were minimized by observing flames at relatively small pressures ($\leq$50 kPa) with either relatively large coflow velocities (air/fuel velocity ratios up to nine) or with relatively large source fuel Froude numbers when coflow velocities were small. The burner was placed within a windowed cylindrical chamber and directed vertically upward along the chamber axis. The windowed chamber had a diameter of 300 mm and a length of 1200 mm. Optical access was provided by two pairs of opposing windows having diameters of 100 mm and centered on a horizontal plane located 500 mm above the base of the windowed chamber. The flames were positioned so that their full lengths could be observed and photographed through the windows.

The burner was a coaxial-tube arrangement with the fuel flowing from the inner port (1.6-, 3.2-, and 4.8-mm inside diameters with the outer wall of the tube tapered to provide a negligible thickness at the tube exit) and air flowing from a concentric outer port (60-mm inside diameter). The inner port had sufficient length to provide fully developed laminar pipe flow at the burner exit. The outer port had several layers of beads and screens to provide a uniform nonturbulent flow at the burner exit. Flame lengths were limited so that test conditions approximated flames in a uniform air coflow based on earlier laser velocimetry measurements of flow velocity distributions.[17,18] The burner tube exit was placed 10 mm above the last screen of the air coflow so that the flames were free to attach somewhat below the burner exit (which often was the case unless liftoff conditions were approached).

Fuel was supplied to the inside port from commercial gas cylinders. Fuel flow rates were controlled and metered using critical flow orifices in conjunction with pressure regulators; the flow properties of the orifices were calibrated using wet-test meters. Air was supplied from the room using critical-flow orifices to control and meter airflow rates. The exhaust products were diluted with air to reduce flow temperatures and then removed using the laboratory vacuum pump system. The flames were ignited using a small torch that was removed from the flowfield after the flames had stabilized.

Instrumentation

Dark-field photographs of the flames were obtained using a 35-mm reflex camera. The photographs were subsequently printed using a 100 × 125 mm film format and then scanned. Flame shapes were measured directly from the scanned images, using objects of known size to calibrate vertical and horizontal distances. Experimental uncertainties (95% confidence) of luminous flame diameters and lengths were less than 2%.

The dark-field color photographs sufficed to locate luminous-flame boundaries as either the outer extremity of yellow luminosity caused by continuum radiation from soot or the inner boundary of blue luminosity from the flame sheet (which exhibited a significant afterglow of OH luminosity for the low-pressure flames observed during the present experiments). To locate the flame sheet, however, dark-field photographs were obtained using a narrowband filter designed to pass radiation from the excited CH band associated with radical reactions at the flame sheet (430-nm center frequency with a 10-nm half-width pass band). This luminosity was relatively weak, but the present flames were very steady so that exposure times could be increased to obtain satisfactory photographs. The outer extremity of the CH image was taken as the flame-sheet location because CH luminosity is not associated with fuel-lean regions of the present flames. Experimental uncertainties of the flame-sheet measurements are the same as the luminous flame boundary measurements.

Test Conditions

Test conditions are summarized in Table 1. Present measurements considered methane-, acetylene-, ethylene-, and propane-fueled flames; earlier measurements considered propylene- and 1,3-butadiene-fueled flames. Gas purities were greater than 99% by volume for all of the fuel gases except acetylene, which only had a 98% purity by volume, because of contamination by acetone, which is present in commercial acetylene gas cylinders for safety purposes. The effect of acetone on the properties of flames similar to the present flames was evaluated during earlier experiments.[17,18]

Table 1 Summary of test conditions[a]

Parameter[b]	CH_4	C_2H_2	C_2H_4	C_3H_6	C_3H_8	C_4H_6
Fuel flow rate, mg/s	0.49–3.12	0.41–4.88	0.50–4.66	1.53–4.08	0.59–3.81	0.74–2.71
Re	2.7–45.6	2.9–54.1	3.6–47.6	38–101	4.9–48.5	18–66
u_{∞}/u_{fo}	0.008–7.14	0.0058–5.01	0.009–8.80	0.3–7.0	0.012–5.71	0.8–32.5
p, kPa	21.3–49.4	4.1–21.3	8.5–21.5	19–50	11.3–35.2	19–50
d, mm	1.6, 4.8	1.6, 4.8	1.6, 4.8	4.8	1.6, 4.8	4.8
μ_{fo}, mg/s-m	48.0	51.7	49.7	49.3	47.0	49.8
L_f, mm	5.7–41.5	5.0–54.9	7.1–47.0	41–108	9.4–51.3	21–75
$w_{1/2}$, mm	6.5–17.7	7.9–24.4	7.9–24.7	5.9–13.1	8.1–22.4	4.3–10.0
Z_{st}	0.0552	0.0704	0.0638	0.0636	0.0603	0.0668

[a]Air port inside diameter of 60 mm with burner directed vertically upward. Reactant temperatures of roughly 300 K.
[b]Commercial gases in cylinders with purities as follows: greater than 98.0% by volume for C_2H_2 and greater than 99.0% by volume for the rest.

This was done by comparing observations with and without acetone vapor present, using the acetone removal system described by Hamins et al.[20] to create an acetone-free acetylene fuel stream. The effect of acetone on luminous flame shapes and laminar smoke-point flame lengths was found to be small.[17,18]

Theoretical Methods

Flame-shape predictions were obtained using the simplified analysis of Lin et al.[5] for laminar diffusion flames in still air and Lin and Faeth[9] for laminar diffusion flames in coflowing air. In both instances a set of easily used equations was sought, along with recommendations for selecting the thermochemical and transport properties appearing in the equations, rather than more complete methods that would require numerical solution using a computer. The approach used for flames in still gases was to extend the analysis of Spalding,[2] which is described in more detail by Kuo,[3] as discussed by Lin et al.[5]; the approach used for flames in coflowing gases was to extend the analysis of Mahalingam et al.,[8] as discussed by Lin and Faeth.[9]

Except for ambient flow properties, the major assumptions of flame-shape analyses in still and coflowing gases were the same,[9] as follows: 1) steady, axisymmetric laminar-jet diffusion flames at constant pressure in an unbounded environment having uniform properties (velocities and scalar properties); 2) effects of buoyancy and associated changes of potential energy are negligible; 3) flow Mach numbers are small so that effects of kinetic energy and viscous dissipation are negligible; 4) the flames have large aspect ratios so that diffusion of mass (species), momentum, and energy in the streamwise direction is small; 5) for the same reasons the solution of the governing equations can be approximated by far-field conditions where the details of the initial conditions can be replaced by integral invariants of the flow for the conservation of mass, momentum, and energy; 6) similarly, the convection velocities of the flow can be approximated by ambient streamwise velocities for the coflow case; 7) all chemical reactions occur within a thin-flame sheet with fast chemistry so that fuel and oxidant are never simultaneously present at finite concentrations; 8) the diffusivities of mass (of all species), momentum, and energy are all equal; 9) all thermophysical and transport properties are constant throughout the flame; and 10) effects of radiation are small. The first three assumptions are justified as conditions of the present experiments. The fourth and fifth assumptions are justified for most of the present measurements because the present flames generally had large aspect ratios, for example, some measurements involve $(L_f - L_o)/d$ as small as 1.0 but most of the measurements involve $(L_f - L_o)/d$ in the range 6–22. The sixth assumption is widely used to approximate wake-like boundary-layer flows at large aspect ratios.[9] The seventh assumption, prescribing a thin flame sheet, has a long history of effective use to find the shapes of laminar diffusion flames, dating back to Burke and Schumann.[1] The remaining assumptions are not satisfied by laminar-jet diffusion flames, however, and are only adopted so that simple flame-shape formulas can be found based on the past success of similar approximations to find the shapes of the luminous soot boundaries of laminar-jet diffusion flames at the laminar smoke point (see Refs. 5 and 9 and references cited therein).

Under these assumptions a simple formula can be obtained for flame-sheet and luminous-flame lengths both in still and strongly coflowing gases, as follows[9]:

$$(L_f - L_o)/d = C_f C_n ReSc/Z_{st} \tag{1}$$

where $C_n = \frac{3}{32}$ and $\frac{2}{32}$ for weak and strong coflow and C_f is roughly 0.5 and 1.0 for the flame-sheet location and for the location of the luminous-flame boundary at laminar smoke-point conditions, respectively. (More accurate selections of C_f will be considered later.) The algorithm for computing flame properties from Eq. (1) was completed by using the values for the Schmidt number and the viscosity of air at the average of the adiabatic flame temperature and the ambient temperature from Braun et al.[21] Typical of past work with hydrocarbon-fueled laminar-jet diffusion flames burning in air, the value of the Schmidt number did not change significantly over the test range; thus, $Sc = 0.76$ was used for all of the results considered during the present investigation. Similarly, the correlations of flame lengths were improved during past work by introducing the empirical virtual origin parameter L_o/d (see Refs. 5 and 9). The effect of a virtual origin was not very significant for present conditions, however, so that $L_o/d = 0$ was used instead.

The expressions for luminous-flame diameters differ for laminar-jet diffusion flames in still air, given in Ref. 5, and in coflowing air, given in Ref. 9. For flames in still air, the expression becomes[5]

$$wZ_{st}/d = 3^{\frac{1}{2}}\zeta\left(\zeta^{-\frac{1}{2}} - 1\right)^{\frac{1}{2}} \tag{2}$$

whereas the corresponding equation for flames in coflowing air becomes[9]

$$wZ_{st}/d = [-\zeta(u_{fo}/u_{ao})Z_{st}\ell_n\{\zeta\}]^{\frac{1}{2}} \tag{3}$$

And in both cases

$$\zeta = (x - L_o)/(L_f - L_o) \tag{4}$$

and the values of the flame diameter at the midposition of the flames, where $\zeta = \frac{1}{2}$, are given as follows for flames in still air[5]:

$$w_{\frac{1}{2}} Z_{st}/d = 0.557 \tag{5}$$

whereas the corresponding equation for flames in coflowing air becomes[9]

$$w_{\frac{1}{2}} Z_{st}/d = [Z_{st}(u_{fo}/u_{ao})\ell_n\{2\}/2]^{\frac{1}{2}} \tag{6}$$

Other expressions for the maximum value of w, w_{MAX}, can be found in Refs. 5 and 9, but the differences between $w_{1/2}$ and w_{MAX} are not large.

Results and Discussion

Flame Appearance

Photographs of a soot-free acetylene-fueled laminar-jet diffusion flame in coflowing air at near liftoff conditions are illustrated in Fig. 1. The figure on the left is a black-and-white image of a conventional dark-field color photograph. The figure at the right is a black-and-white image of a dark-field color photograph obtained using the CH filter. Both images are essentially the same indicating that the flame sheet in the absence of soot luminosity is indicated equally well by conventional dark-field color photographs as well as the image obtained from CH luminosity alone.

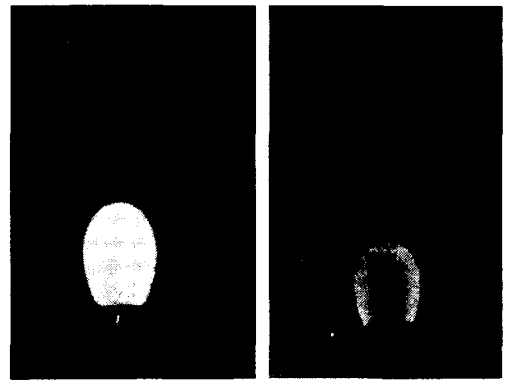

Fig. 1 Photographs of a soot-free acetylene-fueled laminar-jet diffusion flame burning in coflowing air near the liftoff condition, without (left) and with (right) the C-H filter. Test conditions are d = 1.6 mm, p = 4.1 kPa, and u_{ao}/u_{fo} = 0.05.

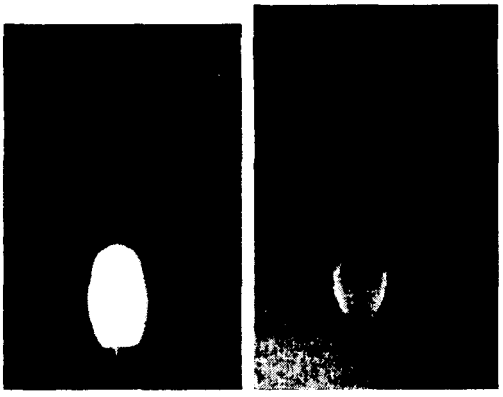

Fig. 2 Photographs of a soot-containing acetylene-fueled laminar-jet diffusion flame burning in coflowing air at conditions between laminar soot and smoke points, without (left) and with (right) the C-H filter. Test conditions are $d = 1.6$ mm, $p = 8.2$ kPa, and $u_{ao}/u_{fo} = 0.06$.

Photographs of a soot-containing acetylene-fueled laminar-jet diffusion flame in coflowing air are illustrated in Fig. 2 for conditions intermediate between the laminar soot and smoke points. Similar to Fig. 1, the figure on the left is a black-and-white image of a conventional dark-field color photograph, whereas the figure at the right is a black-and-white image of a dark-field color photograph obtained using the CH filter. In this case the conventional color photograph image is longer than the color images obtained using the CH filter because of the presence of yellow luminosity from hot soot particles present beyond the flame-sheet in the fuel-lean region of the flame. (This is more evident based on direct viewing of the flame by eye or from the conventional color image where the yellow color can be seen.) Similar to Fig. 1, however, both images are identical near the burner exit where no soot was present. Thus, it was possible to locate the image of the flame sheet using the CH filter even in the presence of significant soot luminosity from the fuel-lean portion of the flame once the laminar soot-point condition was exceeded.

Flame Lengths

Luminous-flame lengths are defined in the following as the streamwise distance between the burner exit and the farthest downstream plane normal to the flame axis that contacts a luminous region of the flame, at the laminar smoke point, similar to Lin and Faeth.[9] For flames in coflowing air, this length was associated with the end of the flame luminosity at the flame axis. For the flames of Lin et al.[5] in still air, however, this location was either along the axis or at an annular soot layer for the closed- and open-tip flames observed near laminar smoke-point conditions for nonbuoyant flames in still gases.[6] This distinction was not necessary for flame-sheet lengths, however, because this length was always associated with the end of flame luminosity at the flame axis, as observed either using the CH filter for soot-containing flames or observed both with and without the CH filter for soot-free flames.

For present conditions, only fuel flowed from the fuel port so that simple one-dimensional conservation of mass principles apply, and an expression for flame length as a function of the fuel flow rate can be obtained from Eq. (1) and the definition of the Reynolds number, as follows:

$$L_f - L_o = 4C_f C_n Sc\, \dot{m}_f/(\pi Z_{st}\mu) \tag{7}$$

Noting that $L_o \ll L_f$ from Table 2, Eq. (7) implies that both the flame-sheet length (at the axis) and the luminous-flame length (at the laminar smoke point) are proportional to the parameter $\dot{m}_f/(Z_{st}\mu)$ because C_f, C_n, and Sc are not affected by either fuel type or the value of $\dot{m}_f/(Z_{st}\mu)$ for present conditions. Similar behavior concerning relationships between fuel flow rates and laminar smoke-point flame lengths for buoyant flames has been recognized for some time[14,22,23] and has also been observed for nonbuoyant flames at the laminar smoke point as suggested by Eq. (5).[24,25]

Table 2 Summary of flame-length correlations[a]

Flame system	Source	L_o/d	C_f	C_n
Smoke-point flame length in still air, $Fr_f = \infty$	Lin et al.[5]	−3.2	1.13	$\frac{3}{32}$
Smoke-point flame length in coflowing air: $u_{ao}/u_{fo} > 1$ and $Fr_o > 1$	Lin and Faeth[9]	1.4	1.05	$\frac{2}{32}$
Soot-free flame length in still air; $u_{ao}/u_{fo} < 0.2$ and $Fr_f \gg 5$	Present study	0.0	0.52	$\frac{3}{32}$
Soot-free flame length in still air; $u_{ao}/u_{fo} = 0$ and $Fr_f = \infty$	Sunderland et al.[4]	2.7	0.56	$\frac{3}{32}$
Soot-free flame length in coflow; $u_{ao}/u_{fo} > 0.5$ and $Fr_o > 1$	Present study	0.0	0.54	$\frac{2}{32}$

[a]Empirical flame length parameters based on Eq. (1) for soot-free flames and for soot-containing flames at the laminar smoke point for flames in still ($u_{ao}/u_{fo} < 0.2$) or coflowing ($u_{ao}/u_{fo} > 0.5$) air.

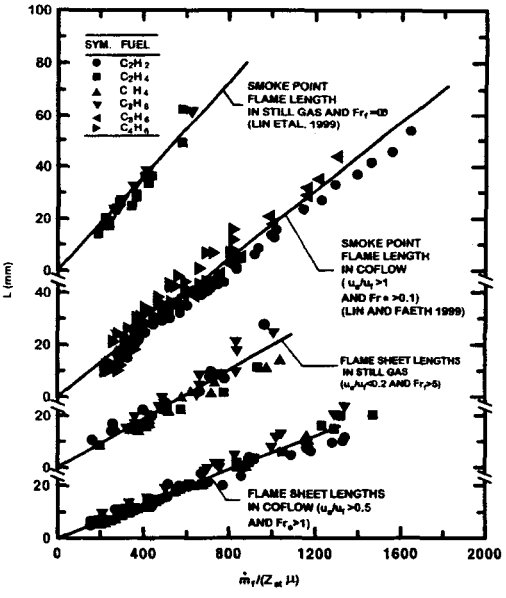

Fig. 3 Flame-sheet and luminous-flame lengths (the latter at the laminar smoke point) of laminar-jet diffusion flames in still air and coflowing air. Measurements from Lin et al.,[5] Lin and Faeth,[9] and the present investigation.

Measured flame-sheet and luminous-flame lengths (the latter at the laminar smoke-point condition) are plotted according to Eq. (7) in Fig. 3 for nonbuoyant diffusion flames in both nearly still and relatively strong coflowing air. The values of C_f and C_n for the correlations were taken from Table 2, whereas $Sc = 0.76$ for all of the present results as noted earlier. Thus, Eq. (7) combined with present methods of finding flame physical properties and the values of C_f and C_n from Table 2 yield excellent correlations for the four flame length conditions that are considered in Fig. 3. The measured flame-sheet results include conditions in both soot-free (blue) flames as well as conditions beyond the laminar soot point (but prior to the laminar smoke point) where soot is present and the flame exhibits yellow soot luminosity. Similar to the discussion of Fig. 2, however,

the presence of soot in the present laminar-jet diffusion flames did not have a significant effect on the flame-sheet length. The values of C_f at the luminous-flame length at the laminar smoke-point condition are roughly twice as large as the values of C_f for the flame-sheet length (see Table 2); thus, the presence of hot soot particles in the fuel-lean portion of the flame significantly extends (by up to a factor of roughly 2) the region where flame luminosity is observed.

The measurements illustrated in Fig. 3 could be grouped into conditions where $u_a/u_f > 0.5$ and the various lengths correlated reasonably well with the coflow correlation with $C_n = \frac{2}{32}$ (as long as $Fr_a > 1$) and $u_{ao}/u_{fo} < 0.2$ where the various lengths correlated reasonably well with the still gas correlation with $C_n = \frac{3}{32}$ (as long as $Fr_f > 5$). Intermediate values of u_{ao}/u_{fo} yield intermediate values of flame lengths (or C_n) as will be discussed in more detail later. In view of the simplicity of the theory, it is remarkable that the predictions are reasonably good. Thus, transition from strong to weak coflow increases both flame-sheet and luminous-flame lengths by roughly 50%. The reason that values of u_{ao}/u_{fo} are significantly less than unity bound conditions between strong and weak coflow is that jet-exit conditions decay rapidly toward ambient conditions so that even relatively small ambient velocities can affect mixing in the important region near the flame tip for flame length behavior, particularly for the relatively large aspect ratio flames (typical of the behavior of hydrocarbon/air flames that have relatively small stoichiometric ratios or small values of Z_{st}) that were considered during the present investigation.

Flame Diameters

It is evident that the normalized characteristic flame diameter $w_{1/2}Z_{st}/d$ for laminar-jet diffusion flames is a constant for flames in still air from Eq. (2) and is inversely proportional to the square root of air/fuel velocity ratio for flames in coflowing air from Eq. (3), independent of flow transport properties. This relationship is illustrated in Fig. 4 for nonbuoyant diffusion flames in coflow for flame-sheet diameters with $u_{ao}/u_{fo} > 0.5$ and $Fr_a > 1$ along with the predictions of Eq. (3). The measurements scatter about the predictions, but the scatter progressively decreases as the normalized flame length increases. Thus, small flame aspect ratios appear to be mainly responsible for the scatter seen in Fig. 4. This conclusion is similar to the findings of Lin and Faeth[9] for laminar smoke-point conditions.

It is also of interest to consider the behavior of the normalized characteristic flame diameter as the value of u_{ao}/u_{fo} increases for conditions representative of nonbuoyant laminar-jet diffusion flames in still air to strongly coflowing air. This transition is considered in Fig. 5, which provides characteristic flame diameter expressions particularly suitable for both large and small values of u_{ao}/u_{fo}. Results illustrated in Fig. 5 show the transition between estimates of the characteristic flame diameter in still gas to estimates in strongly coflowing gas at values of $u_{ao}/u_{fo} \approx 0.1$; measured results in both regimes exhibit significant degrees of scatter, and the large coflow predictions generally underestimate the measurements.

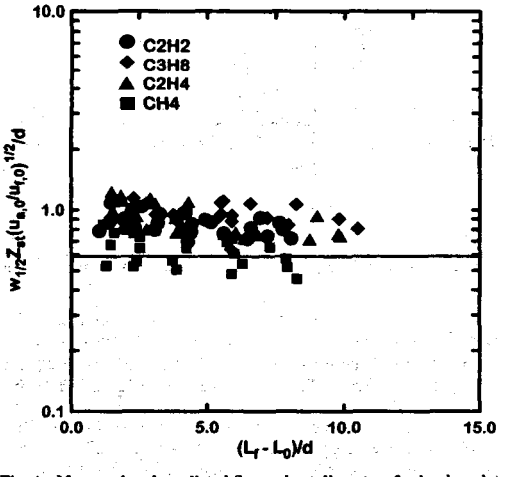

Fig. 4 Measured and predicted flame-sheet diameters for laminar-jet diffusion flames in coflow as a function of air/fuel velocity ratios and flame sheet length.

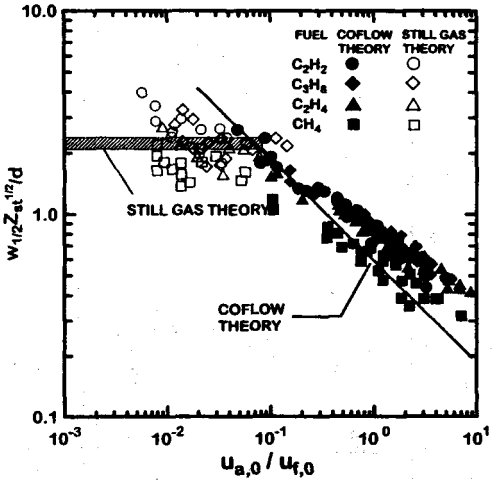

Fig. 5 Measured and predicted flame-sheet diameters as a function of air/fuel velocity ratios.

Flame Shapes

Measured and predicted flame shapes will be compared as the final step in the evaluation of the simplified flame-shape analyses leading to Eqs. (1–4) for nonbuoyant laminar-jet diffusion flames in still and coflowing air. These evaluations will consider a range of flame aspect ratios in order to explore the robustness of the predictions. Both soot-free and soot-containing flames will be considered in the following so that effects of soot on the location of the flame sheet can be evaluated for nonbuoyant laminar-jet diffusion flames.

Examples of measured and predicted flame shapes for soot-free methane/air flames having various coflow velocity ratios are illustrated in Fig. 6. For these soot-free flame conditions the measured flame shapes with and without the CH filter are identical, with both observations giving the correct flame-sheet location. Predictions of flame-sheet locations using the simplified theories are also shown on the plot; all of the measurements are for $u_{ao}/u_{fo} > 0.5$ and are compared with predictions for flames in coflowing air, Eq. (3). The comparison between measurements and predictions is excellent, properly accounting for effects of variations of air coflow, in view of the simplicity of the flame-shape analyses.

Examples of measured and predicted flame-sheet shapes for soot-containing ethylene/air flames having various coflow velocity ratios are illustrated in Fig. 7. For these soot-containing flame conditions measured flame shapes with and without the CH filter are no longer identical with the luminous-flame shape obtained without the filter extending farther downstream as a result of the presence of yellow soot luminosity from soot present in the fuel-lean region of the flame. None of the conditions shown in Fig. 7 correspond to laminar smoke-point conditions; therefore, only laminar flame-sheet predictions are shown on the plot. Similar to Fig. 6 for soot-free flames, the comparison between measurements and predictions is excellent, indicating that the presence of soot in these flames

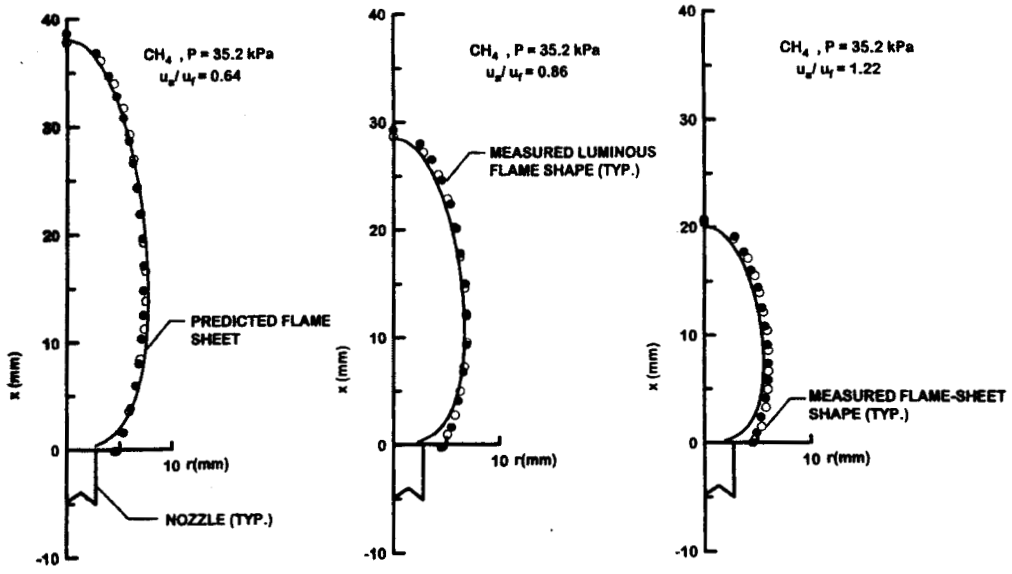

Fig. 6 Measured flame-sheet and luminous-flame shapes and predicted flame-sheet shapes for soot-free methane-fueled laminar-jet diffusion flames having a burner diameter of 4.8 mm at various air coflow velocity ratios.

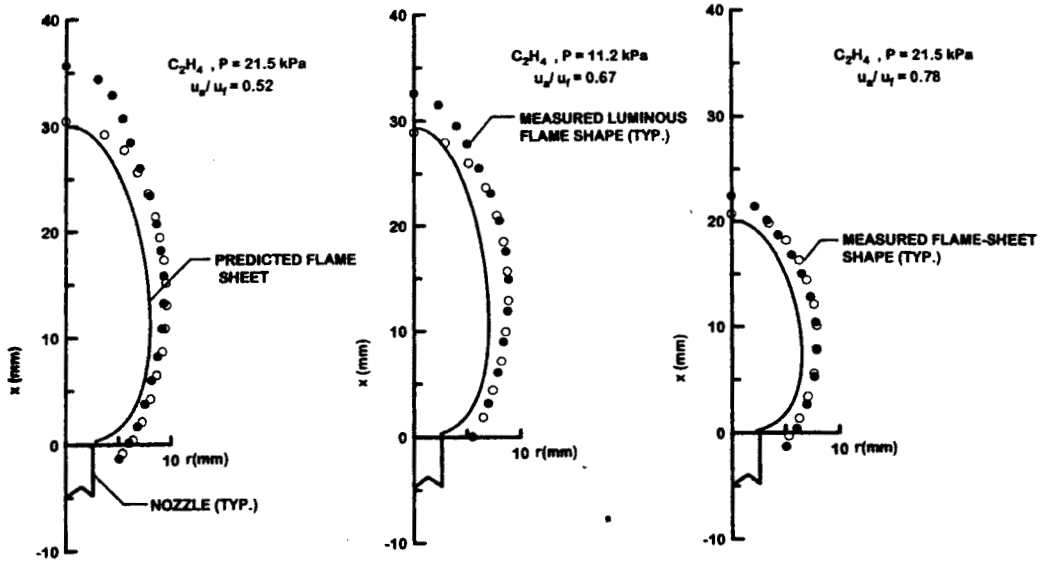

Fig. 7 Measured flame-sheet and luminous-flame shapes for soot-containing ethylene-fueled laminar-jet diffusion flames having a burner diameter of 4.8 mm at various small air coflow velocity ratios.

does not have a significant impact on predictions of flame-sheet location.

Examples of measured and predicted flame-sheet shapes for both soot-free and soot-containing flames involving other fuels, propane/air and acetylene/air flames, having various velocity ratios are illustrated in Figs. 8 and 9. Similar to Fig. 7, results with and without the CH filter are not always the same with the luminous-flame boundary extending beyond the flame sheet because of luminosity from soot in the fuel-lean portion of the flame in some instances. Only predictions for the flame-sheet shape in still air are shown because these flames are not at laminar smoke-point conditions and have small air/fuel velocity ratios; notably, the comparisons between predicted and measured of flame-sheet shapes are excellent. (Corresponding comparisons between measured and predicted luminous-flame shapes at laminar smoke-point conditions can be found in Lin and Faeth.[9])

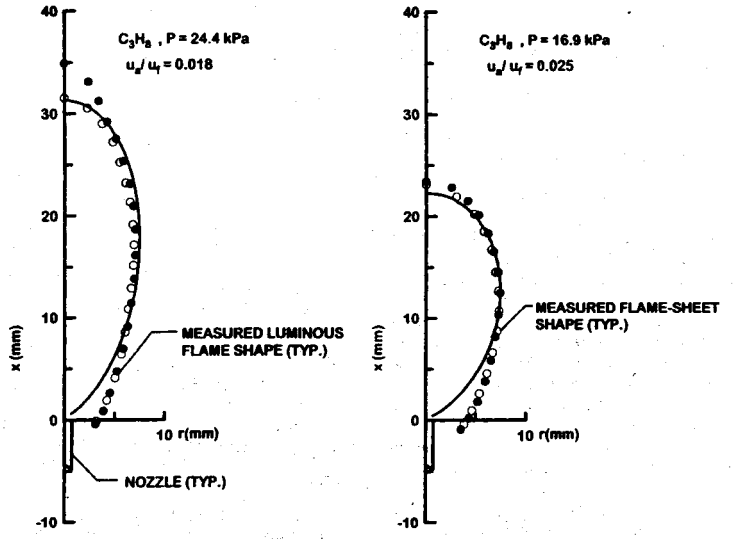

Fig. 8 Measured flame-sheet and luminous-flame shapes and predicted flame-sheet shapes for both soot-containing and soot-free propane-fueled laminar-jet diffusion flames having a burner diameter of 1.6 mm at various small air coflow velocity ratios.

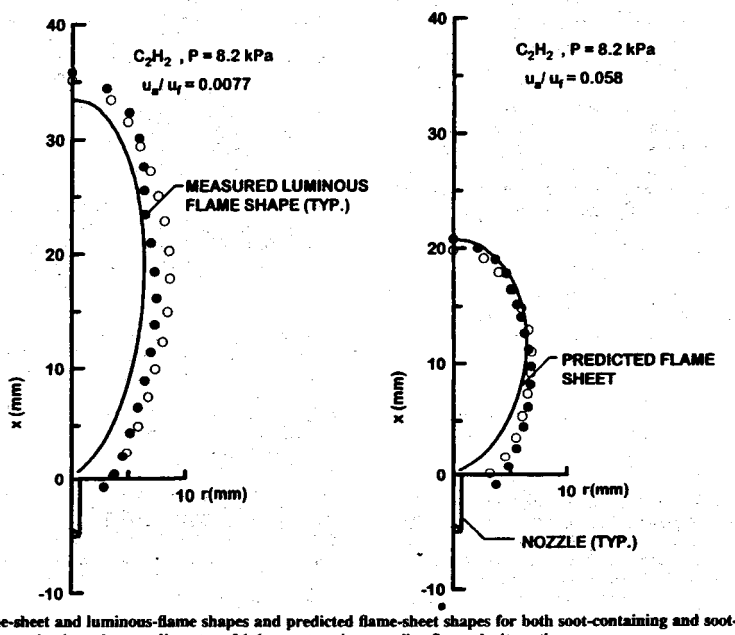

Fig. 9 Measured flame-sheet and luminous-flame shapes and predicted flame-sheet shapes for both soot-containing and soot-free acetylene-fueled laminar-jet diffusion flames having a burner diameter of 1.6 mm at various small coflow velocity ratios.

Conclusions

The luminous flame-sheet and luminous-flame boundaries of steady, nonbuoyant round hydrocarbon-fueled laminar-jet diffusion flames in still and coflowing air were studied both experimentally and theoretically. Present conditions included acetylene-, methane-, propane-, and ethylene-fueled flames having reactant temperatures of 300 K, ambient pressures of 4–50 kPa, jet-exit Reynolds numbers of 3–54, initial air/fuel velocity ratios of 0–9, and luminous flame lengths of 5–55 mm. The present flames involved both soot-free and soot-containing flames but the latter were not emitting soot and generally did not approach laminar smoke-point conditions. Both new and earlier[5,9] measurements were used to evaluate predictions of luminous flame-sheet and luminous-flame boundaries based on extension of simplified analyses from Spalding[2] and Mahalingam et al.[8] The major conclusions of the study are as follows:

1) The present simplified analysis of nonbuoyant laminar-jet diffusion flames in coflow, extended from Mahalingam et al.,[8] provided reasonably good predictions of flame-sheet shapes of both soot-free and soot-emitting flames for $u_{ao}/u_{fo} > 0.5$ and $Fr_a > 1$ after appropriate selection of empirical parameters for the simplified theory summarized in Table 2.

2) The simplified analysis of nonbuoyant laminar-jet diffusion flames in still air from Spalding[2] provided reasonably good predictions of flame-sheet shapes of both soot-free and soot-containing flames in slow-moving coflow for $u_{\infty o}/u_{fo} < 0.2$ and $Fr_f > 5$ after appropriate selections of empirical parameters for the simplified theory summarized in Table 2.

3) Based on present findings about flame-sheet and luminous-flame boundaries of nonbuoyant laminar-jet diffusion flames in still and coflowing air, flame-sheet and luminous-flame lengths increase linearly with fuel flow rates but are relatively independent of jet-exit diameter, pressure, and air/fuel velocity ratio (for flames in coflow). Finally, flames in still air are roughly 50% longer than flames in reasonably strong coflow ($u_{\infty o}/u_{fo} > 1$) at comparable conditions.

4) Based on present findings about flame-sheet and luminous-flame boundaries of nonbuoyant laminar-jet diffusion flames in still and coflowing air, characteristic flame-sheet and luminous-flame diameters vary linearly with jet-exit diameter and are relatively independent of flow physical properties and jet-exit Reynolds numbers. For flames having significant coflow levels ($u_{\infty o}/u_{fo} > 1$), however, the characteristic luminous flame diameters are also proportional to the square root of $u_{fo}/u_{\infty o}$.

5) Luminous-flame lengths progressively increased compared to flame-sheet lengths as the laminar smoke point was approached for nonbuoyant laminar-jet diffusion flames in both still and coflowing air. In both cases luminous-flame lengths at the laminar smoke point were roughly twice as long as flame-sheet length as a result of the presence of hot luminous soot particles in the fuel-lean portions of the soot-containing flames.

Limitations of the present findings should be noted, as follows: these results should be used with caution outside the present test range until the results are definitively confirmed for longer-term microgravity conditions where the intrusion of effects of transient flame development and buoyancy are absent (notably, both these effects tend to reduce the luminous flame dimensions[6]); these results were developed for luminous flame shapes and the simplified theories should not be assumed to apply to other important flame structure properties (temperatures, velocities, species concentrations, etc.) where good performance of such simplified methods has not been established and frankly seems unlikely.

Acknowledgments

This research was supported by NASA Grants NCC3-661, NAG3-1878, and NAG3-2048 under the technical management of D. L. Urban and Z.-G. Yuan of the NASA John H. Glenn Research Center, Dayton, Ohio.

References

[1]Burke, S. P., and Schumann, T. E. W., "Diffusion Flames," *Industrial and Engineering Chemistry*, Vol. 20, No. 10, 1928, pp. 998–1004.

[2]Spalding, D. B., *Combustion and Mass Transfer*, Pergamon, New York, 1979, pp. 185–195.

[3]Kuo, K. K., *Principles of Combustion*, Wiley, New York, 1986, pp. 360–370.

[4]Sunderland, P. B., Mendelson, B. J., Yuan, Z.-G., and Urban, D. L., "Shapes of Buoyant and Nonbuoyant Laminar Jet Diffusion Flames," *Combustion and Flame*, Vol. 116, No. 3, 1999, pp. 376–386.

[5]Lin, K.-C., Faeth, G. M., Sunderland, P. B., Urban, D. L., and Yuan, Z.-G., "Shapes of Nonbuoyant Round Luminous Hydrocarbon/Air Laminar Jet Diffusion Flames," *Combustion and Flame*, Vol. 116, No. 3, 1998, pp. 415–431.

[6]Urban, D. L., Yuan, Z.-G., Sunderland, P. B., Linteris, G. T., Voss, J. E., Lin, K.-C., Dai, Z., Sun, K., and Faeth, G. M., "Structure and Soot Properties of Nonbuoyant Ethylene/Air Laminar Jet Diffusion Flames," *AIAA Journal*, Vol. 36, No. 8, 1998, pp. 1346–1360.

[7]Williams, F.A., *Combustion Theory*, 2nd ed., Benjamin/Cummings Publishing, Menlo Park, CA, 1985, pp. 38-47.

[8]Mahalingam, S., Ferziger, J. H., and Cantwell, B. I., "Self-Similar Diffusion Flames," *Combustion and Flame*, Vol. 82, No. 2, 1990, pp. 231–234.

[9]Lin, K.-C., and Faeth, G. M., "Shapes of Nonbuoyant Round Luminous Laminar Jet Diffusion Flames in Coflowing Air," *AIAA Journal*, Vol. 37, No. 6, 1999, pp. 759–765.

[10]Hussman, A. W., and Maybach, G. W., "The Film Vaporizer Combustor," *SAE Transactions*, Vol. 69, 1961, pp. 563–574.

[11]Bahr, D. W., "Gas Turbine Engine Emission Abatement—Status and Needed Advancements," *Gas Turbine Combustion Design Problems*, edited by A. H. Lefebvre, Hemisphere, Washington, DC, 1979, pp. 205–223.

[12]Haynes, B. S., and Wagner, H. G., "Soot Formation," *Progress in Energy and Combustion Science*, Vol. 7, No. 4, 1981, pp. 229–273.

[13]Wu, K.-T., and Essenhigh, R. H., "Mapping and Structure of Inverse Diffusion Flames of Methane," *Proceedings of the Combustion Institute*, Vol. 20, Combustion Inst., Pittsburgh, PA, 1984, pp. 1925–1932.

[14]Glassman, I., "Soot Formation in Combustion Processes," *Proceedings of the Combustion Institute*, Vol. 22, Combustion Inst., Pittsburgh, PA, 1988, pp. 295–311.

[15]Sugiyama, G., "Nonluminous Diffusion Flame of Diluted Acetylene in Oxygen Enriched Air," *Proceedings of the Combustion Institute*, Vol. 25, Combustion Inst., Pittsburgh, PA, 1994, pp. 601–608.

[16]Du, J., and Axelbaum, R. L., "The Effect of Flame Structure on Soot-Particle Inception in Diffusion Flames," *Combustion and Flame*, Vol. 100, No. 3, 1995, pp. 367–375.

[17]Lin, K.-C., "Hydrodynamic Effects on Soot Formation in Laminar Hydrocarbon-Fueled Diffusion Flames," Ph.D. Dissertation, Dept. of Aerospace Engineering, Univ. of Michigan, Ann Arbor, MI, June 1996.

[18]Lin, K.-C., and Faeth, G. M., "Hydrodynamic Suppression of Soot Emissions in Laminar Diffusion Flames," *Journal of Propulsion and Power*, Vol. 12, No. 1, 1996, pp. 10–17.

[19]Dai, Z., and Faeth, G. M., "Hydrodynamic Suppression of Soot Formation in Laminar Coflowing Jet Diffusion Flames," *Proceedings of the Combustion Institute*, Vol. 28, Combustion Inst., Pittsburgh, PA, 2000, pp. 2085–2092.

[20]Hamins, A., Gordon, A. S., Saito, K., and Seshadri, K., "Acetone Impurity in Acetylene from Tanks," *Combustion Science and Technology*, Vol. 45, No. 5, 1986, pp. 309, 310.

[21]Braun, W. G., Danner, R. P., and Daubert, T. E., *Technical Data Book—Petroleum Refining*, 3rd ed., American Petroleum Inst., Washington, DC, 1976, Chaps. 11 and 13.

[22]Schug, K. P., Manheimer-Timnat, Y., Yaccarino, P., and Glassman, I., "Sooting Behavior of Gaseous Hydrocarbon Diffusion Flames and the Influence of Additives," *Combustion Science and Technology*, Vol. 22, Nos. 5 and 6, 1980, pp. 235–250.

[23]Gomez, A., Sidebotham, G., and Glassman, I., "Sooting Behavior in Temperature-Controlled Laminar Diffusion Flames," *Combustion and Flame*, Vol. 58, No. 1, 1984, pp. 45–57.

[24]Sunderland, P. B., Mortazavi, S., Faeth, G. M., and Urban, D. L., "Laminar Smoke-Points of Nonbuoyant Jet Diffusion Flames," *Combustion and Flame*, Vol. 96, No. 1, 1994, pp. 97–103.

[25]Urban, D. L., Yuan, Z.-G., Sunderland, P. B., Lin, K.-C., Dai, Z., and Faeth, G. M., "Smoke-Point Properties of Nonbuoyant Round Laminar Jet Diffusion Flames," *Proceedings of the Combustion Institute*, Vol. 28, Combustion Inst., Pittsburgh, PA, 2000, pp. 1965–1972.

J. P. Gore
Associate Editor